2019-01-01

A Coupled Modeling Framework For Allocation Design In Land-Use And Land-Cover Changes To Optimize Biofuel Feedstock Production

Ana C. Cram
University of Texas at El Paso

A COUPLED MODELING FRAMEWORK FOR ALLOCATION DESIGN IN LAND-USE AND LAND-COVER CHANGES TO OPTIMIZE BIOFUEL FEEDSTOCK PRODUCTION

ANA CATALINA CRAM

Doctoral Program in Environmental Science and Engineering

APPROVED:

Jose F. Espiritu, Ph.D., Chair

Heidi A. Taboada, Ph.D.

Ivonne Santiago, Ph.D.

Juan Noveron, Ph.D.

Stephen L. Crites, Jr., Ph.D.
Dean of the Graduate School

Dedication

Every word written in this document, every sleepless night, and every effort I made to complete this project, is dedicated to my beloved children, Christopher and Matias.

I do not expect you to follow my steps. I expect you to follow your own dreams and fight as hard as I did to achieve them. We all have different abilities than others but do not ever let that discourage you from pursuing what you most desire in life. Remember that the only limit there is is the one that we impose on ourselves.

A COUPLED MODELING FRAMEWORK FOR ALLOCATION DESIGN IN LAND-USE AND LAND-COVER CHANGES TO OPTIMIZE BIOFUEL FEEDSTOCK PRODUCTION

by

ANA CATALINA CRAM, M. S.

DISSERTATION

Presented to the Faculty of the Graduate School of

The University of Texas at El Paso

in Partial Fulfillment

of the Requirements

for the Degree of

DOCTOR OF PHILOSOPHY

Environmental Science and Engineering Program

THE UNIVERSITY OF TEXAS AT EL PASO

August 2019

Acknowledgements

I want to thank Dr. Jose Espiritu for all his patience, guidance and understanding. My most enormous gratitude goes to him and to Dr. Heidi Taboada, for always believing and supporting me in the many difficult times I faced throughout this journey. I take from them forever the most significant learning a student can receive, beyond any classroom.

I would also like to thank the rest of my dissertation committee members, Dr. Ivonne Santiago, and Dr. Juan Noveron, for being part of this project and for every encouraging word I received from them.

Also, I thank the University of Texas at El Paso for providing me with the tools I needed to achieve academic success.

Special thanks to the National Institute of Food and Agriculture (NIFA) for providing funding under the Hispanic Serving Institutions (HSI) Program, under award numbers 2015-38442-24112 & 2016-38422-25542. Also, many thanks to Dr. Irma Lawrence, who is responsible of the HSI program. The role she plays with the Hispanic community exceeds any expectation making a significant impact on many of our lives.

I also want to acknowledge Dr. Nancy Cavallaro, Dr. Randi Johnson, Dr. Ali Mohamed and Olivia Moreno, for all their support during my internships at NIFA in Washington, D.C.

Finally, I thank all my family and friends for understanding my distance, for the constant encouragement and for the unconditional love I received from all of you.

Abstract

Environmental awareness has increased the demand for renewable energy. Notably, the production of biofuels from feedstock is gaining interest as a viable measure to reduce fossil fuels consumption. Nevertheless, it is crucial to identify the trade-offs between bioenergy crop cultivation and the environmental impact on land, water, and atmosphere.

Intensifying biofuel cultivation trigger effects associated with Land Use and Land-use-change, which are complex to assess. While hydrological models had been used to investigate the environmental impacts of land-use changes on water and soil quality, their quantitative assessment is often incomplete. Changes in land use and agricultural activities also contribute to Greenhouse Gas (GHG) emissions known to influences atmospheric force change.

In order to supply the growing biofuel demand, sustainable approaches where natural resources are efficiently used must be developed. One key challenge on these approaches is optimal land use allocation to reduce the trade-offs between agroecosystems and the environment.

This research proposes a coupled modeling framework to optimize land use allocation for biofuel feedstock production at the watershed scale. The model estimates the potential effects on water quality, water demand, soil erosion, and GHG emissions from cultivating and producing biofuels from first-generation and second-generation feedstocks and provides optimal landscape scenarios. This framework couples the Soil and Water Assessment Tool (SWAT) and the Greenhouse gases, Regulated Emissions, and Energy use in Transportation Model (GREET) to quantify the potential effects on soil quality, water quality and emissions produced from changing the land use to cultivate biofuel feedstock instead of regional crops. The integrative approach incorporates a Multi-Objective Genetic Algorithm (MOEA) to assess land-use allocation,

maximizing biomass production while minimizing the environmental impacts on soil, water, and atmosphere.

Table of Contents

List of Tables

List of Figures

Chapter 1: Introduction

Chapter 1 will review the political efforts made to increase the production of biofuels. Some information of the Climate Change 2014: Mitigation of Climate Change report (Blanco et al. 2014) will be presented to provide an overview of the main contributor to the rising anthropogenic CO_2 concentration levels in the atmosphere and how Land-Use and Land-Change are linked to biofuel feedstock production and climate change. Also, this chapter provides with information on how we can reduce such emissions by increasing the production of biofuel feedstock to produce clean, renewable fuels. In this context, the optimal Land-Use and Land-Cover change design are required, and the means to achieve optimal allocation design will be explained.

1.1 Introduction

Ethanol continues to reduce Greenhouse Gas (GHG) emissions while serving as one of the most effective and low-cost fuel products. Furthermore, the use of ethanol in gasoline decreases harmful pollutants in tailpipe emissions such as carbon monoxide, exhaust hydrocarbons, benzene, and fine particulate matter, all of which are known to cause serious health effects (Renewable Fuels Association, 2015). In a study performed by the University of California-Berkeley, it was found that replacing gasoline with biofuels would extend human lives across the United States: “A biofuel eliminating even 10-percent of current gasoline pollutant emissions would have a substantial impact on human health in this country, especially in urban areas.” (The Coming of Biofuels, 2009)

Meanwhile, crude oil has been moving in the opposite direction. The environmental impacts of petroleum extraction, refining, and consumption continue to deteriorate as the production of oil has become more dependent on unsustainable sources like tar sands and tight oil

from fracking. In comparison to conventional crude oil, these sources require more energy for extraction and often are 15 to 20% more carbon-intensive (Renewable Fuels Association, 2015).

The Energy Independence and Security Act (EISA), signed by former President George W. Bush in 2007, aims to reduce the U.S. dependence on petroleum and to improve vehicle fuel economy. EISA mandates, through the Renewable Fuel Standard, to increase the supply of renewable alternative fuel sources, requiring a minimum of 36 billion gallons of renewable fuels annually by 2022 in transportation fuel sold in the United States. Furthermore, it aims to reduce energy consumption by increasing the standards for fuel economy passenger cars and light trucks, with the Corporate Average Fuel Economy (CAFE), at 35 miles per gallon. EISA requests federal agencies including the Secretary of Energy, the Secretary of Agriculture, the administrator of the Environmental Protection Agency and the National Academy of Science to conduct studies and report impacts of renewable fuel standards. Under this law, greenhouse gas emissions are projected to decrease by 9% by 2030 (US Congress, 2007).

Parallel to these efforts, the Low Carbon Fuel Standard (LCFS) established in 2007, through California's Governor Executive Order, aims to reduce greenhouse gas emissions from petroleum-based transportation fuels using a market-based cap and trade approach. Petroleum-based fuels producers are required to reduce the carbon intensity of their products under the LCFS. This reduction begins at 0.25% in 2011 and reaching a total reduction of 10% in 2020. LCFS allows importers, refiners, and wholesalers to develop low carbon fuel products and buy credits from low carbon alternative fuels companies (California Air Resources Board, 2009).

The LCFS established a scale of carbon content for every fuel included in the standard. This scale was developed by performing a life cycle assessment (LCA) that included the initial point of extraction and ended at the final point of sale (cradle-to-gate). the Greenhouse gases,

Regulated Emissions, and Energy use in Transportation Model (GREET) was employed to quantify the carbon intensity value for each fuel technology, which is expressed in terms of CO2-equivalent per megajoule of energy and has both direct and indirect emissions components. It should also be mention that the University of California Berkeley and Davis campuses have actively participated with the development, supporting, and implementation of the LCFS (California Air Resources Board, 2009).

New laws that promote the development of alternative renewable fuels and low carbon fuel products, forces to reduce current fuel consumption, requires lowering the carbon intensity on petroleum-based fuels and that aim to reduce GHG emissions are based on, or at least coincide with scientific reports on climate change across the world.

1.2 International Panel on Climate Change

The International Panel on Climate Change (IPCC) is a scientific and intergovernmental board, dedicated to providing the world with most updated scientific and objective information concerning climate change and its potential economic and political impacts. It works under the supervision of the United Nations (UN). The most recent report, Climate Change 2014: Mitigation of Climate Change (Blanco et al. 2014) attributes, primarily, the rising of anthropogenic CO2-concentration levels in the atmosphere to the combustion of fossil fuels. The second-largest component for the increased atmospheric CO-2 concentration from human activity is attributed to land use, land-use change, and forestry (LULUCF) (Figure1.1).

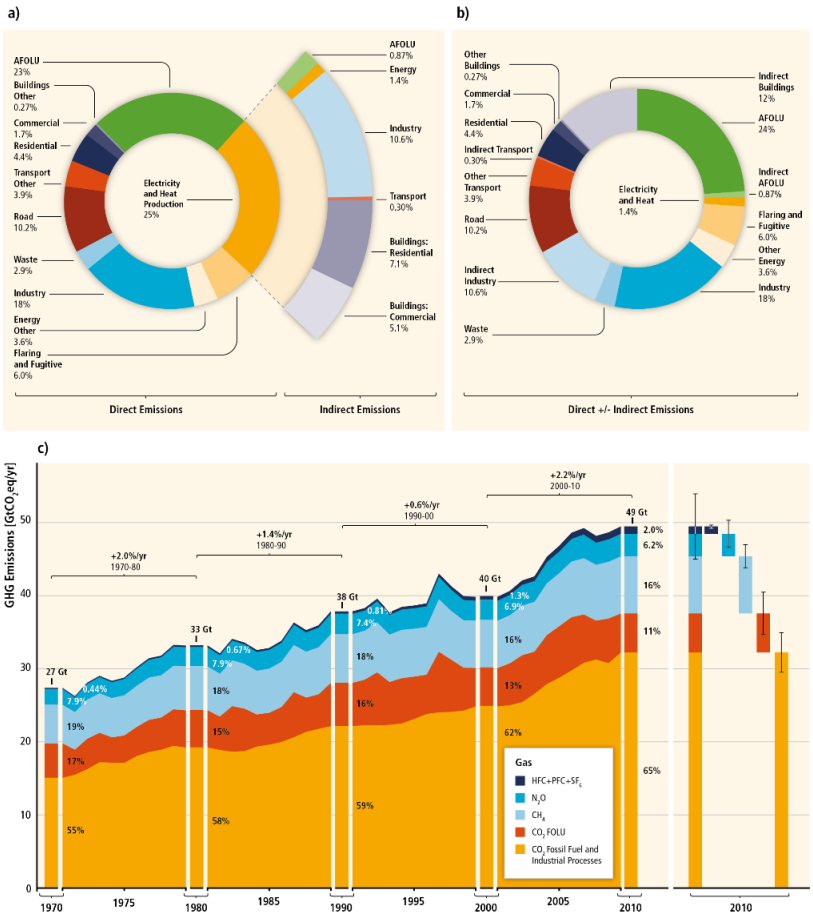

Figure 1.1: Direct and Indirect Greenhouse Gas Emissions (Blanco et al. 2014).

Measured on a 100-year GWP-weight, carbon dioxide (CO_2) and land-use-change covered more than 75% of the anthropogenic GHG emissions in 2010. Since 1970, global anthropogenic emissions have increased considerably. Methane (CH_4) and nitrous oxide (N_2O) have increased around 45% each, while fossil CO_2 have increased more than double. Florentine gases used to cover only 0.4% of GHG emissions in 1970, whereas in 2010 it increased to 2% (Blanco et al. 2014) .

Between 1970 and 2010, GHG emissions associated with agriculture, deforestation, and other land-use change (AFOLU) increased by 20%, from 99 GtCO2eq to 12GtCO2eq (Figure 1.2). By 2010, the emissions of GHGs from the AFOLU sector represented 20-25% of the global emissions. During the period 1970-2010, both the FOLU sub-sector and the agricultural sector

exhibited emissions rises. However, databases considerably show variation and uncertainty. In the agriculture subsector, CH_4 and N_2O were the most significant contributors to the total emissions in 2010. These emissions represent more than 80% of the total, which are mainly attributed to rice cultivation, enteric fermentation, use of synthetic fertilizers, manure and manure management. Higher increments in N_2O emissions have been seen from 1970 to 2010, ranging from 45-75% in comparison with CH_4, with only a 20% increase (Blanco et al. 2014).

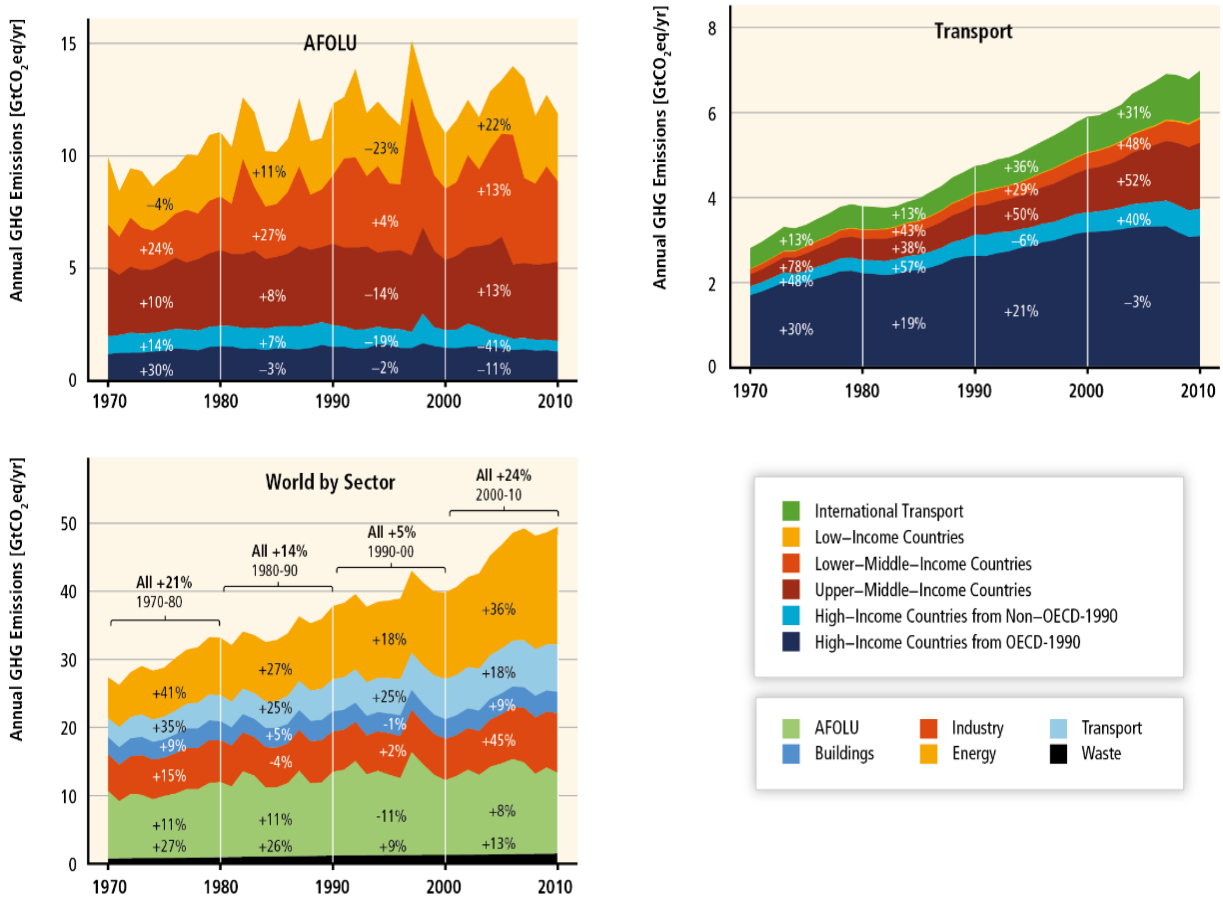

Figure 1.2: Greenhouse Gas Emissions by Sector (Blanco et al. 2014).

The transportation sector has also contributed to global GHG emissions. Between 1970 to 2010 the emissions grew from 2.8 GtCO2eq to 7 GtCO2eq. The largest share of the transport emissions is contributed by the Organization for Economic Co-operation and Development

(OECD) 1990 countries. However, the upper-middle-income countries and bunkers have the highest growth rate emissions in the transport sector. In general, the transportation graph in figure 1.2 shows a gradual increase in annual GHG emissions and a noticeable decline right before 2010. The principal drivers for the CO_2 emission growth in the transport sector over the past few decades are the increasing demand for freight and passenger transport, high fuel-consuming stock of vehicles and limited availability of low-carbon fuels, relatively low oil prices, among others. After 2002, the growth in Chinese exporting industries coincides with the market growth rate of international transport emissions. This suggests that world trade agreements and trade policies influence transport emissions (Blanco et al. 2014).

Furthermore, as a result of the increment in oil prices in 2008, and the global recession of 2009, fossil fuel consumption in OECD countries decreased. These events can explain the 2.0% decline of CO_2 emissions in 2008 and 3.6% in 2009. Similarly, as standards of living increases and economic activity rises, the demand for personal transportation also increases. These trends explain the strong correlation between per capita transport emissions and high-income countries (Blanco et al. 2014).

Bioenergy deployment offers significant mitigation potential. However, management practices and efficiency of bioenergy systems should be approached in terms of sustainability. The implementation of bioenergy systems needs to balance a wide range of environmental, economic, and social objectives that often are not fully compatible, as they can cause both positive and negative effects. The results depend on (1) the type of technology applied; (2) the pace, magnitude, and place of application; (3) the land class used (marginal lands, croplands, grassland, and forest); and (4) framework and practices implemented, considering how these displace or integrate with the current land use (Blanco et al. 2014).

The theoretical amount of bioenergy production that can be obtained through the implementation of demonstrated technologies or practices is known as technical bioenergy potential. The estimate global technical bioenergy potentials in 2050 by resource are shown in figure 1.3. Ranges were based on many studies that addressed the food/fiber first principle and different constraints concerning environmental and resources limitations, excluding explicit costs (Blanco et al. 2014).

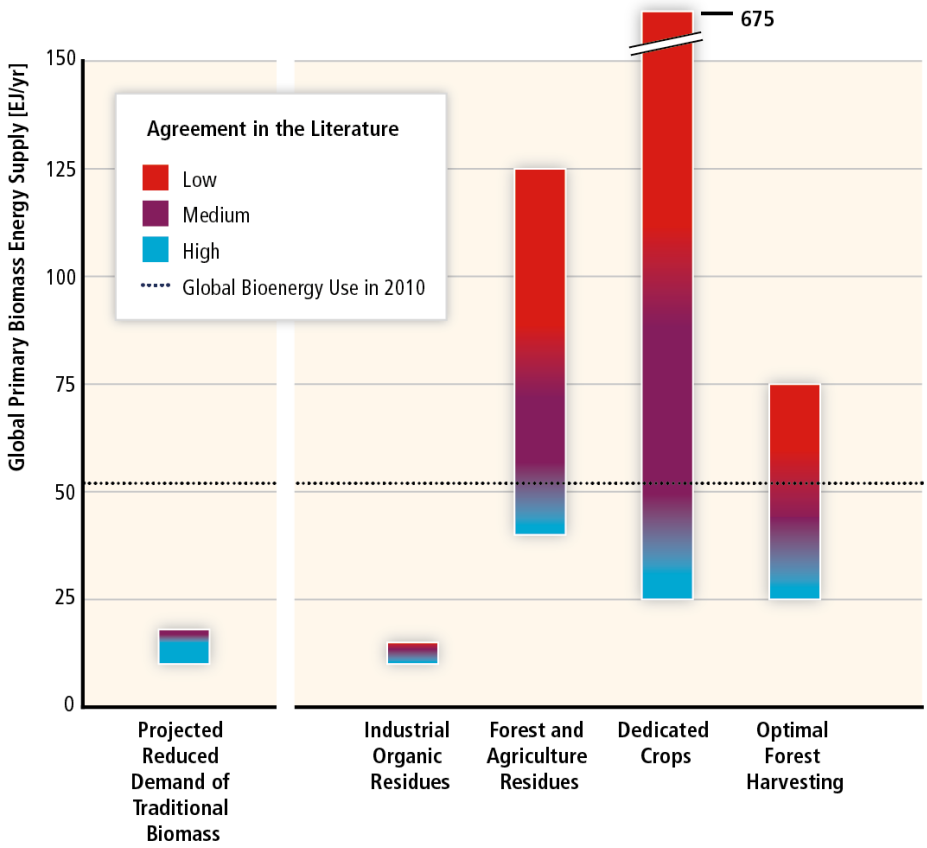

Figure 1.3: Estimate Global Technical Bioenergy Potentials by Resource (Blanco et al. 2014).

Dedicated crops are the most extensive range of estimates of technical bioenergy potential in 2050. Dedicated biomass yields include perennial grasses (miscanthus and switchgrass) and annual (sugar, cereals and oil crops). Generally, the potentials are calculated through the product of the area available for energy crops by the yield per unit area and year. There is a broad consensus that sustainable solutions lean towards conservative policies for implementation

focused on the rational management of impacts on water systems, multifunctional land use, and land-use zoning approaches, among others (Blanco et al. 2014).

Some bioenergy schemes suffer losses of biosphere C. In some cases, the annual savings of GHG obtained by the replacement of fossil fuels are surpassed a hundred times by these schemes. When a dynamic baseline takes into account future trends in global agricultural land use, impacts can significantly be reduced. Positive effects from Land Use Change (LUC), on a smaller scale, have also been observed, for example, when crops grow on carbon-poor soils or grown with high levels of fertilizers and are replaced by semi-perennial crops, perennial grasses or woody plants. In particular, Miscanthus has excellent performance at reducing overall GHG emissions and recover soil organic carbon. Successional perennial crops have grown, over a period of 20 years, in degraded USA areas for economic agriculture avoiding the initial carbon debt costs and indirect costs of land use related with food-based biofuels (Smith et al. 2014; Gibbs et al., 2008; Chum et al., 2011; Kløverpris and Mueller, 2013; Tilman et al., 2006; Harper et al., 2010; Sterner and Fritsche, 2011; Sochacki et al., 2012; Brandão et al., 2011; Gelfand et al., 2013).

There are advantages and disadvantages in the increased removal of biomass in long term rotation forests. Positive overall mitigation effects happen when most of a forest is used as a feedstock for bioenergy, sequestering carbon in soil throughout harvest cycles, particularly in younger forests. In general, there are positive benefits when using feedstock for bioenergy that is easy to decompose. On the contrary, slow decomposing feedstock reduces the accumulation of carbon on soil resulting in net emissions. To increase forest carbon stocks, it is essential to anticipate future bioenergy markets that promotes optimized management practices or establish managed plantations on marginal lands (Smith et al. 2014; Cherubini et al., 2012; Daigneault et al.,

2012; Ximenes et al., 2012; Lamers and Junginger, 2013; Latta et al., 2013; Zanchi et al., 2012; Repo et al., 2011; Sedjo and Tian, 2012).

Cellulosic biomass has the potential to produce bioethanol with relatively low carbon content when avoiding indirect Land Use Change (iLUC). For instance, comprehensive national land management strategies can be developed for the sustainable plantation of Miscanthus to provide fuel for land transport. Although uncertainty exists when quantifying iLUC it has been shown that high-yield bioenergy crops could diminish their effects (Smith et al. 2014; Dornburg et al., 2010; Scown et al., 2012; Van Dam et al., 2009; b; Wicke et al., 2009; Fischer et al., 2010; de Wit et al., 2011, 2013; van der Hilst et al., 2012; Rose et al., 2013).

The estimated bioenergy contribution to primary global energy supply by 2050 is 50% (80-190 EJ/yr) on the two mitigation levels modeled in the Special Report on Renewable Energy Sources and Climate Change (SRREN) scenarios. Similarly, the Global Energy Assessment (GEA, 2012) estimated 80-140 EJ by 2050, considering extensive use of second-generation feedstock and agriculture, to compensate co-processing of biomass with natural gas or coil in carbon dioxide capture and storage, and the adverse impacts of food production and land use (Smith et al. 2014; IPCC, 2011; GEA, 2012).

There is broad agreement about the restoring benefits in degraded lands from ecosystem services and perennial crops plantation. The positive effects include erosion control, agroforestry systems, improvement of water retention, and precipitation at the regional scale. Nevertheless, changing management practices may shift the net GHG equilibrium and obtain efficient, sustainable implications (Smith et al. 2014; Faaij, 2006; Wicke et al., 2011; Immerzeel et al., 2013; Davis et al., 2013).

Integrated models on land, food, water and biodiversity that simulates future bioenergy supply depend on the relationship between: (1) Bioenergy production and food-fiber production; (2) The scale of bioenergy output from waste and residues, or at least lessen competitiveness in land use; (3) The potential in which biomass can be planted in areas that currently harvest some, or could harvest in the future; and (4) The yield and volume of biomass. Biomass yields may vary due to variances in natural fertility, crop type, prior land use, management, and technology. Assumptions on energy crop yields mainly cause differences in future demand for energy crops. Similarly, significant implications for evaluating the degree of land competition between biofuels and these land uses are derived from assumptions about yields, management and policies on forthcoming food/feed crops (Smith et al. 2014; Rogner et al., 2012; Garg et al., 2011; Sochacki et al., 2013; Berndes et al., 2013; Nijsen et al., 2012; Haberl et al., 2010; Batidzirai and Faaij, 2012; Smith et al., 2012a; Johnston et al., 2009; Lal, 2010; Beringer et al., 2011; Pacca and Moreira, 2011; Smith et al., 2012b; Erb et al., 2012a; Popp et al., 2013; Batidzirai et al., 2012; De Wit et al., 2013).

Nevertheless, there are different versions of potential landscape transformation in all regions among models. Systematizing the effects of mitigation on regional land cover is a complicated task. While some models consider significant land change, others do not. In perfect scenarios, many regions exhibit growth of energy cropland and forest land by 2030. However, some models show substantial expansions while others not so much. Land change scenarios increased ranges from 450 ppm in comparison to the 550 ppm scenarios. However, there is a declining share. These results are consistent with the declining land-related mitigation rate with policy stringency (Smith et al., 2014).

The production of bioenergy from crops at large scale may have an impact on water quality and availability since feedstock depends on the type quality and quantity of local freshwater resources, and compete with other the usage of agricultural, urban, industrial and power generation of that region. Existing pressures on water resources could also be further intensified with the irrigation of energy crops. Excluding areas with severe water-scarce for bioenergy production would decrease the global technical bioenergy potential by 17% until 2050 (Smith et al. 2014; Gerbens-Leenes et al., 2009; Coelho et al., 2012; Popp et al., 2011; Van Vuuren et al., 2009).

With an aim to mitigate climate change, the prices of global food may be affected if the production of bioenergy feedstock requires extra land that would displace food production. However, effective and sustainable land-use planning in large bioenergy projects reduces the economic and environmental risks by minimizing water competition. Land-use change may pressure biodiversity if bioenergy production is not managed correctly. Nevertheless, the establishment of bioenergy crops in marginal lands with appropriate agricultural management brings an excellent opportunity to achieve positive environmental and economic outcomes (Smith et al. 2014; Groom et al., 2008; Nijsen et al., 2012)

1.3 Optimal Allocation Design in Land-Use and Land-Cover Changes

In order to optimize the production of biofuel feedstock, it is necessary to quantify the impacts of Land-Use and Land-Cover changes. In this context, all possible Land-Use and Land-Cover changes combinations must be evaluated to determine the optimal settings that yield better environmental performance. For instance, consider the field in figure 1.4. If the aim is to determine the optimal Land-Cover change for biofuel feedstock production considering replacing the

regional crops for switchgrass or miscanthus, then both Land-Cover changes must be evaluated separately to find the crop that yields better environmental performance.

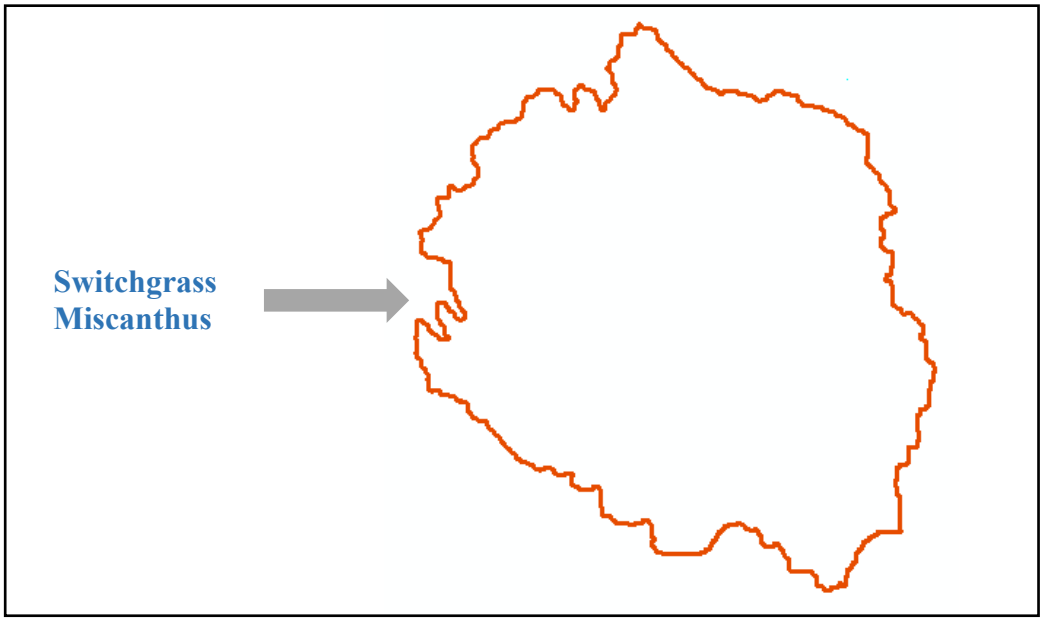

Figure 1.4: Land-Cover change combinations

However, changing the land cover for switchgrass or miscanthus might not be the optimal settings for the best environmental performance. Perhaps, changing the land cover for switchgrass on one side of the field and miscanthus on the other side of the field yields better environmental performance. Furthermore, additional Land-Use must be considered. For instance, the application of 30 kgs of fertilizer. In this example, consider figure 1.5. Under these conditions, four different combinations must be evaluated separately to determine the optimal settings that yield better environmental performance.

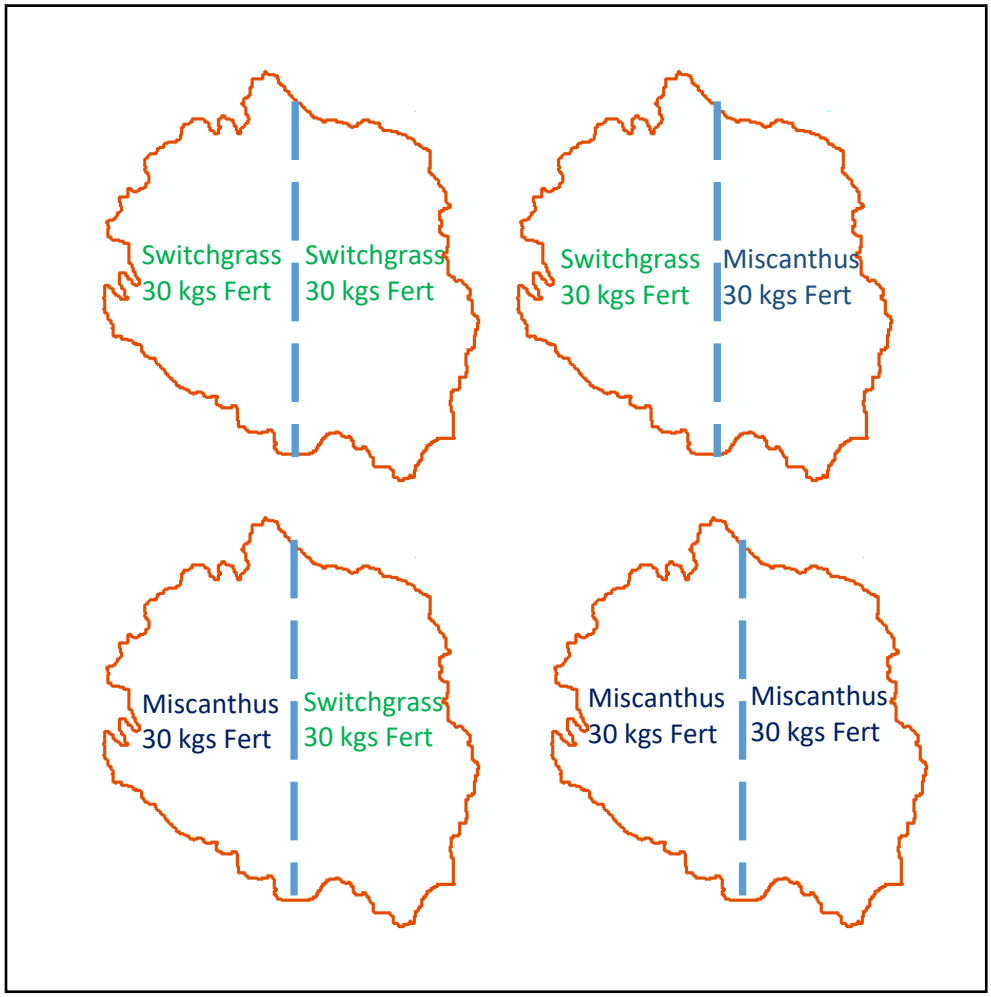

Figure 1.5: Possible Land-Cover combinations with two management practices and two fields.

As the number of management practices increases, also, the number of combinations increase. For instance, when there are two fields and four management practices, the total possible combinations that must be evaluated to obtain the optimal setting that yields better environmental performances increases to 16. If the number of management practices increases to six, the total possible combinations also increase to 36.

Similarly, when the number of fields increases, the total possible combinations that must be evaluated also increase. Consider figure 1.6. In this example, the field is divided into four sections. Under these conditions, when two different management practices, a total of 16 different

combinations must be evaluated to determine the optimal settings that yield better environmental performance.

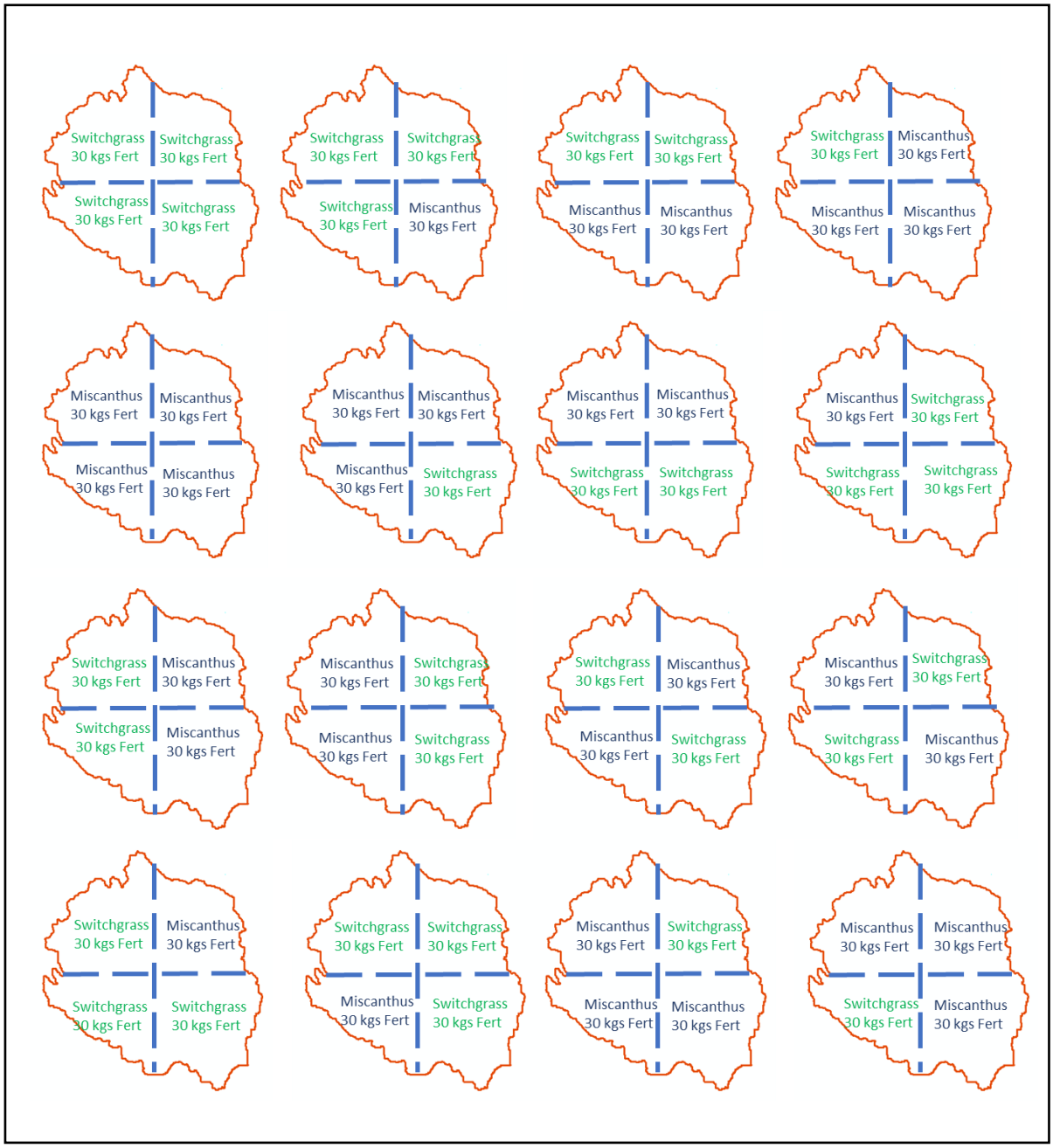

Figure 1.6: Possible Land-Cover combinations with two management practices and four fields

Similarly, as the number of management practices increases, also, the number of combinations increases. For instance, when there are four fields and four management practices, the total possible combinations that must be evaluated to obtain the optimal setting that yields

better environmental performances increases to 256. If the number of management practices increases to six, the total possible combinations also increase to 1,296.

Mathematically, this can be modeled as:

$$Total\ number\ of\ combinations = Number\ of\ management\ practices^{Number\ of\ fields} \quad \text{(Eq. 1.1)}$$

Using this mathematical model, we can determine the total number of combinations that should be evaluated to obtain the optimal settings that yield better environmental performance. For instance, when there are six different management practices and 24 different fields, the total combinations that would have to be evaluated is 4,738,381,338,321,616,896. Therefore, this problem is unfeasible to solve and becomes an NP-Hard problem. However, we can address this problem by using metaheuristic optimization involving several conflicting objectives to obtain a near-optimal solution. Different Multi-optimization methodologies are later explained in chapter 5.

1.4 Chapter Conclusions

In this chapter, the importance of creating and using biofuels was established, supported with the political efforts made to increase the production of clean, renewable fuels which coincides with the latest scientific findings on biofuel production, Land-Use, and Land-Cover changes and climate change.

The mathematical process to obtain the total number of combinations to determine the optimal Land-Use and Land-Cover change design for the production of biofuel feedstock was explained, and it was concluded that as the number of management practices and the number of fields increase, the problem is unfeasible to solve. The following chapter will present how different authors, in literature, have used simulation models to address different assessments and how some have used metaheuristic optimization in their studies.

Chapter 2: Literature Review

This chapter is dedicated to reviewing the studies that approach metaheuristic optimization in hydrologic simulation and life cycle assessment to obtain the best system performance. Some of these authors have coupled simulation models to Multi-objective evolutionary algorithms involving several conflicting objectives to obtain a near-optimal solution

2.1 Literature Review

In an attempt to optimize the performance of hydrologic simulation models, many researchers have applied and coupled Evolutionary Algorithms with the Soil and Water Assessment Tool (SWAT). Among the optimization tools that have been developed include calibrating genetic algorithms. For instance, Ercan et al. (2016) employed a Non-Dominated Genetic Algorithm II (NSGA-II) to create an open-source software library for multi-objective calibration of SWAT models. The developed library was demonstrated using six objective functions on the Upper Neuse Watershed in North Carolina, USA. Zhang et al. (2013a) employed a Python-based parallel computing set, PP-SWAT to run simultaneously a multi-method Genetically Adaptive Multi-Objective Optimization Algorithm (AMALGAM) addressing multiple objectives for efficient calibration of SWAT. The PP-SWAT efficiency includes multiple parameter adjustment schemes that can be selected by the user for model preference, working on different scales and in a reasonable time. However, PP-SWAT does not intend to address model structure errors. Similarly, Confesor et al. (2007) applied a multi-objective evolutionary algorithm (MOEA) with Pareto optimization to automatically calibrate the daily streamflow of the Calapooia watershed in SWAT. In order to determine the Pareto optimal set, the nondominated sorting genetic algorithm II (NSGA-II) and SWAT were called from a parallel genetic algorithm in FORTRAN. The optimized calibration considered a total of 139 parameter values simultaneously.

Alternatively, Ki et al. (2015) developed a method to optimize the execution of SWAT by recompiling the source code (rev 622) with non-commercial Intel FORTRAN compiler in Ubuntu 12.04 LTS Linux Plata accelerating a single SWAT run when using a large number of hydrological response units.

Others have improved SWAT's performance by developing extensions to the model during dry and wet seasons. For example, Zhang et al. (2015) developed an extended SWAT model to improve performance during the dry season. The proposed model calibrated separately, for dry and wet periods, and the resulting optimal solutions for each period were combined into a runoff series. The outputs of the proposed model were compared to those outputs by the original SWAT in the Jinjiang watershed, which is typically a subtropical monsoon climate in China. On the other hand, Hejazi et al. (2008) used a multi-objective genetic algorithm (NSGA-II) to calibrate storm-event distributed hydrologic model which impacts watershed runoff by reservoir release and storage. In order to find the objective function that would result in better calibration and the neglected human interface error in reservoir released or the inaccurate storage-release function that would affect calibration, reservoirs release determined by the hydraulic structure and adding reservoir release were evaluated and compared. In terms of spatial distribution and parameter values robustness, the calibration procedure that considered human interface resulted in better modeling and observed hydrograph.

Recent articles have made improvements for the prediction in hydrologic models at the watershed level by developing sub-models linking SWAT with various databases. Wagena et al. (2017) developed a new physically based routine for SWAT, which quantifies N_2O emissions from agroecosystems. An existing nitrification routine was modified to predict and capture N_2O flux during denitrification during the process. The emissions were predicted by coupling the carbon

(C), and nitrogen (N) cycles with the PH and soil moisture/temperature in SWAT. The modified SWAT uses reduction functions to predict total denitrification (N_2+ N_2O) and partitions N_2 from N_2O. Similarly, improvements for the prediction of the model have been achieved through the application of algorithms and regression models. Noori et al. (2016) coupled SWAT and artificial neural network (ANN) to improve daily flow predictions on watersheds. The hybrid model integrated a quasi- distributed watershed model and an artificial neural network (ANN) to improve daily flow prediction in unmonitored watersheds. Leave one side out jackknifing techniques were employed to obtain streamflow data from 29 watersheds near the city of Atlanta, the United States and the information were used to build the predictive flow models during warm and cool seasons. SWAT was first used to simulate daily streamflow, and the baseflow and stormflow simulation by SWAT were used as inputs for the ANN. On the other hand, Bucak et al. (2017) developed an integrated modeling approach by linking SWAT with a Support Vector Regression model (ε-SVR) to predict the future water levels of Lake Beysehir which can be impacted by climate change and land use.

Those who have coupled SWAT with other models created controlled tools to optimize land use and management practices. A new approach for land use optimization to non-point source pollution control was developed by Zhang et al. (2013b). Pollution loads were simulated under different land-use scenarios in the upstream watershed in Beijing, China by coupling SWAT and the Conversion of Land Use and its Effect at Small regional extent (CLUE-S). Similarly, SWAT and the Water Evaluation And Planning system (WEAP) were combined to design demand-side measures for the urban, tourism, industrial and agricultural sectors to improve water management in the rural upstream sub-catchment of the Pinios river basin which suffers from water shortages attributed to crop irrigation practices (Psomas et al, 2016). Pai et al. (2012) developed a graphical

user interface (GUI) to map SWAT simulations using spatial and non-spatial SWAT outputs. The GUI generates the maps from the HRU layer to a field boundary layer defined by the user assisting field scale visualization through four different aggregation methods. This interface could benefit the communication between model outputs and watershed managers or target conservation practices on a field-scale.

Optimization controlled models that associates SWAT with other simulation models have also been developed to minimize cost using best management practices while preserving water quality. Cools et al. (2011) presented a modeling approach to find the most suitable set of reduction measures, in terms of cost-effectiveness, to achieve an in-stream concentration target. The model was developed by coupling SWAT, and the Environmental Costing Model (ECM) associating the modeled in-stream concentration to the corresponding emission reduction and marginally decreased cost curves for substances that demand oxygen and nutrients. The results indicated that the most effective measures are winter cover crops, dairy cattle, tuned fertilization, among others. In the same way, Arabi et al. (2006) presented a genetic algorithm-based spatial search procedure in combination with SWAT to optimize the selection and placement of best management practices in terms of cost-effectiveness, reducing sediment, phosphorus, and nitrogen monthly loads. The model was tested using two small watersheds in the Midwest portion of the United States. The main objective was to significantly reduce the cost of commonly used strategies while meeting water quality goals.

Different studies have employed other hydrological models to find best land use allocations using modern heuristic optimization techniques to minimize sediment yields and nutrient concentrations considering operation and implementation cost maximizing the benefits from agricultural exploitation and water quality. A new approach based on a randomized adaptive Tabu

search heuristic to find an optimum combination of land use allocation was developed by coupling the runoff model AnnAGNPS and the channel network model CCHE1D. The proposed optimal land use planning showed improvements on the tradeoffs between costs and benefits for an experimental watershed located in northern Mississippi (Qi and Altinakar, 2011). Also, Chichakly et al. (2013) developed an integrated method for stormwater best management practices for watersheds. The approach is based on a multi-scale, multi-objective framework where the non-dominated solutions concerning the management plan implementation cost and sediment loading are pruned regarding sensitivity dominance to anticipate fluctuations in precipitation patterns. Optimal cost best management practices were precomputed using Geographic Information Systems (GIS). Each solution was formulated as a real-value vector of treatment level and applied a multi-objective optimization technique based on differential evolution to create nondominated solution sets. The optimal solutions were added to the preoptimized best management practice map.

Including environmental impacts in feasibility, analyses are crucial to improve sustainable living practices. Several studies that have been published in the peer-reviewed literature describing applications of LCA methodologies with optimization frameworks are described by Pieragostini et al. (2012) offering a state-of-the-art in optimization methodologies and tools based on Life Cycle Assessment (LCA). For instance, Azapagic and Clift (1999a, 1999b) used a cradle to gate approach and employed the methodology by Heijungs et al. (1992). The best possible routes for environmental management of the product was identified through a multi-objective-Pareto system which was executed using Xpress MP. Furthermore, Using Eco-indicator 99 Hugo and Pistikopoulos (2005) presented a methodology for the explicit inclusion of LCA principals as part of investment decisions associated with supplying chain networks. The mathematical framework

included a Multi-Objective Mixed Integer Linear Programming and a Multi-period/parameter optimization. Also, Tan (2004) developed a software model for the comparison of 10 different GREET fuel-cycle inventory enhanced with probabilistic uncertainty propagation (PUP) and probabilistic compromise programming (PCP) features. The proposed model called POLCAGE 1.0 (possibilistic LCA using GREET and EDIP) was coded in Visual Basic and Microsoft Excel. The model was later used as an alternative approach to the work of Azapagic and Clift in 1999, applying a Zimmermann's symmetric fuzzy linear programming method to produce a single optimal solution (Tan, 2005).

In order to minimize the overall environmental impact of the operating conditions of an ethylene process utility plant, Eliceche et al. (2007) used a cradle-to-gate approach applying the methodology of Heijungs et al. (1992) and a Waste Reduction (WAR) algorithm. The mathematical formulation employed was a Mixed Integer Nonlinear Programming (MINLP) computed on CONOPT and OSL/Generalized Algebraic Modeling System (GAMS). Guillén-Gosálbez et al. (2008) developed an optimal design of chemical processes by coupling mixed-integer modeling techniques with environmental concerns based on LCA. The methodology of the design considered the Eco-indicator 99, which was executed in SimaPro. Similarly, Zhou et al. (2009) developed a cradle-to-grave LCA tool which optimizes multi-objective of material selection by combining artificial neural networks (ANN) with genetic algorithms. The environmental impacts were computed in SimaPro using Eco-indicator99.

Others have applied these techniques for the optimization of supply chains to minimize environmental impacts or maximize profits. Bojarski et al. (2009) considered economic and environmental issues by optimizing the planning and design of the supply chain. The LCA was performed with IMPACT 2002+. The results were used to create impact maps with compromising

supply chain activities and nodes. The objective of such maps was to identify and invest in the most promising subject to reduce environmental burdens. A multi-objective MILP was the mathematical formulation using Pareto and weight sum method. Net present value, damage categories impact, and overall impact factor as the objective function. Pinto-Varela et al. (2010) developed a model for planning and design of supply chain structures to maximize annual profits and minimize environmental impacts. In order to quantify the damage to human health, the Eco-indicator was employed while the profits and environmental impacts were evaluated through the use of an adapted symmetric fuzzy linear programming (SFLP). Lastly, the methodology employed for the supply chain was the Resource-TaskNetwork (RTN) modeled with mixed-integer linear programming (MILP) optimization problem. Similarly, Luz Santos and Legey (2010) associated a cradle-to-gate LCA for hydro/thermal plants and a mixed-integer linear programming model to minimize investment, operation, and environmental costs. The methodologies employed for the proposed model were ExtrenE project and CAAGE EGHT, which was executed in Xpress-MP.

Different studies have also applied optimization techniques seeking to improve the performance of energy systems in ecological terms. For instance, Carvalho et al. (2011) implemented a cradle-to-gate approach for energy systems. SimaPRO LINGO was employed to minimize environmental impacts related to production equipment and consumption resources. The methodology based on a Mixed Integer Linear Programming (MILP) couples with the information obtained through the LCA performed. The objective function considered the Eco-indicator 99 Single Score and CO_2 emissions as well as energy price, resources and compensation possibilities from selling surplus electricity to the electric grid. Furthermore, Gebreslassie et al. (2010) presented a decision support tool which includes a cradle-to-gate approach for the design of solar

assisted absorption cooling systems. The mathematical framework is based on a bi-criteria mixed-integer nonlinear programming (MINLP) optimization problem and Pareto/ε-c M. The optimization considers the minimization of environmental impacts over the entire life cycle and associated total cost for cooling systems. The methodology follows the Eco-indicator 99, and the simulation models include TRNSYS DICOPT, SNOPT, and CPLEX/GAMS. Similarly, Liu et al. (2010) presented an optimal design control tool for various energy technology alternatives to improve environmental performance and energy efficiency. The mathematical formulation is based on a mixed-integer optimization technique for energy systems design problem with a Pareto/ε-c M as the solution strategy to simultaneously optimize economic and environmental criteria. Also, Pietrapertosa et al. (2009) proposed an analytical methodology to evaluate energy system associating LCA, ExternE, and Comprehensive Analysis. The mathematical formulation followed a Multi-Period Linear Programming and computed in GEMIS and MARKAL.

2.2 CHAPTER CONCLUSIONS

In this chapter, some studies that have used different optimization techniques in hydrologic simulation and Life Cycle Assessment Models were presented. However, very little literature regarding the optimization in Land-Use and Land-Cover changes for biofuel feedstock production was found. Therefore, there is a vast opportunity to create and expand these studies. In the next chapter, the hydrologic simulation model, SWAT, will be introduced.

Chapter 3: Soil and Water Assessment Tool

This chapter is dedicated to introducing the Soil and Water Assessment Tool model (SWAT). The focus is to provide an overview of the methods used to measure or calculate the hydrologic simulation process for the input parameters.

3.1 SWAT

Developed by the United States Department of Agriculture (USDA) Agricultural Research Services (ARS), the Soil and Water Assessment Tool (SWAT) is a useful tool for evaluating water re-source and nonpoint pollution problems at the watershed scale, for a broad range of environmental conditions worldwide. The model is the result of almost 30 years of efforts and has been used by several U.S. federal agencies, including the USDA within the Conservation Effects Assessment Project (CEAP) and the U.S. Environmental Protection Agency (USEPA). SWAT has gained international acceptance and, as previously mentioned, it has been used in numerous peer-reviewed journals for hydrological analysis, pollutant load assessments, comparisons with other models, streamflow calibration and different optimization studies (Gassman et al. 2007).

SWAT is a physically-based, basin-scale simulation model which can run continuously over long-time periods. Its primary purpose is to predict the effects of agricultural management practices on water, sediment, and chemical yields in watersheds. It requires specific weather and hydrology data, soil properties and temperature, plant growth nutrient parameters, and land management practices (Gassman et al. 2007).

When a watershed is defined, SWAT divides it into multiple sub-basins. Sub-basins are located in a specific geographical location in the watershed and are spatially connected. The sub-basin can be delineated in two ways: (1) From boundaries defined by surface topography so that the total sub-basin area flows towards the sub-basin outlet; or (2) From grid cell boundaries. Grid

cells are often attractive to use because most spatial inputs are grid-based, such as Digital Elevation Model (DEM), Next-Generation Radar (NEXRAD) and Land Use/Land Cover (LULC). However, they do not retain topographic stream paths and routing reaches (Arnold et al. 2012).

Sub-basins are further subdivided into particular land use, management, and soil characteristics called, Hydrologic Response Units (HRUs), and will contain at least one HRU, a stream channel and the main channel or reach. Also, a pond and wetland can be included within a sub-basin (Arnold et al. 2012).

Rather than a field, HRUs imply the total sub-basin area with unique land use, management, and soil. While individual fields with specific characteristics are scattered throughout the sub-basin, these areas are grouped considering similarities to create HRUs. This SWAT feature is convenient in simulating since it is faster to execute similar land use and soil areas than individual fields (Arnold et al. 2012).

Since HRUs do not interact with sub-basins, loadings from each HRUs are evaluated separately and then added together to define the loadings from the sub-basin. The spatial relationship is specified at the sub-basin level. For instance, if the land use area has significant interaction with another, it is defined as sub-basin, rather than as an HRU (Arnold et al. 2012).

HRUs increases the accuracy in the prediction of loadings from the sub-basin. The growth behavior of plants significantly varies among species. The net amount of incoming runoff to the main channel is more precise when the diversity in plant cover is considered (Arnold et al. 2012).

In order to increase the complexity of the dataset, a higher number of sub-basins in the watershed should be defined when configuring the SWAT model, rather than increasing the number of HRUs. In many cases, 1-10 HRUs is recommended for a given sub-basin (Arnold et al. 2012).

The main channel in the watershed is associated with each sub-basin. Loadings and outflow from the upstream enter the main channel of the watershed from the sub-basin into the related reach segment(s) (Arnold et al. 2012).

Tributary channels distinguish inputs for the channelized flow of surface runoff produced in a sub-basin. These channels estimate the time concentrations flow to the main channel produced in the sub-basin and transmission losses from runoff. Its inputs define the sub-basin longest flow path, which in some cases would be the main channel. If so, both dimensions, tributary channel and main channel, will be the same. However, in other sub-basins, their dimensions will be significantly different from each other (Arnold et al. 2012).

The interfaces in Geographic Information System (GIS) allow HRUs to be created with water as the land use, to process United States Geological Surveys (USGS) land use maps. This, however, should be avoided if possible. Modeling water bodies should be done, representing ponds, wetlands, or reservoirs (Arnold et al. 2012).

Reservoirs are commonly used for lakes for naturally occurring water bodies that have been altered or influenced by man. However, SWAT does not refer to reservoirs as human-made water bodies. Instead, they are modeled on the stream network of the watershed. Also, differences in size between impoundments on and off the main channel network need to be addressed. Because on the main channel, impoundments tend to be larger, different file extensions store inputs. This way, both pond and wetlands may be defined within each sub-basin. These impoundments cannot receive water from other sub-basins; therefore, water is created in the sub-basin. On the other hand, all upstream sub-basins water contributed to the channel network can supply to reservoirs. (Arnold et al. 2012).

Loading of water, sediment, and nutrients from land regions in watersheds are directly modeled by SWAT. Nevertheless, sources not associated with land regions may contribute to loadings to the stream network in some watersheds. These are called point sources. A sewage treatment plant is the most common point source in SWAT. Users are allowed to include daily or average daily loadings from a point source to the main channel. Both loadings from point sources and loadings created by land areas are routed through the channel network. Access to sub-basin maps can happen depending on the interface being used. For instance, GIS interface produces the maps to get a clear view of the spatial relationship between sub-basins. On the other hand, when using the Windows interface, the user must use drag/drop objects and connecting arrows to set up the spatial position of sub-basins and to show flow direction. SWAT does not have access to maps or displays, but it uses the information from the configuration files (.fig) to connect sub-basins and the watershed. (Arnold et al. 2019).

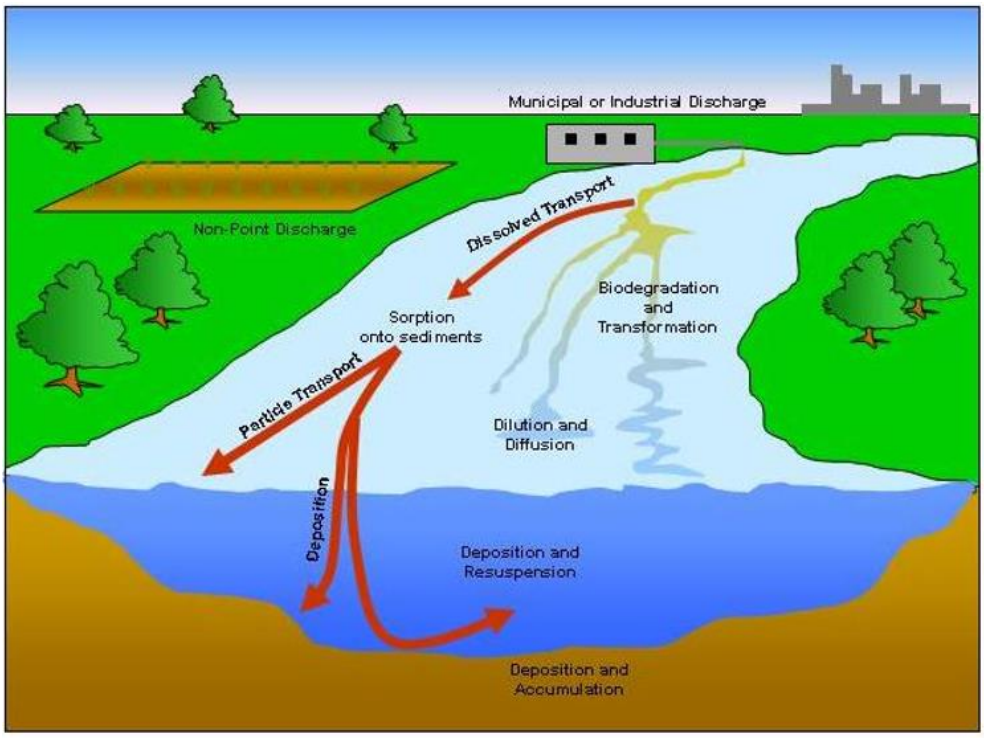

Figure 3.1: In-stream processes modeled by SWAT (Neitsch et al., 2011).

Regardless of the complexity of the problem assessed with SWAT, the driving force of how everything works in the watershed is water balance. The accurate prediction of pesticide and nutrients movements and sediments relies on the quality of hydrologic cycle simulation and how close it mimics the process of the watershed. The hydrology simulation of a watershed can be separated into two main components, land phase, and routing phase. The hydrologic cycle in land phase controls loading amounts of water, sediment, nutrient, and pesticide to the main channel in every sub-basin. The hydrologic cycle in the routing phase is defined as the movement of water, sediment, nutrients, etc. over the channel network to the outlet of the watershed (Neitsch et al., 2011).

The water balance equation used by SWAT to simulate the hydrologic cycle follows:

$$SW_t = SW_0 + \sum_{i=1}^{t}\left(R_{day} - Q_{surf} - E_a - w_{seep} - Q_{gw}\right) \qquad \text{(Eq. 3.1)}$$

where SW_t is the total soil water content (mm H_2O), SW_0 is the initial soil water content on day i (mm H_2O), t is the time (days), R_{day} is the amount of precipitation on day i (mm H_2O), Q_{swf} is the amount of surface runoff on day i (mm H_2O), E_a is the amount of evapotranspiration on day i (mm H_2O), W_{seep} is the amount of incoming water to the vadose zone coming from the soil profile on day i (mm H_2O), and Q_{gw} is the return flow amount on day i (mm H_2O) (Neitsch et al., 2011).

The model reflects differences in evapotranspiration for various crops and soils through the subdivision of the watershed. Runoff is estimated for every HRU separately, and it is routed to acquire the total runoff for the watershed (Neitsch et al., 2011).

The flow that occurs along a sloping surface is known as surface runoff or overland flow. It happens whenever the ground surface water application is higher than the rate of infiltration. Surface depression starts to fill when the application rate exceeds the infiltration rate. Furthermore,

if the application rate remains higher until all surface depression has filled, then surface runoff will start (Neitsch et al., 2011).

SWAT simulates surface runoff volumes and peak runoff rates for every HRU using daily or sub-daily rainfall amounts. In order to calculate surface runoff, SWAT uses an adjusted SCS curve number method (USDA Soil Conservation Service, 1972) or the Green & Amp infiltration method (Green and Ampt, 1911).

The SCS runoff equation became popular after more than 20 years of studies involving the relationship between rainfall and runoff from small rural watersheds across the U.S., in the 1950s. The empirical model was developed to calculate the amount of runoff under different land use and soil types (Rallison and Miller, 1981).

The following equation represents the SCS curve number (SCS, 1972):

$$Q_{surf} = \frac{(R_{day} - I_a)^2}{R_{day} - I_a + S)} \quad \text{(Eq. 3.2)}$$

where Q_{surf} is the accumulated runoff or rainfall excess (mm H2O), R_{day} is the rainfall depth for the day (mmH_2O), I_a is the initial abstractions including surface storage, interception and infiltration before runoff (mmH_2O), and *S*, the retention parameter (mmH_2O). Spatial variations in the retention parameter can happen due to changes in soils, land use, slope, management, and changes in soil water content. The retention parameter is defined as follows:

$$S = 25.4\left(\frac{1000}{CN} - 10\right) \quad \text{(Eq. 3.3)}$$

Where *CN* is the curve number for the day. Commonly, the initial abstractions I_a, approximates as 0.2S. Therefore, equation 3.2 becomes:

$$Q_{surf} = \frac{\left(R_{day} - 0.2S\right)^2}{R_{day} + 0.8S)} \quad \text{(Eq. 3.4)}$$

Figure 3.2 displays the different curve number values with the relationship between runoff and rainfall. Notice that Runoff only occurs when $R_{day} > I_a$.

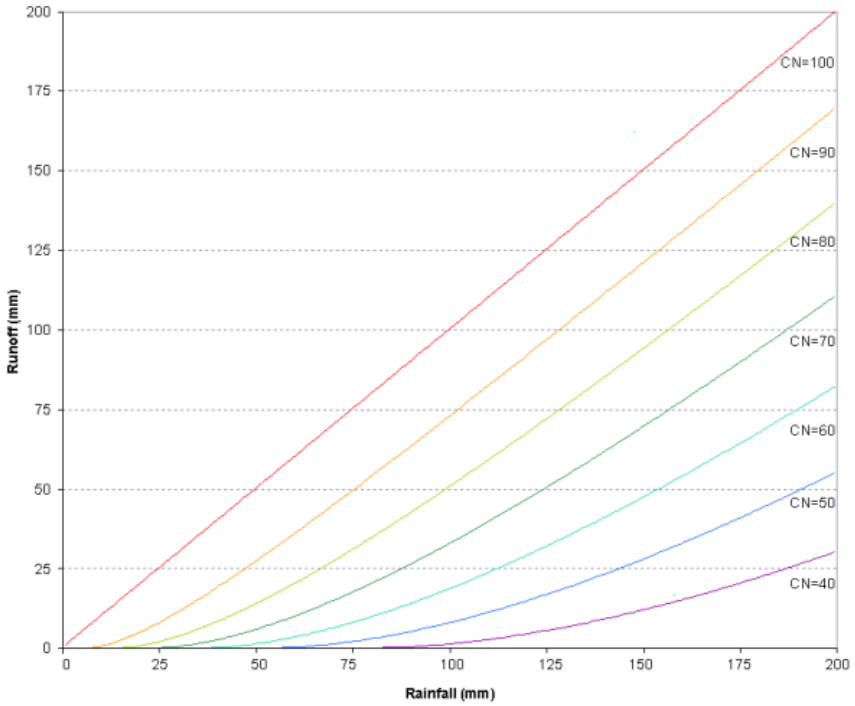

Figure 3.2: Relationship of runoff to rainfall in the SCS curve number method (Neitsch et al., 2011).

Erosion is the action caused by water flow or wind that take away soil, rocks, or dissolved organic matter from one location to another (Neitsch et al., 2011).

When raindrop impact land areas, containing rills and channels, soil particles on unprotected land surfaces can be detached and transported to the rills. The particles move from the small rills into larger rills, later into passing channels ending in continuously flowing rivers. Erosion can occur with or without human influence. When human influence is not involved, it is known as geological erosion. However, accelerated erosion occurs when the rate of erosion increases by the influence of human activity (Neitsch et al., 2011).

Erosion can have significant impacts on natural resources and watersheds. Water supply and flood control are the main reasons why reservoirs are built. When erosion occurs upstream of

a reservoir, the water holding capacity decreases as sediment settles at the bottom of the reservoir. Also, the highest profiles in organic matter and nutrients are found at the soil surface. Soil reserves of nitrogen and phosphorus, needed by plants to grow, are depleted by excessive erosion degrading the soil until plant life is unbearable. Water balance of a watershed change when erosion is severe since it increases the amount of water lost to evapotranspiration (Neitsch et al., 2011).

In order to calculate the erosion caused by rainfall and runoff, SWAT utilizes the Modified Universal Soil Equation (MUSLE)(Williams, 1975). The MUSLE is defined as follows:

$$sed = 11.8(Q_{surf} \times q_{peak} \times area_{hru})^{0.56} \times K_{USLE} \times C_{USLE} \times P_{USLE} \times LS_{USLE} \times CFRG \quad \text{(Eq. 3.5)}$$

where *sed* is the sediment yield (metric tons) on a given day, Q_{surf} is the surface runoff volume (mm H2O/ha), q_{peak} is the peak runoff rate (m3/s), $area_{hru}$ is the area of the HRU (ha), K_{USLE} is the USLE soil erodibility factor (0.0013 metric ton m2 hr/(m 3-metric ton cm)), C_{USLE} is the USLE cover and management factor, P_{USLE} is the USLE support practice factor, LS_{USLE} is the USLE topographic factor, and $CFRG$ is the coarse fragment factor (Neitsch et al., 2011).

3.2 NITRATE TRANSPORT

When surface runoff, lateral flow or percolation happen, nitrate in soil surface may be transported. In order to estimate the nitrate quantity moved with water, the nitrate concentration in the moving water is evaluated. The mass of nitrate soil loss from the soil surface is obtained through the product of nitrate concentration and the volume of water moving in each pathway (Neitsch et al., 2011).

SWAT calculates the nitrate concentration in the mobile water with the following equation:

$$conc_{NO3,mobile} = \frac{NO3_{ly} \times \left\lfloor \frac{-w_{moile}}{(1-\theta_e) \times SAT_{ly}} \right\rfloor}{w_{mobile}} \quad \text{(Eq. 3.6)}$$

where $conc_{NO3,mobile}$ is the nitrate concentration in the mobile water for a specific layer (Kg N/mm H_2O), $NO3_{ly}$ is the nitrate quantity in the layer (kg N/ha), w_{mobile} is the moving water quantity in the layer (mm H_2O). The quantity of water lost by surface runoff, filtration, or lateral flow is equal to the quantity of mobile water in the layer:

$$w_{mobile} = Q_{surf} + Q_{lat,ly} + w_{perc,ly} \qquad for\ top\ 10\ mm \qquad \text{(Eq. 3.7)}$$

$$w_{mobile} = Q_{lat,ly} + w_{perc,ly} \qquad for\ lower\ soil\ layers \qquad \text{(Eq. 3.8)}$$

where w_{mobile} is the quantity of water moving in the layer (mm H_2O), Q_{surf} is the surface runoff produced on a particular day (mm H_2O), $Q_{lat,ly}$ is the layers' discharged water by lateral flow (mm H_2O), and $w_{perc,ly}$ is the quantity of infiltrating water to the underlying soil layer on a specific day (mm H_2O). Within the top 10 mm of soil, surface runoff, and transport of nutrients interact (Neitsch et al., 2011).

SWAT calculates the amount of nitrate removed in surface runoff with the following equation:

$$NO3_{surf} = \beta_{NO3} \times conc_{NO3,mobile} \times Q_{surf} \qquad \text{(Eq. 3.9)}$$

where $NO3_{surf}$ is the amount of nitrate removed in surface runoff (kg N/ha), β_{NO3} is the nitrate infiltration coefficient, $conc_{NO3,mobile}$ is the nitrate concentration of moving water for the top 10 mm of soil (kg N/mm H_2O), and Q_{surf} is the surface runoff produced in a particular day (mm H_2O). The nitrate infiltration coefficient can be defined by the user to establish the concentration of nitrate in surface runoff to a portion of the concentration in infiltration (Neitsch et al., 2011).

SWAT calculates the amount of nitrate removed in lateral flow with the following equations:

$$NO3_{lat,ly} = \beta_{NO3} \times conc_{NO3,mobile} \times Q_{lat,ly} \qquad for\ top\ 10\ mm \qquad \text{(Eq. 3.10)}$$

$$NO3_{lat,ly} = conc_{NO3,mobile} \times Q_{lat,ly} \qquad for\ lower\ layers \qquad \text{(Eq. 3.11)}$$

where $NO3_{lat,ly}$ is the amount removed of nitrate in lateral flow from layer (kg N/ha), β_{NO3} is the nitrate infiltration coefficient, $conc_{NO3,mobile}$ is the concentration of nitrate in the moving water for the layer (kg N/mm H_2O), and $Q_{lat,ly}$ is the layers' discharged water by lateral flow (mm H_2O) (Neitsch et al., 2011).

SWAT calculates the nitrate transported to the underlying layer by infiltration with the following equation:

$$NO3_{perc,ly} = conc_{NO3,mobile} \times w_{perc,ly} \quad \text{(Eq. 3.12)}$$

where $NO3_{perc,ly}$ is the amount of nitrate transported to the underlying layer by infiltration (kg N/h), $conc_{NO3,mobile}$ is the nitrate concentration in the moving water for the layer (kg N/mm H_2O), and $w_{perc,ly}$ is the quantity of infiltrated water to the underlying soil layer in a specific day (mm H_2O) (Neitsch et al., 2011).

3.3 Chapter Conclusions

In this chapter, the SWAT hydrologic simulation model was introduced. This model can be used to assess Land-Use and Land-Cover changes to analyze the environmental impacts on soil and water from the production of biofuel feedstock production at the watershed scale. The next chapter introduces the Greenhouse Gases, Regulated Emissions, and Energy Use in Transportation Model (GREET), which is a Life Cycle Assessment tool to quantify the greenhouse gas emissions in every stage of the process of different fuel technologies, including biofuel production.

Chapter 4: Greenhouse Gases, Regulated Emissions, and Energy Use in Transportation Model

This chapter is dedicated to introducing the Greenhouse Gases, Regulated Emissions, and Energy Use in Transportation Model (GREET) which is a Life Cycle Assessment model. The focus is to provide an overview of the methods used to quantify the greenhouse gas emissions associated with the production of different fuel technologies, in every cycle stage of the process.

4.1 GREET

The Argonne National Laboratory developed the Greenhouse Gases, Regulated Emissions, and Energy Use in Transportation Model (GREET) with support from the U.S. Department of Energy's (DOE's) Office of Energy Efficiency and Renewable Energy. It is an LCA tool available for the public and stakeholders to study several fuel and vehicle cycles. GREET considers the processes associated with producing and using fuels through the fuel-cycle model. Furthermore, the processes associated with manufacturing and discarding vehicles, including recycling, is considered through the vehicle-cycle model. The model is employed to evaluate emissions of greenhouse gases (CO_2, CH_4 and N_2O) as well as pollutant emissions such as carbon monoxide (CO), volatile organic compounds (VOCs), mono-nitrogen oxides (NOx), sulfur oxides (Sox), particulate matter with diameter less than or equal to 10 micrometers (PM10), and particulate matter with diameter less than or equal to 2.5 micrometers (PM2.5) derived from fossil/petroleum fuels and total energy use (including the energy in renewable biomass) (Frank et al. 2011).

Numerous vehicle/fuel systems are considered in the GREET model. The diagram in figure 4.1 displays some of the different fuel types such as gasoline, diesel, biofuels, hydrogen, natural-gas-based fuels, and electricity. However, more than 100 fuel production pathways from various

energy feedstocks are considered in the model. The yellow boxes list feedstocks and the red boxes list fuels produced by feedstocks.

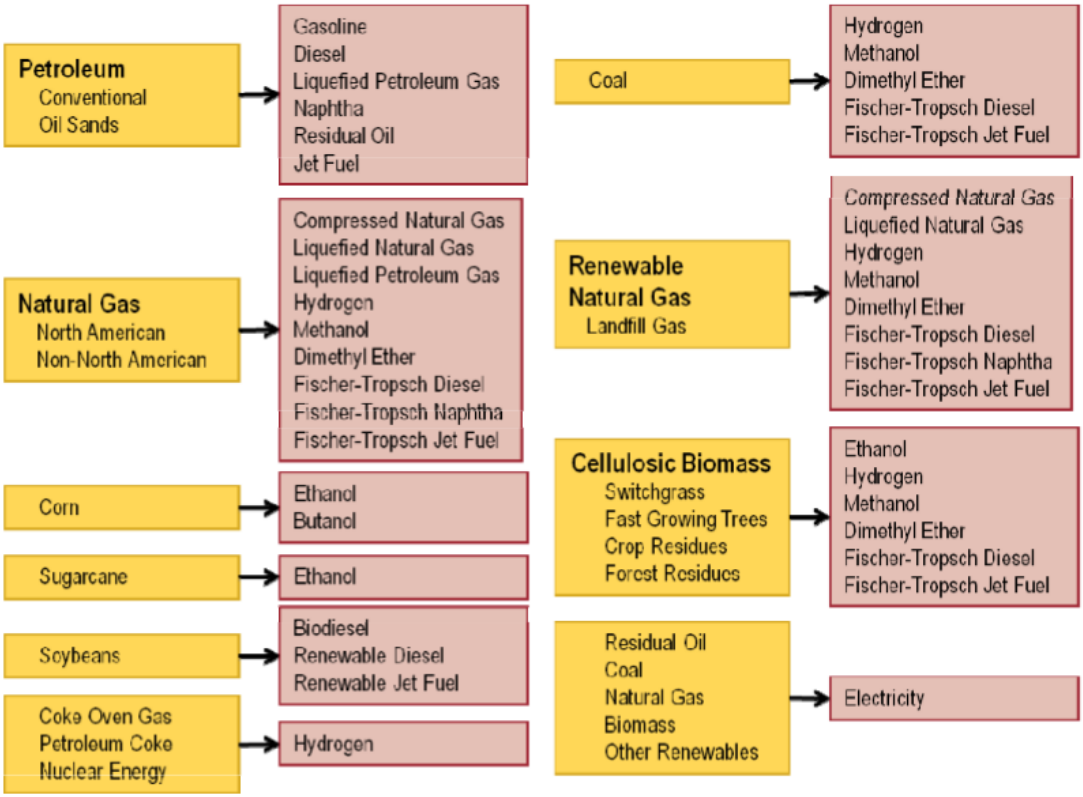

Figure 4.1: GREET Model Diagram (Yellow boxes list feedstocks; red boxes list fuels produced from feedstocks) (Frank et al. 2011).

The diagram in figure 4.2 displays the biofuel production options in the GREET model. Also, numerous vehicle technologies are considered by GREET. Such technologies include diesel engines, gasoline engines, hybrid electric vehicles with diesel and gasoline engines, plug-in hybrid electric vehicles with diesel and gasoline engines, battery-powered electric vehicles and fuel cell vehicles (Frank et al. 2011).

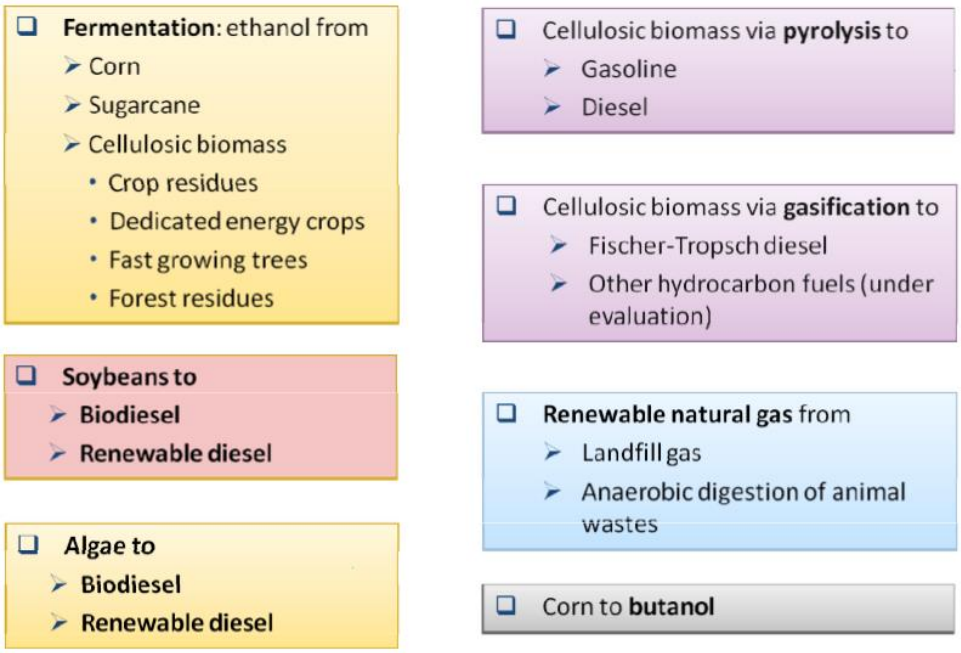

Figure 4.2: Potential Biofuel Production Pathways (Frank et al. 2011)

A life cycle frequently involves several stages, such as production, transportation, distribution, and end-use. The GREET model represents each stage as a stationary or transportation process. Emissions can be released in each process in different ways: (1) energy for the process provided by the combustion of process fuels, (2) escapes usually related to storage and transportation of volatile fuels (GREET LCA Mode, 2014).

To better describe how GREET calculates the emissions from transportation cycles (CO_2, CH_4, and N_2O) and other pollutants, figure 4.3 illustrates the calculations' flow in the model. A list of resources, related quantities, and escape rates are specified to account energy inputs to a process. In the same way, different technologies are considered to account for process emissions. Each pollutant criteria consist of a set of emission factors which define the different technologies and every resource employed in a process can be designated to one or more technologies. The complete life cycle is modeled by incorporating processes into pathways (GREET LCA Model, 2014).

Only one product defines each pathway. The energy and emissions associated with each pathway are calculated by combining all the resources and technologies applied in the processes of a pathway. Such calculations are used when they are inputs to a process as upstream values for the corresponding product. Circular references are resolved using iterative calculations (GREET LCA Model, 2014).

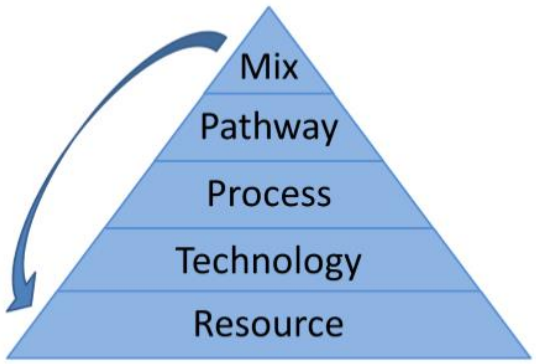

Figure 4.3: GREET pyramid (GREET LCA Model, 2014).

The description of every concept is next.

4.2 RESOURCES

The inputs and outputs of the GREET process define the resources which are organized in groups. The model currently has 11 groups to choose from including fertilizers for agriculture: (1) Petroleum fuel; (2) Natural gas fuel; (3) Coal fuel; (4) Fossil fuel; (5) Renewable; (6) Biomass; (7) Nuclear; (8) Non-fossil fuel; (9) Fertilizer; (10) Pesticide; and (11) Renewable natural gas. These groups are categories that belong to resources, and each resource can be associated with one or more groups (GREET LCA Model, 2014).

Seven physical properties can also define each resource: (1) Carbon ratio; (2) Sulfur ratio; (3) $\rho(f)$ Density; (4) $hhv(f)$ (High-heating value); (5) $lhv(f)$ (Low-heating value); (6) State of matter (solid, liquid, gas); and (7) Marker value (GREET LCA Model, 2014).

Also, 5 properties for resources can be defined by the user: (1) Name; (2) List of compatible resources; (3) Group membership; (4) Main resource (i.e., natural resource, such as coal, wind, natural gas, oil); (5) Gases created during evaporation (GREET LCA Model, 2014).

The ratios of sulfur and carbon are required for combustible fuels. Such ratios are used to evaluate the effect of combustion by quantifying SO_x and CO_2 balance. The conversion of mass, volume and energy, and the estimated ratios allocation between outputs and coproducts are carried out by the density and heating values. Additionally, the estimated ratios allocation may be done through the market value. These properties are all taken into account to estimate and report results. When a resource has no upstream energy and emission associations, it is called a primary resource. For instance, natural resources such as coal, uranium ore, crude oil, etc. are defined as primary resources. When evaporation happens, pollutant emissions are produced through material losses. GREET specifies what pollutants are attributed to such produced emissions (GREET LCA Model, 2014).

4.3 TECHNOLOGIES

Technology is used to model a combustion process or chemical reaction to quantify the emissions associated with the process. The type of fuel and the emission factor $Em_f(f,t)$ defines each technology, which is measured by grams of pollutant per Joule (g/J) of fuel consumed. GREET currently evaluates 9 different pollutants: (1) VOC; (2) CO; (3) NO_x; (4) PM10; (5) PM2.5; (6) SO_x; (7) CH_4; (8) CO_2; (9) N_20 (GREET LCA Model, 2014).

GREET allows to customized different values for different years so that the emission factors for each pollutant are arranged as a time series. This is done through an emission factor table where the rows and columns are pollutants and years, respectively (GREET LCA Model, 2014).

4.4 SULFUR AND CARBON BALANCE

Occasionally the technology table does not specify the SO_x emission factor. However, it must be calculated. When liquid or gaseous fuels are utilized, the SO_x emission factor is calculated with the following equation:

$$ef(f, SO_x) = \frac{\rho(f)}{hv(f)} \frac{sr(f)}{sr(SO_2)} \quad \text{(Eq. 4.1)}$$

Likewise, when solid fuels are utilized, the SO_x emission factor is calculated with the following formula:

$$ef(f, SO_x) = \frac{1}{hv(f)} \frac{sr(f)}{sr(SO_2)} \quad \text{(Eq. 4.2)}$$

where $sr(f)$ is the process of fuel's sulfur ratio and $sr(SO_2)$ is the SO_2 sulfur ratio, and the mass units are in parts per million (ppm).

The emission factor for CO2, when liquid or gaseous fuel is utilized, is calculated with the following equation:

$$ef(CO_2) = \frac{1}{cr(CO_2)} \left[\frac{\rho(f) cr(f)}{hv(f)} - (ef(VOC) cr(VOC) + ef(CO) cr(CO) + ef(CH_4) cr(CH_4)) \right] \quad \text{(Eq. 4.3)}$$

Likewise, when solid fuels are utilized, the CO_2 emission factor is calculated with the following formula:

$$ef(f, CO_2) = \frac{1}{cr(CO_2)} \left[\frac{cr(f)}{hv(f)} - (ef(f, VOC) cr(VOC) + ef(f, CO) cr(CO) + ef(f, CH_4) cr(CH_4)) \right] \quad \text{(Eq. 4.4)}$$

where $cr(f)$ is the process fuel's carbon ratio and $cr(VOC)$, $cr(CO)$ and $cr(CH_4)$ is the carbon ratios for the corresponding pollutants (GREET LCA Model, 2014).

4.5 INPUT

Every fuel production pathway is modeled using an input-output process for each stage. An input may be defined from 7 attributes: (1) Name; (2) $a(f)$ (quantity); (3) Source type; (4) Mixor pathways reference; (5) List of technologies with shares; (6) Parameters for sequestration; (7) Emission mass ratios (GREET LCA Model, 2014).

The source type specifies the process in which the upstream values are calculated for the inputs. There are four different sources: (1) Primary Resource; (2) Pathway Mix; (3) Output of a Previous Process; (4) Single Pathway. There is no upstream value associated with an input when the source is defined as a Primary Resource. When there is a pathway that will be used to evaluate the upstream emissions and energy values, it is indicated by the single pathway. Similarly, when multiple pathways with corresponding shares are utilized, they are indicated by Pathway Mixes. For instance, when the electricity utilized is produced by a shared combination of coal and NG power (GREET LCA Model, 2014).

The emissions and energy of the Mixor pathway are utilized as upstream values for producing a resource when the source is a Pathway Mixor Single Pathway (GREET LCA Model, 2014).

GREET calculates the energy associated with producing an input f with the following equation:

$$E(f) = a(f)E_{up}(f) \qquad \text{(Eq. 4.5)}$$

Emissions are estimated using the following equations:

$$Em(f) = a(f)Em_{up}(f) + a(f)\sum_{t\in T} s(f,t)Ef(f,t) + Em_{other} \qquad \text{(Eq. 4.6)}$$

$$= a(f)\left(Em_{up}(f) + \sum_{t\in T} s(f,t)Ef(f,t)\right) + Em_{other} \qquad \text{(Eq. 4.7)}$$

Therefore, the sum of the upstream emissions, technologies, and non-technology related emissions equals the emissions (GREET LCA Model, 2014).

4.6 PROCESSES

Since most of the calculations are done at the process, this is considered the main component of the model. There are two types of process: (1) stationary process and (2) transportation process. Both process types are modified to be represented as a canonical input-output value for calculation purposes (GREET LCA Model, 2014).

4.6.1 Canonical Process

Four different components define the emissions and energy associated with a process: (1) Input; (2) Outputs; (3) co-products; and (4) additional emissions (GREET LCA Model, 2014). GREET calculates the energy balance vector associated with a process with the following equation:

$$E_b = \frac{E(I) - E(P)}{a(f_o)(1 - l_r(f_o))} \quad \text{(Eq. 4.8)}$$

where

$$E(I) = \sum_{f \in I} E(f) \quad \text{(Eq. 4.9)}$$

Equation 4.4.1 provides $E(I)$ and $E(P)$ is the energy accredited to co-products. The loss rate is defined by $l_r(f_o)$ for the main output, $0 \leq l_r < 1$.

Likewise

$$Em_b = \frac{Em(I) - Em(P) + Em_{other}}{a(f_o)(1 - l_r(f_o))} \quad \text{(Eq. 4.10)}$$

The user can specify emissions associated with losses using Em_{other} and the emissions attributed to coproducts are defined by $Em(P)$ (GREET LCA Model, 2014).

In order to account for a coproduct's energy and emissions either of the following displacement methods can be used:

$$E(P) = \sum_{f_p \in P} E(f_p) \quad \text{(Eq. 4.11)}$$

$$Em(P) = \sum_{f_p \in P} Em(f_p) \quad \text{(Eq. 4.12)}$$

The energy ($E(P)$) and emissions ($Em(P)$) associated with every co-product depend on the treatment method applied (GREET LCA Model, 2014).

The equations employed to estimate the allocation to the production of the main output are the following:

$$E(f_p) = (1 - r_e)E(I) \quad \text{(Eq. 4.13)}$$

$$Em(f_p) = (1 - r_{em})Em(I) \quad \text{(Eq. 4.14)}$$

The ratios of energy and emissions are denoted by r_e and r_{em}, respectively. Four different allocation methods can be used: (1) Energy; (2) Mass; (3) Market Value; and (4) Volume. These methods are chosen considering the physical properties that were defined for the process output and the co-product (GREET LCA Model, 2014).

The ratios for energy allocation are calculated with the equation:

$$r_e = r_{rm} = \frac{e(f_o)}{e(f_p) + e(f_o)} \quad \text{(Eq. 4.15)}$$

An intermediate share *s* is defined when a non-energy allocation is employed, and it is based on the quantity of main output and co-product:

$$s = \frac{a(f_o)}{a(f_o) + a(f_p)} \quad \text{(Eq. 4.16)}$$

Since r_{em} and *s* are equal to each other, the energy ratio can be evaluated with the equation:

$$\Big(e(I) - e(f_o) - e\big(f_p\big)\Big)\, s + e(f_o) = r_e e(I) \qquad \text{(Eq. 4.17)}$$

The result for the simplification of the above equation is:

$$r_e = s - \frac{e(f_o)}{e(I)}\left(\frac{s}{s_e} - 1\right) \qquad \text{(Eq. 4.18)}$$

where s_e is:

$$s_e = \frac{e(f_o)}{e\big(f_p\big) + e(f_o)} \qquad \text{(Eq. 4.19)}$$

The assumption made by displacement is that a conventional product f_c is moved by the co-product of the process (GREET LCA Model, 2014). . This ensures that the model defines at least one pathway for f_c so that its upstream values are used to evaluate $E(f_p)$ and $Em(f_p)$with the following equations:

$$E(f_p) = a(f_c)E_{up}(f_c) \qquad \text{(Eq. 4.20)}$$

$$Em(f_p) = a(f_c)Em_{up}(f_c) \qquad \text{(Eq. 4.21)}$$

The structure of a stationary process can be compared to the canonical process. However, the stationary process might include a group object to specify inputs differently. Either an amount or an efficiency attribute is considered in each group. It is possible to convert the efficiency attribute into an amount (GREET LCA Model, 2014).

$$a(G) = \frac{a(f_o)}{\eta} = \sum_{f_i \in G} a(f_i) \qquad \text{(Eq. 4.22)}$$

The inputs within the group are obtained from the group amount in the following way. G_1 denotes the predetermined inputs within the group.

$$\hat{a}(G) = a(G) - \sum_{f \in G_1} a(f) \qquad \text{(Eq. 4.23)}$$

$$a(I) = a(G) + \sum_{f \in I-G} a(f_i) \quad \text{(Eq. 4.24)}$$

Shares specify the remaining inputs. The amount for the inputs that have shares instead of amount attributes are calculated with the following equation:

$$a(f) = s(f)\hat{a}(\mathrm{G}), \text{for } f \in G - G_1 \quad \text{(Eq. 4.25)}$$

The stationary process adapts to the canonical process when each attributed input amount in a group is estimated (GREET LCA Model, 2014).

4.7 ALGORITHM

The process in which energy and emissions results are estimated for each pathway is described in the following pseudo-code. The zeros in the vector *v(f)* represent empty spaces for basic resources, and the one corresponds to the index of *f* in the vector for basic fuels (GREET LCA Model, 2014).

$$v(f) = (0, 0 \ldots 0, 1, 0 \ldots ., 0)$$

Input: *max_it* ≥0, *tol* ≥ 0
While *dif f* ≥ *tol* or *it* ≤ *max_it* **do**
    diff = 0
    for each resource res **do**
        for each pathway *path* that has *res* as output **do**
            if *path* has *feed* **then**
                $Eenem_{prev} = Enem_{up}(feed)$
            else
                $EM_{prev} = 0$
            end if
            for each *proc* in the *path* **do**
                $E_b = 0, Em_b = 0, Enem = (E_b, Em_b)$
                for each input *f* in proc **do**
                if sources of *f* is in previous **then**
                $Enem_{up}(f) = Eenem_{prev}$
                else if source if *f* is well **then**
                $Enem(f) = e(f)v(f)$
                else if source if *f* is Pathway Mix **then**
                $Enem_{up}(f) = Eenem_{prev}(pathway)$
                end if

calculate E(f) ad Em(f) as shown in 5 and 6, correspondingly
end for
calculate E_b *and* Em_b as shown in 7 and 9, correspondingly
end for
$Enem_{prev}(path) = Enem(path)$
$Enem(path) = (E_b, Em_b)$, energy an emission balance of the last process of the pathway
$diff = diff + (Enem_{prev}(path) - Enem(path))^2$
end for
end for
it + = 1
end while

4.8 CHAPTER CONCLUSIONS

In this chapter, the GREET Life Cycle Assessment model was introduced. This model can be used to quantify the greenhouse gas emissions associated with the production of biofuel feedstock production. Therefore, SWAT and GREET can be used simultaneously for a more complete sustainable approach in Land-Use and Land-Cover change design considering the environmental impacts on soil and water from replacing regional crops, at the watershed scale, and the atmospheric impacts associated to the production of biofuel feedstock and their conversion to biofuel. The next chapter introduces different optimization techniques that take into account two or more conflicting objectives, and that can be considered to solve large and complex design problems.

Chapter 5: Optimization Techniques

This chapter is dedicated to introducing the general optimization concept, as well as different optimization techniques, that can be used to solve complex problems when two or more conflicting objectives are considered.

5.1 Optimization

Optimization, also known as constrained optimization or mathematical programming, can be defined as the mathematical procedure to determine the optimal allocation of limited resources. The problem consists of maximizing or minimizing one or more objective functions by finding the best combination of activities without exceeding the resources that are available (Schrage, 2009). In linear programming, a single objective optimization problem can be formulated as follows:

$$Minimize \sum_{j=1}^{n} c_j x_j \qquad \text{(Eq. 5.1)}$$

$$subject\ to \sum_{j=1}^{n} a_{ij} x_j = b_i, \quad i = 1, 2, \ldots, m$$

$$x_j \geq 0, \qquad j = 1, 2, \ldots, n.$$

where $c_j x_j$ is the objective function and x_j is the independent variable. The optimal solution is subject to the constraints $a_{ij} x_j = b_i$ and non-negative constraints $x_j \geq 0$ (Bazaraa et al, 2010).

Applied optimization problems often require detecting multiple local and global optima of a specific objective function. However, the optimal result may not be feasible in real-world problems due to physical constraints. In this case, multiple solutions can be evaluated to approximate the optimal solution (Das et al., 2011).

As the name suggests, multi-objective optimization techniques seek to find optimal solutions to problems with multiple objectives. Therefore, a solution that is optimum concerning a single criterion does not satisfy this type of problems (Ghosh and Dehuri, 2004).

A multi-objective optimization problem can be expressed mathematically as follows:

$$\text{Minimize } f_m(X) \qquad m = 1, 2, \ldots\ldots, M \qquad \text{(Eq. 5.2)}$$

$$Subject\ to: g_j(x) \leq 0 \qquad j = 1, 2, \ldots\ldots, J$$

$$x^{lower} \leq x \leq x^{upper}$$

where $f_m(x)$ is the objective function for every mth element of the transpose of the row vector $f = (f_1, f_2, \ldots\ldots, M)$, x is the independent variable, $g_j(x)$ is the feasible solution space and x^{lower} and x^{upper} are the lower and upper bounds of the independent variable. If there are trade-offs among the M objective functions, we can conclude that there are multiple solutions to the optimization problem described in equation 5.2 (Li et al., 2008, Deb, 2001)

The procedure of a multi-criterion optimization is different from a single criterion optimization. The main goal of a single criterion optimization is to find the global optimal solutions. On the other hand, when multiple objectives are considered, each objective may have a different individual optimal solution. The objective functions may conflict with each other resulting in significant difference in the optimal solutions. These conflicting objective functions forces the production of an optimal solution set, rather than only one solution. The purpose for the optimality of numerous solutions is that a single solution cannot be considered better than others without taking into account all the objective functions. Such optimal solutions are called Pareto-optimal which are named after the economist Vilfredo Pareto who established this concept in 1896 (Ghosh and Dehuri, 2004).

To illustrate the Pareto optimal solution, let us consider a problem in which the objective is to minimize both time and space complexity (Figure 5.1).

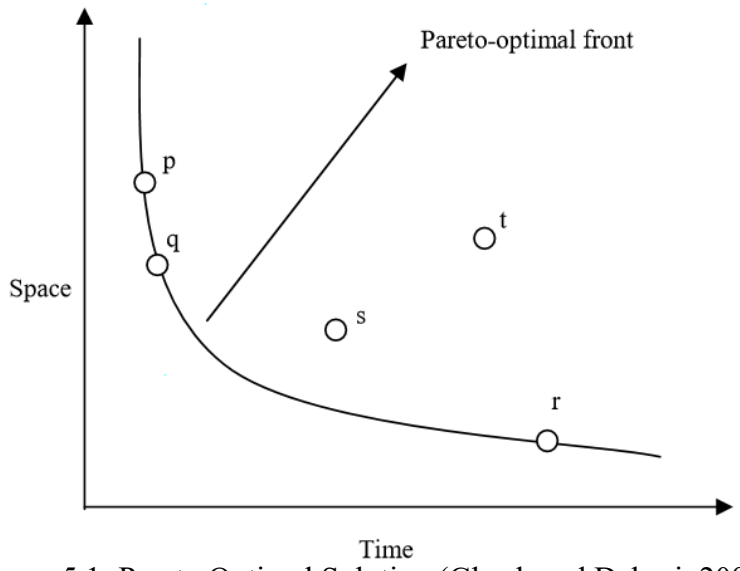

Figure 5.1: Pareto Optimal Solution (Ghosh and Dehuri, 2004).

The possible solution ‘p’ minimizes the time but maximizes the space complexity. In contrast, the possible solution ‘r’ maximizes the time but minimizes the space complexity. When both objectives are considered, neither solution is optimal. Therefore, solution ‘p’ is not better than ‘r’ and vice versa. Many solutions also belong to the Pareto optimal set, such as ‘q’, which cannot be sorted given the performance metrics taking into account both objectives. The Pareto-optimal solutions are all those that are found on the curve (Ghosh and Dehuri, 2004).

Other solutions that do not belong to the Pareto optimal set exist. For instance, in figure 5.1, if solutions ‘t’ and ‘q’ are compared, it is evident that ‘t’ is not better in any of the objectives. In this case, ‘t’ is outside the Pareto optimal set, and it is considered to be a dominated solution or inferior solution (Ghosh and Dehuri, 2004).

To demonstrate how a set of solution =s become a Pareto-optimal set let us consider a problem having m objectives ($f_i = 1, 2, 3, \ldots, m \; where \; m > 1$). Any two solutions having ‘t’ decision

variables each (v^1 and v^2) can either dominate the other or not dominate the other. Solution v^1dominates v^2 if the following conditions are true:

1. The solution v^1 is not inferior than v^2 in all objectives, or $f_i(u^{(1)}) \geq f_i(u^{(2)}), \forall i = 1,2,3 \ldots, m.$
2. The solution $v^1$is firmly better than v^2 in at least one objective, or $f_i(u^{(1)}) \succ f_i(u^{(2)})$ for at least one, I ∈ {1,2,3,…., m} ($\succ = better\ and\ \prec$ = worse)

If at least one of the above conditions is violated, the solution v^1 does not dominate the solution v^2. If v^1 dominates v^2 than v^2 is dominated by v^1, or v^1 is nondominated by v^2, ultimately, it can be said that v^1 is the nondominated solution (Ghosh and Dehuri, 2004).

According to the Local Pareto-optimal set and Global-Pareto optimal set, we can confirm that a set of solutions belong to a local or global Pareto-optimal set. In the Local Pareto-optimal set, if for every member *v* in a set of Q, ∃ no solution *u* satisfy $\|v - u\|_\infty \leq \varepsilon$, where ε is a small positive number that dominates any element in the set Q; hence, the solution in the set Q create a local Pareto-optimal set. By definition, if the solution *v* is perturbed the resulting solution *u* dominates any member of that set. Such set is called local Pareto optimal set. In the global Pareto-optimal set, if no solution dominates any member of the set Q in the search space, the solution belonging to the set Q creates a global Pareto-optimal set (Ghosh and Dehuri, 2004).

If for every member u in a set S, ∃ no solution v satisfying ε ≤∞− vu, where ε is a small positive number, which dominates any member in the set S, then the solutions belonging to the set S constitute a local Pareto-optimal set. The definition says that if we are perturbing the solution u in a small amount, then the resultant solution v dominates any member of that set then the set is called local Pareto optimal set (Ghosh and Dehuri, 2004).

The approaches for solving Multi-Objective Evolutionary Algorithms are classified by techniques. These techniques are categories as follows:

a) Priori Technique

b) Progressive Techniques

c) A Posteriori Techniques

Overall, in single-objective optimization exist total order solutions. However, partial order of solutions is generated with multi-objective methods which are guided toward a possible set of trade-off solutions in objective space. A dominance approach is suitable for Multi-Objective Evolutionary Algorithms considering strict partial orders of points in an objective space (Coello et al. 2007).

It is not necessary to have an exact set of objective functions when solving Multi-Objective problems (MOP). Only the associated fitness for each solution in a neighborhood and selection system. Three fundamental solution techniques exist for MOP: (1) The highest priority objective is the only one considered for optimization; (2) An aggregated weigh sum is applied in which all the objectives are included; (3) Finding the entire Pareto front through a Multi-Objective Algorithms. A numerous set of operators covers each of these techniques which may do an exhaustive search within the objective space, use the initial set of individuals to move towards the Pareto front, or generate random points for testing. The level of priority assigned by the decision-maker, in an attempt to find all solutions, cause solutions variations in P_{true}. The primary aim of optimizing multi-criteria is to obtain the Pareto front. The following techniques exploit different search operators, objective landscapes, and use metrics to evaluate the results (Coello et al. 2007).

5.2 PRIORI TECHNIQUE

This technique requires the definition of the MOP objective ranks by the decision-maker (DM) before the search begins. Such ranks are frequently reflected in the weights related to the total summation of the objectives. The idea is to evaluate and compare solutions according to the

preferences of the DM in a multicriteria problem. In real problems, it is crucial to identify the solution that satisfies the DM's needs. Therefore, it is essential to avoid poor quality objective prioritization since some adequate solutions could not be explored. Regardless of the optimization algorithm used, the priori MOEA techniques have this unavoidable consequence, which is explained next (Coello et al. 2007).

5.2.1 Lexicographic ordering

In this technique, the objectives are ranked by the DM in order of importance. The objective functions are minimized in sequence to obtain the optimal solution, beginning with the objective of the highest rank and continuing in descending order of importance. When the priority is unknown, an objective may be selected randomly at each generation to be optimized. However, this is equivalent to a weighted combination of objectives given that the selection process takes place with the associated probability defined by each weight. In comparison to other techniques, there is a significant difference when using tournament selection with this approach since pairwise comparison reduces scaling information. Nevertheless, the randomness involved in the process makes this approach weak since it only favors specific objectives. As a result, the population converges to a district part of the Pareto front instead of a full delineation. Still, this approach is extremely competitive with other non-Pareto methods due to its simplicity and computational efficiency (Coello et al. 2007).

5.2.2 Linear aggregating functions

The fitness for the linear aggregating function can be computing using:

$$fitness = min \sum_{i=1}^{k} w_i f_i(x) \qquad \text{(Eq. 5.3)}$$

where w_i is greater than cero and i are the weighing coefficients assigned by the DM and k is the number of objective functions in the problem. For normalization purposes, it is frequently assumed that:

$$\sum_{i=1}^{k} w_i = 1 \qquad \text{(Eq. 5.4)}$$

Despite its deficiencies, its simplicity makes the linear fitness technique a widely used scalarizing approach. The parallel lines in figure 5.2 determine if the search finds a Pareto front. Point A is a single Pareto front at minimum cost if A is on the convex hull of the Pareto front. Since there is a smaller aggregate objective function value at point A, point B is not retained. The variances of slopes and intersection points on the convex envelope at contrasting points on PF_{true} are the result of the different weights assigned by the DM. Consequently, all the points of interest in the Pareto front are not found by the linear aggregating algorithm. Therefore, the range of variation in the value or number of points identified on PF_{true} is determined by the variation of weights assigned (Coello et al. 2007).

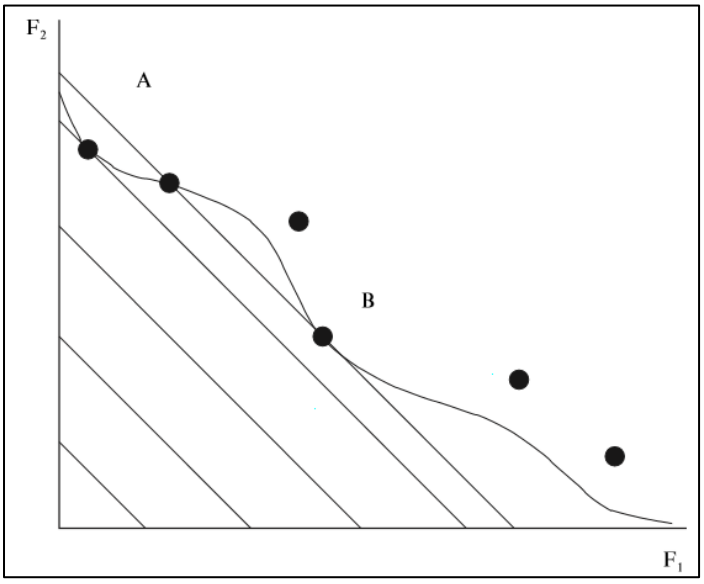

Figure 5.2: Priori weight selection for a bi-objective example in linear aggregating technique, $w_1x_1 + w_2x_2$ (Coello et al. 2007).

5.2.3 Nonlinear aggregating functions

In contrast with the linear aggregating functions, this technique is not often used in literature. Its unpopularity is due to the complicated effort required to accomplish utility functions or appropriate probability of acceptance, and to the various requirements which the objective functions must satisfy. Simultaneously, the quality of the resulting solutions does not always justify the additional overhead (Coello et al. 2007).

To be more specific on the desired goals, the DM could use target vector approaches, which are more popular than multiplicative methods. When combining an evolutionary algorithm and the vector approach, the current solution generated is minimized according to the difference of the vector of the desired goals. Target vector approaches suggest being another aggregating approach. However, they are typically considered different since, under certain conditions, concave portions of the Pareto front are achieved by target vectors, while a linear combination of weight approaches cannot (Coello et al. 2007).

Goal Programming, Goal Attainment, and the min-max algorithm are the most widely used methods that include the target vector approaches (Coello et al. 2007).

Despite the efficiency and simplicity of multiplicative approaches, determining an excellent nonlinear aggregation function is more challenging than determining a linear aggregating function.

Target-vector approaches have the same imperfection since the desirable goals to be achieved must be defined by the DM. Further problems can be encountered when computing these goals as it usually requires additional computational work (Coello et al. 2007).

Another point at issue is that the yield of nondominated solutions is restricted to the definition of the goal within the feasible domain, a condition which limits their applicability. Additionally, desirable solutions may be left unexplored due to the restricted search space caused

when the goals or weights were specified, a common defect in all priori techniques. However, it has been seen that nonlinear aggregating functions approximate, in specific problems, to the Preto optimal set, especially in multi-objective combinatorial optimization problems (Coello et al. 2007).

5.3 PROGRESSIVE TECHNIQUES

Usually, this approach requires the DM to favor the search when defining the goals or scheme of preference. The main problem is that such definitions require an interactive process and may result in inefficient solutions, especially when there are unknown pieces of the problem. Furthermore, contradictions between group preferences may exist, which increases the level of conflict. Nevertheless, complex real-world problems often require narrowing the search to a specific region. Under this condition, the most suitable technique may be an interactive process. It is questionable how the DM would be incorporated into the MOEA since this may cause scalability or intransitivity issues (Coello et al. 2007).

5.4 POSTERIORI TECHNIQUE

The purpose of the posteriori technique is to find P_{true} and PF_{true}. Therefore, the search becomes more comprehensive to create numerous solutions to the Pareto Optimal set. The main difference concerning the prior techniques is that the decision-making process is done after the search has been completed(Coello et al. 2007). The following subsections describe the posteriori sub-techniques:

5.4.1 Independent Sampling Techniques

In this technique, each objective has a weight that varies in every MOEA run, allowing higher portions of the Pareto front. The variation of weights along the evolutionary process is what makes this technique different than the priori linear aggregating function. However, in most cases, these points are not evenly distributed at the Pareto front (Coello et al. 2007).

This approach is convenient to use due to its relative simplicity and efficiency. Nevertheless, when the number of objectives is low, this method may have little utility. It is useful to approximate the Pareto front but only under specific type of problems (Coello et al. 2007).

5.4.2 Criterion Selection Techniques

Proposed by David Schaffer, the Vector Evaluated Genetic Algorithm (VEGA) is considered the first implementation of a MOEA. In this approach, a fraction of the objectives are randomly selected in every generation based on separate objective performance. The solutions generated by the VEGA technique converge to local optima with respect to each objective (Coello et al. 2007).

In a problem with k objectives, the VEGA approach generates a k subpopulation of size M/k where only one of the k objective is considered as a fitness function. This criterion is used to create the mating pool to generate the succeeding population of size M. The crossover and mutation operators are applied typically as in every GA (Coello et al. 2007).

The structural representation of the VEGA process is shown in figure 5.3 below.

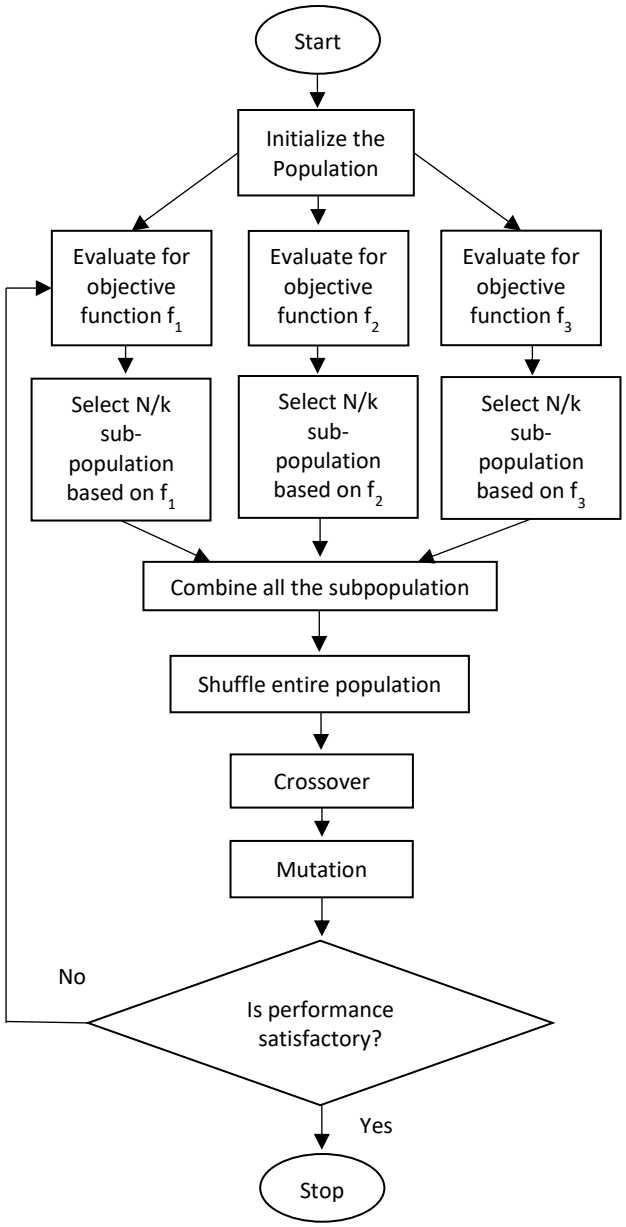

Figure 5.3: Schematic Representation of VEGA

In this procedure, non-dominance is limited to the current population. Dominated solutions in one generation may become dominated by a new solution in succeeding generations. Furthermore, compromise solutions will not survive under this selection methodology since the selection process is based on one-dimensional performance only, without considering the other dimension, a problem known as 'speciation.' To minimize speciation, Schaffer developed two heuristics: (1) Non-dominated selection heuristic; and (2) the mate selection heuristic. In general,

this approach, in the presence of non-convex search spaces, is incapable of producing Pareto-Optimal solutions (Ghosh and Dehuri, 2004).

5.4.3 Aggregation Selection Techniques

This approach uses different weight combinations between generations and each function evaluation, rather than static objective weights. There are different approaches for the distribution of weights such as random assignment, as functions of a specific solution in evaluation, or the chromosome can be encoded with the weight as genes, including them as part of the evolutionary process (Coello et al. 2007).

A set of solutions can be generated with aggregation selection techniques in a single run of a MOEA. However, individuals of PF_{true} may be missed when the weighted sum approach is employed. Furthermore, significant effort is required when using both the constrain/objective combination and hybrid search approaches (Coello et al. 2007).

5.4.4 Constraint Techniques

The ε-constraint approach consists of selecting a primary objective function while the others are bounded with different predefined ε-constraint values. In order to create different points on the Pareto front, the ε-constrain are changed successively, which result in the discovery of elements in the Pareto optimal set. Usually, the distribution of the Pareto front is non-uniform. The main advantage of this technique is its smooth implementation. However, it requires extensive computation effort to generate PF_{known} (Coello et al. 2007).

5.4.5 Pareto Sampling Techniques

Pareto sampling is a technique that takes advantage of the MOEA's population capability to find several elements of the Pareto optimal set in one stochastic computational run. Figure 5.4 shows the concept of two objective Pareto optimality. However, the graphical definition of

dominated and nondominated points within the objective space as well as the solutions that correspond to the variable space must be related. The dominance comparison of points in the objective space with this technique cannot be made due to the strict partial order (Coello et al. 2007).

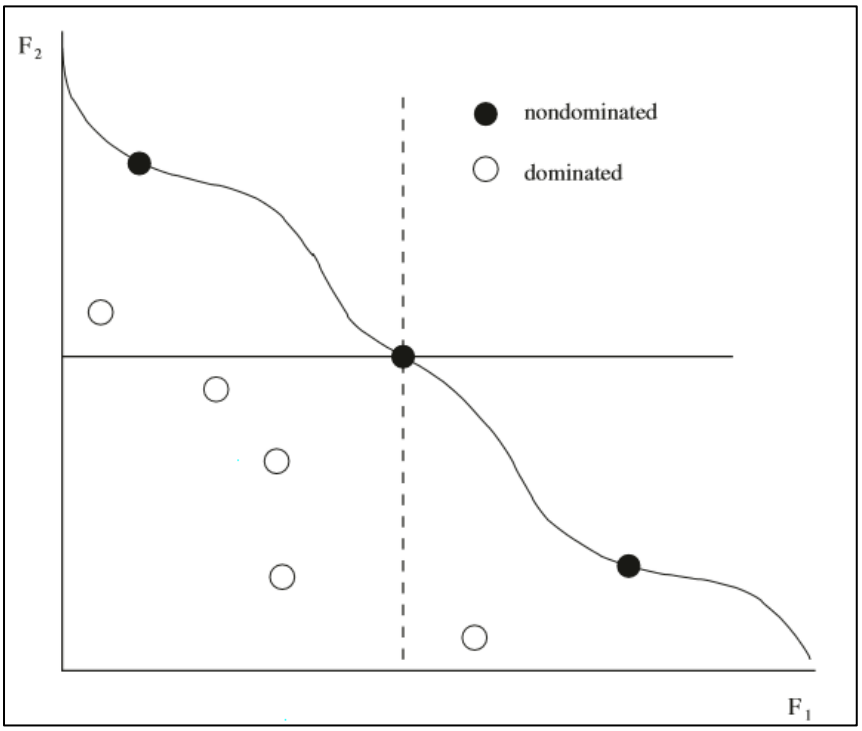

Figure 5.4: Pareto optimality concept associated with non-dominance in a maximization multi-objective problem (Coello et al. 2007).

According to Coello, the four high-level primary goals of any basic algorithm using Pareto-based fitness assignment to identify nondominated vectors from a MOEA's existing population and some operators according to their goals are:

Goal 1. Conserve non-dominated points (elitism vs. non-elitism) with $PF_{current} \rightarrow PF_{known}$

- Dominance-Based ranking – fitness assignment
- Non-Pareto vs. Pareto approaches
- Arching + elitism of chromosome population

Goal 2. Lead PF_{known} towards PF_{true}

- Convergence to true computational Pareto front, PF_{true}
- Generating non-dominated phenotype points
- Explicit/non-explicit building block manipulation
- Quantitative and Qualitative performance metrics and visual comparisons
- Probabilistic MOEA models; local search incorporation, etc.

Goal 3. Create and preserve the diversity of points on the Pareto Front, PF_{known} (phenotype) and Pareto optimal solutions PF_{known} (genotype)

- Diversity preservation
- Niching/fitness sharing and crowding on Pareto front (variations)
- Uniform/Diverse non-dominated PF_{known}

Goal 4. Provide a limited number of PF_{known} points

Based on these goals, the following genetic operations should be included for an effective MOEA, assuming operations on a complete individualism:

- Generating the initial population P with N number of individuals and fitness function. The encoding of the gene's individuals from the problem domain can be binary, integer, or real.
- Based upon scalar multi-objective function such as Pareto ranking ($P \rightarrow P^i$), remove Pareto dominated individuals from P.
- Limit the number of individuals in P^i that belong to small regions of the current PF_{knwon} or P_{known} using density estimators. The methodologies include niching, sharing, and crowding with related parameter values.

- Generate new individuals by applying evolutionary operators such as reproduction, crossover, mutation, etc. and using appropriate parameter values $P^{i} \rightarrow P^{ii}$. The individuals that will reproduce can be selected using ranking, binary tournament selection, or proportional selection.
- Numerous selection operations can be employed to select the individuals for the next generation (population P^{iii}). For instance, one could operate on [P^{ii}] or [$P^{i} \cup P^{ii}$] using ranking. Obviously, $P^{iii}$is $P_{current}$. Better results are generated using elitism since competent individuals are kept.
- If a stopping criterion is not reached, such as convergence criteria or a given number of generations, set P^{iii} to P as $P_{current}$
- Eliminate individuals that are Pareto dominated and infeasible from P^{iii}or repair individuals that are unfeasible. Set P^{iii} to P as $P_{current}$
- Keep and save individuals that are non-dominated and feasible by storing P^{iii} in a file P^{iv}. The non-domination operation is applied to the merged combination as the new population P^{iii} is merged in the file. The P^{iv} file is composed of P_{known} and associated PF_{known}.
- Good performance can also be provided by local search operations in hybrid or memetic MOEA by exploring limit regions in objective space.

The majority of MOEA algorithms structures follow this genetic structure. The meta-level Genetic MOEA pseudo-code is represented in figure 5.5.

Initialize population P and P^{iv}
Evaluate Objective F(x) values over population
Assign Rank Based on Pareto Dominance
Compute Niche Count
Assign Shared Fitness or Crowding
While not terminal condition (number of generations of other)
  Selection of good individuals from $P \rightarrow P^{i}$
  Reproduction, mutation of individuals in $P^{i} \rightarrow P^{ii}$
  Evaluate Objective Values of Children P^{ii}
  Rank ($P^{i} \cup P^{ii}$) $\rightarrow P^{iii}$ based on Pareto Dominance
  Compute Niche Count
  Assign Shared Fitness or Crowding
  Reduce $P^{iii} \rightarrow P$
  Copy $P^{iii} \rightarrow P^{iv}$ based on Pareto Dominance
End While

Figure 5.5: Generic MOEA Pseudo code

The different operators distinguish a MOEA algorithm structure. The following subsections present different structures of MOEAS that have been modified and improved in newer versions (Coello et al. 2007).

5.5 MULTI-OBJECTIVE GENETIC ALGORITHM (MOGA)

The formal algorithmic pseudo code of Multi-Objective Algorithm is shown below (Coello et al. 2007).

Algorithm 1 MOGA algorithm

procedure MOGA ($\mathcal{N}', g, f_x(x_k)$) ▷ $\mathcal{N}'$ members evolved g generations to solve $f_x(x)$
    Initialize Population $\mathbb{p}'$
    Evaluate Objective Values
    Assign Rank Based on Pareto dominance
    Compute Niche Count
    Assign Linearly Scaled Fitness
    Shared Fitness
    for $i = 1$ to g **do**
        Selection via Stochastic Universal Sampling
        Single Point Crossover
        Mutation
        Evaluate Objective Values
        Assign Rank Based on Pareto dominance

14: Compute Niche Count
15: Assign Linearly Scaled Fitness
16: Assign Shared Fitness
17: **end for**
18: **end procedure**

A variation of the MOGA was proposed by Fonseca and Fleming where the number of dominated chromosomes in the current population correspond to the rank of a specific individual. For instance, an individual x_i in generation t, is dominated by P_i^t individuals in the current generation; therefore, the rank assigned to that individual follows the rule: $rank(x_i, t) = 1 + P_i^{(t)}$) (Coello et al. 2007).

Fitness assignment is performed by sorting the population according to rank, interpolating from the best to the worst rank of individuals and using the same rank to average the fitness of individuals. Thus, all of them will be sampled at the same rate keeping the global population fitness constant (Coello et al. 2007).

It is possible to produce a large selection pressure that might lead to early convergence with this fitness assignment methodology. To prevent that, a niche-formation method was used by Fonseca and Fleming so as to distribute the population over the Pareto-optimal region. They used sharing on the objective function values, rather than performing sharing on the parameter values (Coello et al. 2007).

5.6 NONDOMINATED SORTING GENETIC ALGORITHM (NSGA)

Another variation of Goldberg's approach in which the original ranking is modified was proposed by Srinivas and Deb called "Nondominated Sorting Genetic Algorithm" (NSGA). The pseudo code for this MOEA NSGA-I technique I given in Algorithm 2 (Coello et al. 2007).

Algorithm 2 NSGA-I algorithm

1: **procedure** NSGA-I($\mathcal{N}', g, f_j(x_k)$) ▷ $\mathcal{N}'$ members evolved g generations to solve $f_k(x)$

2: Initialize Population $\mathbb{p}'$
3: Evaluate Objective Values
4: Assign Rank Based on Pareto in Each Wave
5: Compute Niche Count
6: Assign Shared Fitness
7: **for** $i = 1$ to g **do**
8: Selection via Stochastic Universal Sampling
9: Single Point Crossover
10: Mutation
11: Evaluate Objective Values
12: Assign Rank Based on Pareto in Each Wave
13: Compute Niche Count
14: Assign Shared Fitness
15: **end for**
16: **end procedure**

These classified solutions are shared along with their fake fitness values to preserve the diversity of the population. At that point, the classified solutions in this group are ignored, and another set of nondominated solutions is considered. This process continues until all solutions in the population are classified. This technique adopts the stochastic remainder proportionate selection. Given that the maximum fitness value belongs to the individuals in the first front, these will get more replicas than the rest of the population Instead of converging quickly, the fitness sharing mechanism in this MOEA causes a computational bottleneck (Coello et al. 2007).

An improved version of the NSGA algorithm is proposed by Deb, called NSGA-II. The pseudo code for the MOEA NSGA-II technique I given in Algorithm 3 (Coello et al. 2007).

Algorithm 3 NSGA-II algorithm

1: **procedure** NSGA-II($\mathcal{N}', g, f_x(x_k)$) ▷ $\mathcal{N}'$ members evolved g generations to solve $f_x(x_k)$
2: Initialize Population $\mathbb{p}'$
3: Generate random population – size $\mathcal{N}'$
4: Evaluate Objective Values
5: Assign Rank (level) Based on Pareto dominance – $sort$
6: Generate Child Population
7: Binary Tournament Selection
8: Recombination and Mutation
9: **for** $i = 1$ to g **do**

10: **for** each Parent and Child in Population **do**
11: Assign Rank (level) based on Pareto – $sort$
12: Generate sets of nondominated vectors along PF_{known}
13: Loop (inside) by adding solutions to next generation starting from the *first* front until $\mathcal{N}'$ individuals found determine crowding distance between points on each front
14: **end for**
15: Select points (elitist) on the lower front (with lower rank) and are outside a crowding distance
16: Create next generation
17: Binary Tournament Selection
18: Recombination and Mutation
19: **end for**
20: **end procedure**

The individuals are sorted and ranked according to the nondomination level. To generate a new pool of offspring an Evolutionary Operations (EVOPs) is applied, after that, the parents and offspring are combined before dividing the new combined pool into fronts. Niching is conducted through the addition of crowding distance to each member. To preserve a diverse front, this crowding distance is used as its selection operator (Coello et al. 2007).

5.7 NICHED-PARETO GENETIC ALGORITHM (NPGA)

The Niched-Pareto Genetic Algorithm (NPGA) was proposed by Horn and colleagues which employs a tournament selection MOEA based on Pareto dominance. The pseudo code for the MOEA NPGA technique I given in Algorithm 4 (Coello et al. 2007).

Algorithm 4 NPGA algorithm

1: **procedure** NPGA($\mathcal{N}', g, f_x(x_k)$) ▷ $\mathcal{N}'$ members evolved g generations to solve $f_x(x_k)$
2: Initialize Population P
3: Evaluate Objective Values
4: **for** $i = 1$ to g **do**
5: Specialized Binary Tournament Selection
6: **Begin**
7: **if** only Candidate 1 dominated **then**
8: Select Candidate 2
9: **else if** Only Candidate 2 dominated **then**
10: Select Candidate 1

```
            else if Both are Dominated or Nondominated then
                Perform specialized fitness sharing
                Return Candidate with lower niche count
            end if
        End
        Single Point Crossover
        Mutation
        Evaluate Objective Values
    end for
end procedure
```

Two random individuals and a subset from the entire population are compared. If one of the random individuals is dominated and the other is nondominated, the nondominated individual wins. Tournament is decided through fitness sharing when both individuals are either nondominated or dominated. A fitness sharing in the objective domain was also proposed, where both the objective and the decision variable domains where combined with a metric, called equivalent class sharing (Coello et al. 2007).

An improved NPGA was developed by Erickson, which applies Pareto ranking and preserves tournament selection. The pseudo code for the MOEA NPGA 2 technique I given in Algorithm 5. Instead of using the current generation, niche counts are evaluated using solutions in the partially filled succeeding generation. This technique is called continuously updated fitness sharing (Coello et al. 2007).

Algorithm 5 NPGA 2 algorithm

```
1: procedure NPGA 2(𝒩′, g, f_x(x_k))   ▷ 𝒩′ members evolved g generations to
   solve f_x(x_k)
2:     Initialize Population ℙ′
3:     Evaluate Objective Values
4:     for i = 1 to g do
5:         Specialized Binary Tournament Selection using rank as domination
   degree
6:         Begin
7:             if Only Candidate 1 dominated then
8:                 Select Candidate 2
9:             else if Only Candidate 2 dominated then
```

```
10:                Select Candidate 1
11:            else if Both are Dominated or Nondominated then
12:                Perform specialized fitness sharing
13:                Return Candidate with lower niche count
14:            end if
15:        End
16:        Single Point Crossover
17:        Mutation
18:        Evaluate Objective Values
19:    end for
20: end procedure
```

5.8 PARETO ARCHIVED EVOLUTION STRATEGY (PAES)

Knowles and Corne designed and implemented the Pareto Archived Evolution Strategy (PAES). The pseudo code for the MOEA PAES technique I given in Algorithm 6 (Coello et al. 2007).

Algorithm 6 PAES algorithm

```
1: procedure NPGA 2(f_x(x_k))
2:   repeat
3:     Initialize Single Population parent, c, and add to archive, 𝔸
4:     mutate c to produce child c′ and evaluate fitness
5:     if c ≻ c′ then
6:       discard c′
7:     else if c ≻ c′ then
8:       replace c with c′ and add c to 𝔸
9:     else if ∃_{c″∈A}(c″ ≻ c′) then
10:      discard c′
11:    else
12:      apply test (c, c′, 𝔸) to determine which becomes the new current solution
       and whether to add c′ to 𝔸
13:    end if
14:  until termination criteria is met
15: end procedure
```

The evolutionary strategy consists of the generation of a single offspring by a single parent in combination with records od nondominated solutions previously found. Every mutated individual is compared to these records. Diversity is also preserved with a crowding procedure

approach. In comparison with traditional niching methods, this procedure has low computational complexity (Coello et al. 2007).

5.9 STRENGTH PARETO EVOLUTIONARY ALGORITHM (SPEA)

Zitzler and Thiele developed the Strength Pareto Evolutionary Algorithm (SPEA) in which different MOEAs were integrated. The pseudo-code for the SPAE technique I given in Algorithm 7 (Coello et al. 2007).

Algorithm 7 SPEA algorithm

1: **procedure** SPEA ($\mathcal{N}', g, f_x(x_k)$)
2: Initialize Population $\mathbb{P}'$
3: Create empty external set $\mathbb{E}'(|\mathbb{E}'| < |\mathbb{P}'|)$
4: **for** $i = 1$ to g **do**
5: $\mathbb{E}' = \mathbb{E}' \cup \mathcal{ND}(\mathbb{P}')$ ▷ Copy members evaluating to be nondominated of P to E
6: $\mathbb{E}' = \mathcal{ND}(E)$ ▷ Keep only members evaluating to nondominated vectors in E
7: Prune $\mathbb{E}'$ (using clustering) if max capacity of $\mathbb{E}'$ is exceeded
8: $\forall_{i \in \mathbb{P}'}$ Evaluate $(\mathbb{P}'_i)$ ▷ Evaluate fitness for all member of $\mathbb{E}'$ and $\mathbb{P}'$
9: $\forall_{i \in \mathbb{E}'}$ Evaluate $(\mathbb{E}'_i)$
10: $\mathcal{MP} \leftarrow \mathcal{T}(\mathbb{P}' \cup \mathbb{E}')$ ▷ Use binary tournament selection with
11: ▷ Replace to select individuals from $\mathbb{P}'+ \mathbb{E}'$
12: ▷ (multiset union) until the mating pool is full
13: Apply crossover and mutation on $\mathcal{MP}$
14: **end for**
15: **end procedure**

The nondominated solutions are copied, in each generation to an external nondominated set, where they a strength value is computed for every solution. Each member of the current population is evaluated according to the strength of all external nondominated solutions that dominate it. Both the closeness to the true Pareto front and even distribution of solutions are considered in SPAE in the fitness assignment process. Rather than using niches based distance, Pareto dominance guarantees that solutions along the Pareto front are found, although the size of the external nondominated set will determine its effectiveness (Coello et al. 2007).

The SPEA2 is a revised version of SPEA. The pseudo code for the MOEA SPAE 2 technique I given in Algorithm 8. There are three main differences that distinguish SPAE2 from SPAE. First, a fine-grained fitness assignment approach is incorporated where the number in which one solution dominated others and the number that was dominated by others is considered. Second, a neighbor density estimation approach is used to guide the search more efficiently. Lastly, to guarantee the conservation of boundary solutions and improved archive truncation technique is employed (Coello et al. 2007).

Algorithm 8 SPEA 2 algorithm

1: **procedure** SPEA2 ($\mathcal{N}', g, f_x(x_k)$)
2: Initialize Population $\mathbb{P}'$
3: Create empty external set $\mathbb{E}'$
4: **for** $i = 1$ to g **do**
5: Compute fitness of each individual in $\mathbb{P}'$and $\mathbb{E}'$
6: Copy all individual evaluating to nondominated vectors $\mathbb{P}'$and $\mathbb{E}'$to $\mathbb{E}'$
7: Use the truncation operator to remove elements from E when the capacity of the file has been extended
8: If the capacity of $\mathbb{E}'$ has not been exceeded then use dominated individuals in $\mathbb{P}'$to fill $\mathbb{E}'$
9: Perform binary tournament selection with replacement to fill the mating pool
10: Apply crossover and mutation to the mating pool
11: **end for**
12: **end procedure**

5.10 CHAPTER CONCLUSIONS

This chapter reviewed different optimization techniques that can be used to solve complex problems. In particular, these techniques can be applied to optimize landscape designs for the production of biofuel feedstock production. In the next chapter, the coupling of the SWAT and GREET model, along with a Multi-Objective Evolutionary Algorithm, as the methodology approach to optimize allocation design in Land-Use and Land-Cover change to produce biofuel feedstock will be explained.

Chapter 6: Methodology

This chapter is dedicated to explaining the methodology approach to optimize the allocation design in Land-Use and Land-Cover change to produce biofuel feedstock. This methodology includes the coupling of the SWAT and GREET models to evaluate the environmental performance on soil and water from replacing regional crops, at the watershed scale, for biofuel crops and their corresponding greenhouse gas emissions associated to the cultivation of these crops and their conversion to biofuel. This methodology also employs a Multi-Objective Evolutionary Algorithm to find the optimal Land-Use and Land-Cover design to increase biomass yields and reduce environmental impacts.

6.1 METHODOLOGY

The main objective of this research is to develop an interactive control model capable of identifying and quantifying the environmental impacts and tradeoffs of land use, land change and management practices on water ecosystem services and atmosphere when traditional land uses are replaced with crops for optimal biofuel production. An integrating modeling approach where hydrologic simulation software and Life Cycle Assessment simulation model are interfaced with a Multi-Objective Optimization Algorithm has significant advantages since no further simplification of the real system, beyond those inherent to the original simulation model, is required. Furthermore, optimal or near-optimal decision alternatives on landscape scenarios are generated through system responses and the optimization algorithm, which can be used as a decision support tool.

In this context, SWAT and GREET were coupled to evaluate LUC and management practices scenarios for biofuel feedstock production. These scenarios are further evaluated with a Multi-Objective Optimization Algorithm to determine optimal LUC and management practice in

order to increase biomass production and decrease the environmental impacts that may occur with the expected increase in biofuel feedstock production.

Figure 6.1 shows the flow chart of the interactive control model coupling SWAT and GREET with the MOEA. First, the GREET's settings and desired pathway are defined. Second, management practices are defined. In this step, SWAT and GREET evaluate the watershed responses from the different land management practices selected. Also, the control model extracts and saves the results in each simulated scenario. These results are later used by the MOEA.

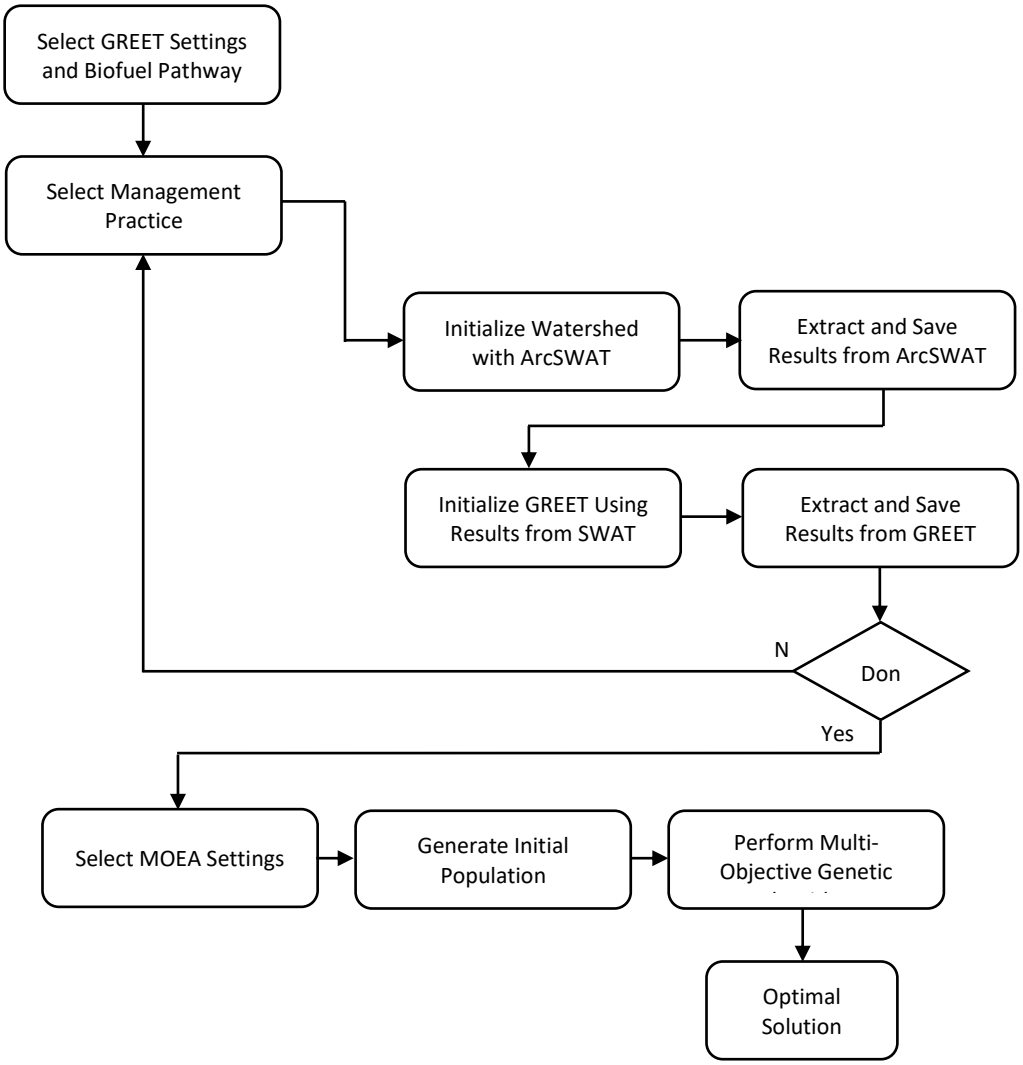

Figure 6.1: Flow Chart of Interactive Control Model

6.2 GREET Settings and Biofuel Pathway

The GREET settings and biofuel pathway selection are executed through a Graphical User Interface (GUI). In this GUI, the users can select different key options for their biofuel production simulation. Figure 6.2 shows the GREET GUI. The Microsoft Excel spreadsheet version of GREET (GREET1_2018.xlsm), specifically the Input worksheet - Section 8, which handles the scenario control variables and input assumptions for the fuel ethanol pathway, is used to interact with the GUI.

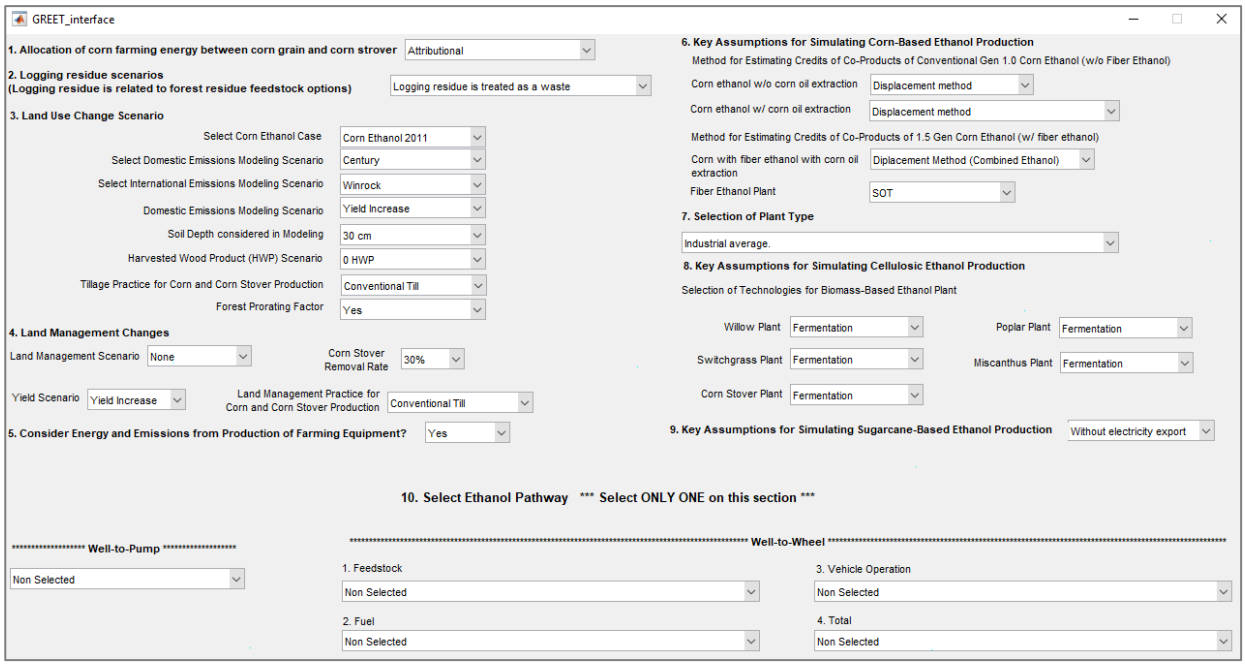

Figure 6.2: Graphical User Interface for GREET

The first category that can be modified for the simulation is the type of allocation of corn farming energy between corn grain and corn stover. The options for this category are: (1) Attributional; (2) Energy allocation; (3) Mass allocation; and (4) Market-value allocation. The second category considers the logging residue scenarios (Logging residue is related to forest residue feedstock options). In this category, the options are: (1) Logging residue is treated as waste; and (2) Logging residue is treated as a co-product.

Next, the Land Use Change scenario include the following categories and options:

1. Select Corn Ethanol Case

a. Corn Ethanol 2011

b. Corn Ethanol 2013

2. Select Domestic Emissions Modeling Scenario

    a. Century

    b. Winrock

    c. Woods Hole

3. Select International Emissions Modeling Scenario

    a. Winrock

    b. Woods Hole

4. Domestic Emissions Modeling Scenario

    a. Yield Increase

    b. Yield Constant

5. Soil Depth considered in Modeling

    a. 30 cm

    b. 100 cm

6. Harvested Wood Product (HWP) Scenario

    a. 0 HWP

    b. Heath

7. Tillage Practice for Corn and Corn Stover Production

    a. Conventional Till

    b. No Till

    c. Reduced Till

    d. US Average

8. Forest Prorating Factor

    a. Yes

    b. No

The third simulation options refer to Land Management Changes Scenarios. The categories and options are as follows:

1. Land Management Scenario
    a. None
    b. Rye Cover Crop
    c. Animal Manure
2. Corn Stover Removal Rate
    a. 30%
    b. 60%
3. Yield Scenario
    a. Yield Increase
    b. Yield Constant
4. Land Management Practice for Corn and Corn Stover Production
    a. Conventional Till
    b. No Till
    c. Reduced Till
    d. US Average

Another simulation option is to consider energy and emissions from the production of farming equipment. These options are Yes or No.

The next simulation options are critical assumptions for simulating corn-based ethanol production. These assumptions are based on the methods for estimating credits and co-products of conventional Gen 1.0 Corn Ethanol (w/o fiber ethanol). The methods available for corn ethanol without corn oil extraction are: (1) Displacement method; (2) Btu-based Allocation; and (3) Market Value-based method. The methods available for corn ethanol with corn oil extraction are: (1) Displacement method; (2) Btu-based Allocation; (3) Market Value-based method; (4) Hybrid allocation method (DGS vs. Ethanol + Corn Oil by Market; Ethanol vs. Corn oil by Energy); (5) Process Level Energy Value-based Allocation; and (6) Marginal Method.

Another set of options for simulating corn-based ethanol production are based on the methods for estimating credits and co-products of 1.5 Gen Corn Ethanol (w/ fiber ethanol). The methods available for corn with fiber ethanol with corn oil extraction are: (1) Displacement Method (Combined Ethanol); and (2) Displacement Method (Separate Ethanol). The methods available for fiber ethanol plant are: (1) SOT; and (2) nth plant.

The next selection for the simulation is the plant type. The different options include the following:

1. Industrial average.
2. User defined average.
3. Plant Specific: Dry Mill with DGS as a process fuel.
4. Plant Specific: Dry Mill with only DDGS as co-product and NG as process fuel.
5. Plant Specific: Dry Mill with only DDGS as co-product and Coal as process fuel.
6. Plant Specific: Dry Mill with only DDGS as co-product and Biomass as process fuel.
7. Plant Specific: Dry Mill with only WDGS as co-product and NG as process fuel.
8. Plant Specific: Dry Mill with only WDGS as co-product and Coal as process fuel.
9. Plant Specific: Dry Mill with only WDGS as co-product and Biomass as process fuel.
10. Plant Specific: Wet Mill with NG as process fuel.
11. Plant Specific: Wet Mill with Coal as process fuel.
12. Plant Specific: Wet Mill with Biomass as process fuel.

An crucial essential assumption for simulating cellulosic ethanol production is the selection of technology for a biomass-based ethanol plant. Willow, poplar switchgrass, miscanthus, and corn stover have the options of being processed using Fermentation or Gasification method.

Similarly, the critical assumptions for simulating sugarcane-based ethanol production can be either (1) Without electricity export or (2) With electricity export.

Finally, the last set of options the user can select refer to the ethanol pathway. This selection will determine system boundary for the LCA, Well-to-Pump (WTP) or Well-to-Wheels (WTW) and the type of ethanol production. The WTP results will provide the CO_2, CH_4 and N_2O emissions from wells to refueling station pumps (in grams per mmBtu of fuel available at fuel pumps). These results are three of the seven optimization objectives in the MOEA. The types of ethanol production for WTP are:

1. Low-Level EtOH blend with Gasoline (E10).
2. E85 for FFV.
3. E85 for Dedi. EtOH Vehicle.

The WTW results provide the CO_2, CH_4 and N_2O emissions for 11 vehicle/fuel systems, each with four different stages: (1) Feedstock; (2) Fuel; (3) Vehicle operation; and (4) Total. The WTW vehicle/fuel systems are:

1. Gasoline Vehicle: Low-Level EtOH with gasoline.
2. EtOH FFV: E85
3. Dedi. EtOH Vehicle: E85
4. SIDI Vehicle: Low-Level EtOH Blend with gasoline (E10)
5. SIDI Dedi. EtOH Vehicle: E85
6. Grid-Independent SI HEV: Low-Level EtOH Blend with gasoline (E10)
7. Grid-Independent SI HEV: E85
8. Grid-Connected SI PHEV: Low-Level EtOH Blend with gasoline CD EtOH LLBlend
9. Grid-Connected SI PHEV: E85
10. Grid-Connected SI PHEV: Low-Level EtOH Blend with gasoline CS EtOH LLBlend
11. Grid-Connected SI PHEV: E85 and Electricity (US Mix) CS EtOH

6.3 Management Practice

The interactive model requires an initial SWAT simulation. The resulting output files for the SWAT simulation that is intended to optimize are used by the Management Practice Interface to rerun SWAT with new management parameter settings. Before selecting the management practices that are desired to evaluate, it is necessary to define the number of HRUs of the initial SWAT simulation. This number needs to be defined only once, and it must remain constant for the entire evaluation. Figure 6.3 shows a new GUI where the number of HRUs are defined. The next step on this GUI is to enter the management file names that correspond to the HRUs that will be excluded for the evaluation of the new management practices. For instance, water or urban HRUs should be excluded from simulating LUC. The management files for each of them should be entered here once at a time by clicking the ADD button each time.

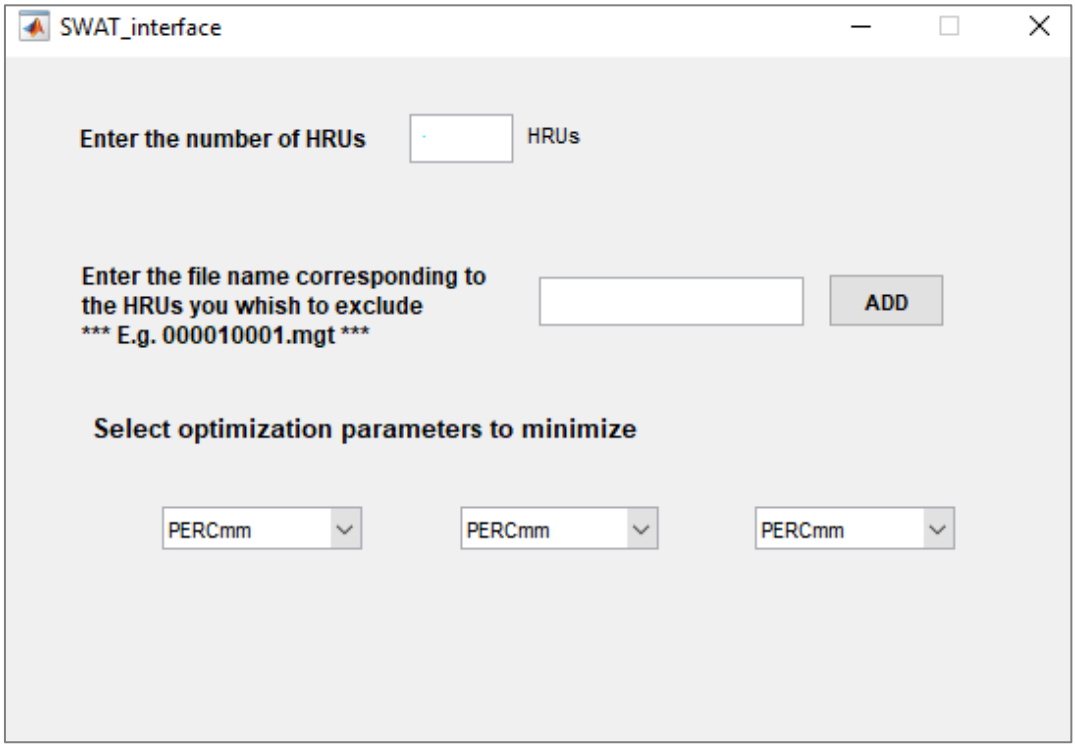

Figure 6.3: SWAT Graphical User Interface

The last step is to select the optimization parameters that will be minimized by the MOEA. The list and description of these parameters are described below:

1. PERCmm. - Water that percolates past the root zone during the time step (mm H2O). There is usually a lag between the time the water leaves the bottom of the root zone and reaches the shallow aquifer. Over a long period of time, this variable should equal groundwater recharge (PERC = GW_RCHG as time $\rightarrow \infty$).
2. GW_RCHGmm. - Recharge entering aquifers during time step (total amount of water entering shallow and deep aquifers during time step) (mm H2O).
3. DA_RCHGmm. - Deep aquifer recharge (mm H2O). The amount of water from the root zone that recharges the deep aquifer during the time step. (shallow aquifer recharge = GW_RCHG - DA_RCHG)
4. SURQ_GENmm. - Surface runoff generated in HRU during time step (mm H2O).
5. SURQ_CNTmm. - Surface runoff contribution to streamflow in the main channel during time step (mm H2O).
6. TLOSSmm. - Transmission losses (mm H2O). Water lost from tributary channels in the HRU via transmission through the bed. This water becomes recharge for the shallow aquifer during the time step. Net surface runoff contribution to the main channel streamflow is calculated by subtracting TLOSS from SURQ
7. LATQGENmm. - Lateral flow generated in HRU during timestep (mm H2O). Water flowing laterally within the soil profile that enters the main channel during time step.
8. GW_Qmm. - Groundwater contribution to streamflow (mm H2O). Water from the shallow aquifer that enters the main channel during the time step. Groundwater flow is also referred to as baseflow.
9. WYLDmm. - Water yield (mm H2O). The total amount of water leaving the HRU and entering main channel during the time step. (WYLD = SURQ + LATQ + GWQ – TLOSS – pond abstractions)
10. SYLDt/ha. - Sediment yield (metric tons/ha). Sediment from the HRU that is transported into the main channel during the time step.

11. USLEt/ha. - Soil loss during the time step calculated with the USLE equation (metric tons/ha). This value is reported for comparison purposes only.
12. NFIXkg/ha. - Nitrogen fixation (kg N/ha). Amount of nitrogen fixed by legumes during the time step.
13. F-MNkg/ha. - Fresh organic to mineral N (kg N/ha). Mineralization of nitrogen from the fresh residue pool to the nitrate (80%) pool and active organic nitrogen (20%) pool during the time step. A positive value denotes a net gain in the nitrate and active organic pools from the fresh organic pool while a negative value denotes a net gain in the fresh organic pool from the nitrate and active organic pools.
14. A-MNkg/ha. - Active organic to mineral N (kg N/ha). Movement of nitrogen from the active organic pool to the nitrate pool during the time step.
15. A-SNkg/ha. - Active organic to stable organic N (kg N/ha). Movement of nitrogen from the active organic pool to the stable organic pool during the time step.
16. F-MPkg/ha. - Fresh organic to mineral P (kg P/ha). Mineralization of phosphorus from the fresh residue pool to the labile (80%) pool (P in solution) and the active organic (20%) pool. A positive value denotes a net gain in solution and active organic pools from the fresh organic pool while a negative value denotes a net gain in the fresh organic pool from the labile and active organic pools.
17. AO-LPkg/ha. - Organic to labile mineral P (kg P/ha). Movement of phosphorus between the organic pool and the labile mineral pool during the time step. A positive value denotes a net gain in the labile pool from the organic pool while a negative value denotes a net gain in the organic pool from the labile pool.
18. DNITkg/ha. - Denitrification (kg N/ha). Transformation of nitrate to gaseous compounds during the time step.
19. NUPkg/ha. - Plant uptake of nitrogen (kg N/ha). Nitrogen removed from soil by plants during the time step.

20. PUPkg/ha. - Plant uptake of phosphorus (kg P/ha). Phosphorus removed from soil by plants during the time step.
21. ORGNkg/ha. - Organic N yield (kg N/ha). Organic nitrogen transported out of the HRU and into the reach during the time step.
22. ORGPkg/ha. - Organic P yield (kg P/ha). Organic phosphorus transported with sediment into the reach during the time step.
23. SEDPkg/ha. - Sediment P yield (kg P/ha). Mineral phosphorus sorbed to sediment transported into the reach during the time step.
24. NSURQkg/ha. - NO3 in surface runoff (kg N/ha). Nitrate transported with surface runoff into the reach during the time step.
25. NLATQkg/ha. - NO3 in lateral flow (kg N/ha). Nitrate transported by lateral flow into the reach during the time step.
26. NO3Lkg/ha. - NO3 leached from the soil profile (kg N/ha). Nitrate that leaches past the bottom of the soil profile during the time step. The nitrate is not tracked through the shallow aquifer.
27. NO3GWkg/ha. - NO3 transported into main channel in the groundwater loading from the HRU (kg N/ha).
28. SOLPkg/ha. - Soluble P yield (kg P/ha). Soluble mineral forms of phosphorus transported by surface runoff into the reach during the time step.
29. P_GWkg/ha. - Soluble phosphorus transported by groundwater flow into main channel during the time step (kg P/ha).
30. BACTPct. - Number of persistent bacteria in surface runoff entering reach (# cfu/100 mL).
31. BACTLPct. - Number of less persistent bacteria in surface runoff entering reach (#cfu/100 mL).
32. TNO3kg/ha. - NO3 in tile (kg N/ha)
33. LNO3kg/ha. - Amount of NO3-N in lateral flow in HRU for the day (kg/N/ha).

After defining these parameters, the next step is to select the type of management practices that are intended to evaluate. Figure 6.4 shows the Management Practice Interface. The management practices selected here will be applied to all HRUs in the simulation, except for those that were excluded in the previous GUI. A fixed scheduling by heat units of 0.15 has been predefined for this operation. The first step is to initiate the growth of a specific land cover/plant type in the HRUs. The plants available are:

1. Alamo Switchgrass
2. Corn
3. Corn Silage
4. Poplar
5. Sorghum Hay
6. Sugarcane
7. Willow
8. Miscanthus

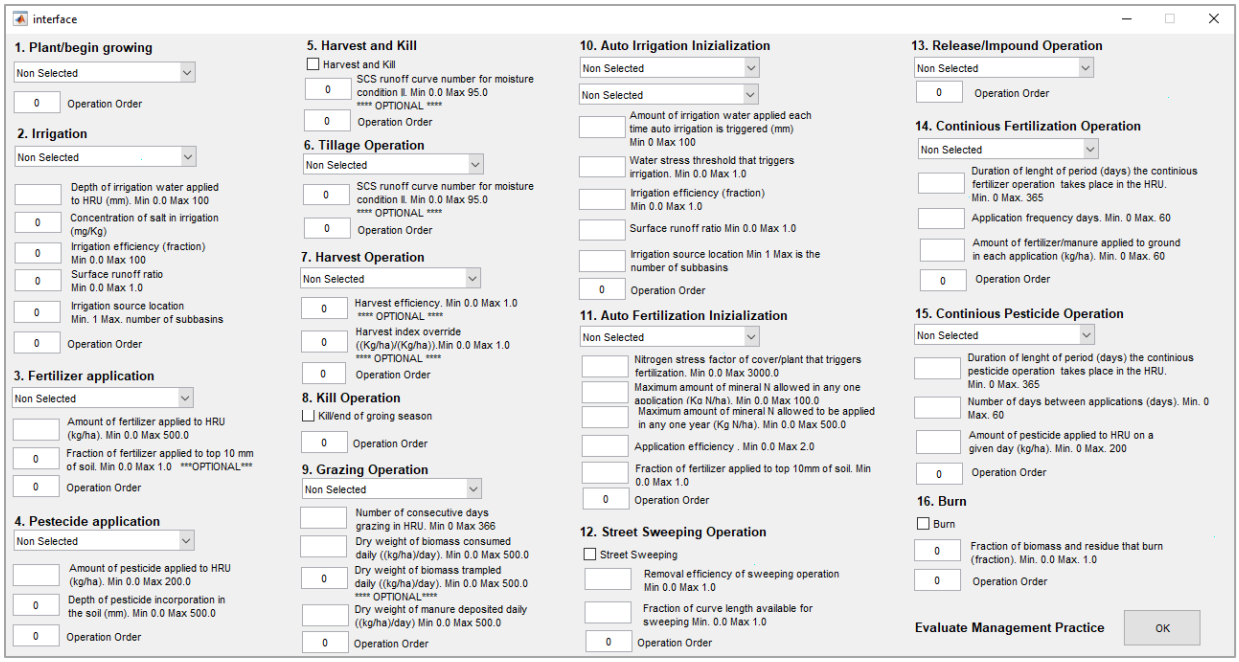

Figure 6.4: Management Practice Interface

In step 2, irrigation can be applied to the HRUs. Irrigation can be obtained from one of the following five types of water sources:

1. Reach
2. Reservoir (must specify reservoir number)
3. Shallow aquifer
4. Deep aquifer
5. Source outside the watershed

If irrigation operation is selected, it is required to specify the depth of irrigation water applied on the HRUs (mm), the concentration of salt in irrigation (mg/kg), the irrigation efficiency (0-1, where 0.1 is 10% of irrigation efficiency) and the surface runoff ratio (0-1, where 0.1 is 10% of surface runoff). Furthermore, unless the water source is outside the watershed, the model must know the location of the water source. If the water supply comes from a reach, shallow aquifer or deep aquifer, the subbasin number in which the source is located must be defined. If the water supply comes from a reservoir, the reservoir number must be defined as well. A fixed scheduling by heat units of 0.15 has been predefined for this operation.

In step 3, fertilizer or manure can be added to the soil. The types of fertilizer/manure that can be selected are listed in table 6.1.

Table 6.1: Fertilizers and manure

1. Elemental Nitrogen	15. 24-06-00	29. 10-20-20	43. 00-06-00
2. Elemental Phosphorous	16. 22-14-00	30. 10-10-10	44. Dairy-Fresh Manure
3. Anhydrous Ammonia	17. 20-20-00	31. 08-15-00	45. Beef-Fresh Manure
4. Urea	18. 18-46-00	32. 08-08-00	46. Veal-Fresh Manure
5. 46-00-00	19. 18-04-00	33. 07-07-00	47. Swine-Fresh Manure
6. 33-00-00	20. 16-20-20	34. 07-00-00	48. Sheep-Fresh Manure
7. 31-13-00	21. 15-15-15	35. 06-24-24	49. Goat-Fresh Manure
8. 30-80-00	22. 15-15-00	36. 05-10-15	50. Horse-Fresh Manure
9. 30-15-00	23. 13-13-13	37. 05-10-10	51. Layer-Fresh Manure
10. 28-10-10	24. 12-20-00	38. 05-10-05	52. Broiler-Fresh Manure
11. 28-03-00	25. 11-52-00	39. 04-08-00	53. Turkey-Fresh Manure
12. 26-13-00	26. 11-15-00	40. 03-06-00	54. Duck -Fresh Manure
13. 25-05-00	27. 10-34-00	41. 02-09-00	
14. 25-03-00	28. 10-28-00	42. 00-15-00	

If the fertilizer operation is selected, the amount of the fertilizer must also be defined. Since surface runoff interacts with the top 10 mm of soil, the fraction of fertilizer that is applied to the top 10 mm can also be specified. The remainder fraction amount will be added to the first soil layer. If the fraction is set to 0, the model applies 80% of the fertilizer to the first soil layer and 20% to the top 100 mm. A fixed scheduling by heat units of 0.15 has been predefined for this operation.

In step 4, a pesticide can be added to the soil. The types of pesticides that can be selected are listed in table 6.2.

Table 6.2: Pesticides

1. Silvex	60. Clomazone	119. Dicofol	178. Iprodione
2. Mecoprop Amine	61. Fluometuron	120. Pronamide	179. Maleic Hydrazide
3. Atrazine	62. Terbufos	121. Fosamine Ammon. Salt	180. Fenarimol
4. Temephos	63. Triclopyr Amine	122. Methomyl	181. Dipropetryn
5. Chlorobenzilate	64. Profenofos	123. Cyromazine	182. Hexythiazox
6. Endothall Salt	65. Dimethoate	124. Thiodicarb	183. Imazaquin Ammonium
7. Fenoxaprop-Ethyl	66. Dodine Acetate	125. Alachlor	184. Metribuzin
8. Naptalam Sodium Salt	67. Malathion	126. Amidochlor	185. Carbaryl
9. Daminozide	68. 2,4-D Acid	127. Clopyralid	186. Terbacil
10. Aldrin	69. DCPA	128. Linuron	187. Methiocarb
11. Fosetyl-Aluminum	70. Dalapon Sodium Salt	129. Clorpyrifos	188. Ethalfluralin
12. Metsulfuron-Methyl	71. Fensulfothion	130. Maneb	189. Diazinon
13. Chloramben Salts	72. DDT	131. Methoxychlor	190. Tebuthiuron
14. NAA Amide	73. MCPA Amine	132. Aminocarb	191. Chlorpropham
15. Amitrol	74. Tribufos	133. Fluvalinate	192. Propanil
16. Cypermethrin	75. Arsenic Acid	134. Oxydemeton-Methyl	193. Methidathion
17. Diethatyl-Ethyl	76. Napropamide	135. Propazine	194. Oryzalin
18. Ancymidol	77. Disulfoton	136. Isazofos	195. Butylate
19. Imazapyr Acid	78. Naled	137. Amitraz	196. Phosphamidon
20. MSMA	79. Dieldrin	138. Bifenox	197. Acifluorfen
21. Esfenvalerate	80. Diflubenzuron	139. Methamidophos	198. Bifenthrin
22. Imazamethabenz-m	81. Dinoseb Phenol	140. Oxythioquinox	199. Tridiphane
23. Imazamethabenz-p	82. Diquat Dibromide	141. Fenamiphos	200. Phenthoate
24. Quizalofop-Ethyl	83. Mancozeb	142. Fenamiphos Sulfone	201. Bendiocarb
25. Asulam Sodium Salt	84. Dalapon	143. Fenamiphos Sulfoxide	202. Thiabendazole
26. Difenzoquat	85. Thidiazuron	144. Ethofumesate	203. Aldicarb
27. Monocrotophos	86. Methanearsonic Acid Na	145. Prochloraz	204. Aldicarb Sulfone
28. Benefin	87. Triphenyltin Hydroxide	146. Isofenphos	205. Aldicarb Sulfoxide
29. Propamocarb	88. Metolachlor	147. Acephate	206. Chloroxuron
30. Dicamba	89. Fonofos	148. Captan	207. Terbutryn
31. Bentazon	90. Trichlorfon	149. Sulfometuron-Methyl	208. PCNB
32. Glufosinate Ammonia	91. Diphenamid	150. Flucythrinate	209. Chloroneb
33. Triadimefon	92. Anilazine	151. Methyl Parathion	210. Etridiazole
34. Fenthion	93. DNOC Sodium Salt	152. Toxaphene	211. Phorate
35. Cyfluthrin	94. EPN	153. Mevinphos	212. Endosulfan
36. Benomyl	95. EPTC	154. Phoskil Parathion (Ethyl)	213. Thiram

37. BHC	96. Ethion	155. Piperalin	214. MCPB Sodium Salt
38. Phenmedipham	97. Ametryn	156. Mepiquat Chlor. Salt	215. Pebulate
39. Desmedipham	98. Norflurazon	157. Oxycarboxin	216. Propiconazole
40. Dicrotophos	99. Triallate	158. Sethoxydim	217. Profluralin
41. Cyanazine	100. Fenac	159. Metiram	218. Thiophanate-Methyl
42. Thiobencarb	101. Fenitrothion	160. Permethrin	219. Picloram
43. Sulprofos	102. 3-CPA Sodium Salt	161. Prometon	220. Tralomethrin
44. MCPA Ester	103. Chlordimeform Hydroclo.	162. Bensulide	221. Trifluralin
45. DCNA (Dicloran)	104. Triforine	163. Paraquat	222. NAA Ethyl Ester
46. Chlorothalonil	105. Carbofuran	164. Flumetralin	223. Siduron
47. Bromoxynil Octan. Ester	106. Fluazifop-P-Butyl	165. Simazine	224. Triclopyr Ester
48. 2,4-DB Ester	107. Chlorsulfuron	166. Methazole	225. Hexazinone
49. Prometryn	108.Oxyfluorfen	167. Pendimethalin	226. Fenbutatin Oxide
50. Ferbam	109. Azinphos-Methyl	168. AC 263,499	227. Vernolate
51. Dichlobenil	110. Thifensulfuron-Methyl	169. Fenvalerate	228. Petroleum oil
52. Formetanate Hydrochlor	111. Dimethipin	170. Pyrazon	229. Oxamyl
53. Ethephon	112. Diclofop-Methyl	171. Propaclor	230. 2,4-D amine
54. Propham (IPC)	113. Bromacil	172. Fomesafen	231. 2,4,5-T Amine
55. Chlordane	114. Phosmet	173. 2,4-DB Sodium Amine	232. Dichlorprop Ester
56. Imazapyr Amine	115. Lindane	174. Metalaxyl	233. Phosalone
57. Chlorimuron-ethyl	116. Lambda-Cyhalothrin	175. Cycloate	
58. Lactofen	117. Dinocap	176. Oxadiazon	
59. Propargite	118. Diuron	177. Glyphosate Amine	

A fixed scheduling by heat units of 0.15 has been predefined for this operation. The variable that must be entered in this operation is the amount of pesticide applied to the HRUs (kg/ha). Also, the depth of pesticide incorporation in the soil (mm) may be defined. However, if this variable is left blank, the model assumes that the pesticide is applied to the surface.

In step 5, the land cover/plant type previously described is harvested as yield from the HRUs and transforms the remaining plant biomass to residue on the soil surface. A fixed scheduling by heat units of 1.2 has been predefined for this operation. Also, an optional variable for SCS runoff curve number for moisture condition II may be specified.

In step 6, residue, nutrients, pesticides, and bacteria are redistributed in the soil profile. For this operation, a fixed scheduling by heat units of 0.15 has been predefined. Also, it is optional to update the moisture condition II curve number. Table 6.3 lists the different types of tillage operations that can be selected.

Table 6.3: Tillage Operations

1. Generic Fall Plowing Operation	54. Rubber-wheel Weed Puller
2. Generic Spring Plowing Operation	55. Multi-weeder
3. Generic Conservation Tillage	56. Moldboard Plow Reg Ge10b
4. Generic No-Till Mixing	57. Chisel Plow Gt21ft
5. Duckfoot Cultivator	58. Chisel Plow Gt15ft
6. Field Cultivator Ge15ft	59. Chisel Plow Le15ft
7. Field Cultivator Lt15ft	60. Coulter-chisel Plow
8. Furrow-out Cultivator	61. Disk Plow Ge23ft
9. Marker (Cultivator)	62. Disk Plow Lt23ft
10. Rolling Cultivator Ge15ft	63. Moldboard Plow Reg 4-6b
11. Rolling Cultivator Lt15ft	64. Moldboard Plow Reg Ge7b
12. Row Cultivator Ge15ft	65. Moldboard Plow Reg Le3b
13. Row Cultivator Lt15ft	66. Moldboard Plow 2-way 4-6b
14. Discovator	67. Moldboard Plow 2-way Ge7b
15. Leveler	68. Moldboard Plow 2-way Le3b
16. Harrow 10 Bar Tine 36 Ft	69. Stubble-mulch Plow Gt15ft
17. Culti-mulch Roller Ge18ft	70. Stubble-mulch Plow Le15ft
18. Culti-mulch Roller Lt18ft	71. Subsoil Chisel Plow
19. Culti-packer Pulverizer	72. Row Conditioner 1 Row
20. Land Plane-leveler	73. Hipper 1 Row
21. Landall, Do-all	74. Rice Roller
22. Laser Planer	75. Paraplow
23. Levee-plow-disc	76. Subsoiler-bedder Hip-rip
24. Float	77. Deep Ripper- Subsoiler
25. Field Cond (scratcher)	78. V-ripper
26. Lister (middle-buster)	79. Bed Roller 4 Row
27. Roller Groover	80. Bedder (disk)
28. Roller Packer Attachment	81. Bedder Disk-hipper
29. Roller Packer Flat Roller	82. Bedder Disk-row
30. Sand-fighter	83. Bedder Shaper
31. Seedbed Roller	84. Disk Border Maker
32. Crust Buster	85. Disk Chisel (mulch Tiller)

33. Roller Harrow 15 Ft	86. Offset Dis/heavduty Ge19ft
34. Triple K	87. Offset Dis/heavduty Le13ft
35. Cultivator 1 Row	88. Offset Dis/heavduty14-18ft
36. Finishing Harrow Ge15ft	89. Offset Dis/lghtduty Ge19ft
37. Finishing Harrow Lt15ft	90. Offset Dis/lghtduty Le13ft
38. Flex-tine Harrow Cl Ge20ft	91. Offset Dis/lghtduty14-18ft
39. Flex-tine Harrow Cl Lt20ft	92. One-way (disk Tiller)
40. Powered Spike Tooth Harrow	93. Tandem Disk Plw Ge19ft
41. Spike Tooth Harrow Gt25ft	94. Tandem Disk, Plw Le13ft
42. Spike Tooth Harrow Le25ft	95. Tandem Disk Reg 14-18ft
43. Springtooth Harrow Ge15ft	96. Tandem Disk Reg Ge19ft
44. Springtooth Harrow Lt15ft	97. Tandem Disk Reg Le13ft
45. Soil Finisher	98. Tandem Disk Plw 14-18ft
46. Rotary Hoe	99. Single Disk
47. Roterra	100. Power Mulcher
48. Roto-tiller	101. Blade 10 Ft
49. Rotovator-bedder	102. Furrow Diker
50. Rowbuck	103. Bedder Disk-Beet Cultivator 8 Row
51. Ripper 10 Ft	104. Cultiweeder 36 Ft
52. Middle Buster 1 Row	105. Packer 40 Ft
53. Rod Weeder	106. Rodweeder/10 Bar Har 36ft

In step 7, harvest operation, grain or plant biomass is removed without killing the plant. A fixed scheduling by heat units of 0.15 has been predefined for this operation. This operation has the option of setting a harvest efficiency to define the fraction of yield biomass removed by the harvesting equipment. If the fraction is close to zero, the biomass cutting clippings are left on the ground. If the fraction is 1.0, all cut biomass is removed. When the harvest efficiency is not set, or zero is entered, the fraction is automatically set to 1.00. Therefore, the entire yield is removed from the HRUs. Another option is to define the harvest index override ((kg/ha)/(kg/ha)). This parameter forces the ratio of yield to total aboveground biomass to the defined value and must be used to specify the amount of biomass cut.

In step 8, kill operation, the plant growth in the HRUs is stopped, and all plant biomass is transformed into residue. The only information required on this operation is the timing, which has been fixed to 0.15 heat units.

In step 9, grazing operation, plant biomass removal, and manure deposition over a specified period are simulated. It is used to mimic pasture or range grazed by animals. A fixed scheduling by heat units of 0.15 has been predefined for this operation. The information required in this operation is the number of consecutive days of the grazing period, the amount of dry weight consumed daily, the amount of manure deposited daily, and the type of manure, which are listed in table 6.4. An optional input is the daily amount of biomass trampled.

Table 6.4: Grazing operations

1. Dairy-Fresh Manure	7. Horse-Fresh Manure
2. Beef-Fresh Manure	8. Layer-Fresh Manure
3. Veal-Fresh Manure	9. Broiler-Fresh Manure
4. Swine-Fresh Manure	10. Turkey-Fresh Manure
5. Sheep-Fresh Manure	11. Duck-Fresh Manure
6. Goat-Fresh Manure	

In step10, auto irrigation initialization, water is applied to the plants as needed. A fixed scheduling by heat units of 0.15 has been predefined for this operation. Automatic irrigation can be triggered either by plant water demand or by soil water content. If auto irrigation is selected, the type of water body the irrigation water is being diverted from must be identified. The options are:

1. Divert water from reach
2. Divert water from reservoir
3. Divert water from shallow aquifer
4. Divert water from deep aquifer
5. Divert water from unlimited source outside the watershed

The source location is specified by entering the number of the reach that water is removed from, the number of the reservoir that the water is removed from, or the number of the subbasin that the water is removed from. The source location is not specified when water is obtained from an unlimited source outside the watershed. The water stress threshold that triggers irrigation must also be specified. The water stress threshold is a fraction of potential plant growth when water

stress is based on plant water demand. If the plant growth falls below this fraction due to water stress, the amount of irrigation water selected will be applied to the HRU (mm) (0.0-100). The factor ranges from 0 to 1. A zero factor indicates no growth of the plant, while a factor of 1 indicates no decrease in plant growth due to water stress. Usually, this factor is set between 0.90 and 0.95. On the other hand, the water stress threshold is the soil water deficit below field capacity (mm H_2O) when the water stress is based on soil water deficit. The model will apply irrigation water when the water content of the soil profile falls below the fraction. In both cases, water will be added to the soil until it is at field capacity if enough water is available from the irrigation source. Irrigation efficiency (0.0-100) and surface runoff ratio (0-1, where 0.1 is 10% surface runoff) also must be specified in this operation.

In step 11, auto fertilization, a nitrogen stress threshold factor applies fertilization in the HRUs. If this operation is used, one fertilizer from table 6.1 must be selected. A fixed scheduling by heat units of 0.15 has been predefined for this operation. Like the water stress threshold, the factor ranges from 0 to 1. A zero factor indicates no growth of the plant, while a factor of 1 indicates no decrease in plant growth due to nitrogen stress. Likewise, this factor is usually set between 0.90 and 0.95. The fraction of total fertilizer applied to the soil surface (0-1), applies the fraction of fertilizer to the top 10 mm of the soil. The remaining fraction is applied below this soil layer. The model sets a fraction of 0.2 if this variable is left in blank. Similarly, if the maximum amount of fertilizer that can be applied during the year (kg N/ha) and the maximum amount of fertilizer that can be applied in any one application (kg N/ha) are left in blank, the model will set these values to 300 and 200, respectively. The application efficiency ranges from 0 to 2. When the efficiency is equal to 1, enough fertilizer is applied to replace the amount of nitrogen removed at harvest. When the efficiency is less than 1, the fertilizer is applied to meet harvest removal plus an extra amount to compensate nitrogen lost during runoff. When the efficiency is greater than 1, the fertilizer is applied at the specified fraction below the amount removed at harvest. When this fraction is left in blank, auto efficiency is set to 1.3.

Although step 12, street sweeping operation, is part of the management practices available in SWAT, this operation is disabled in the management practice interface because urban areas are not considered for LUC.

In step 13, release/impound operation, HRUs can be defined as potholes. These are closed depressional areas, where the drainage network is poorly developed. A fixed scheduling by heat units of 0.15 has been predefined for this operation. The release/impound action options are: (1) initiate water impoundment; or (2) initiate water release.

In step 14, continuous fertilizer operation, manure is distributed across the HRUs. A fixed scheduling by heat units of 0.15 has been predefined for this operation. If this operation is used, one of the fertilizers in table 6.1 must be selected. Also, the application frequency (days), the amount of fertilizer applied to the ground (kg/ha) and the duration (days) the continuous fertilizer operation takes place in the HRUs must be defined.

In step 15, continuous pesticide operation, the same variables as in the continuous fertilizer operation must be defined. The types of pesticide options are listed in table 6.2.

In the last step 16, burn operation, a fraction of biomass and residue that remains after it burns is required. A fixed scheduling by heat units of 0.15 has been predefined for this operation.

In every step mentioned, there is a field called operation order. This number identifies the order sequence of the operations. For every management practice evaluated, a fixed skip a year operation is scheduled.

Once the first management practice is defined, it is necessary to evaluate it by clicking the OK button on the bottom right corner of the management practice interface. This button will change the operation schedule on the management files (.mgt) from the initial SWAT simulation, as seen in figures 6.5 and 6.6. These figures show the management files for HRU 1 (000010001.mgt) before and after the operation schedule is changed.

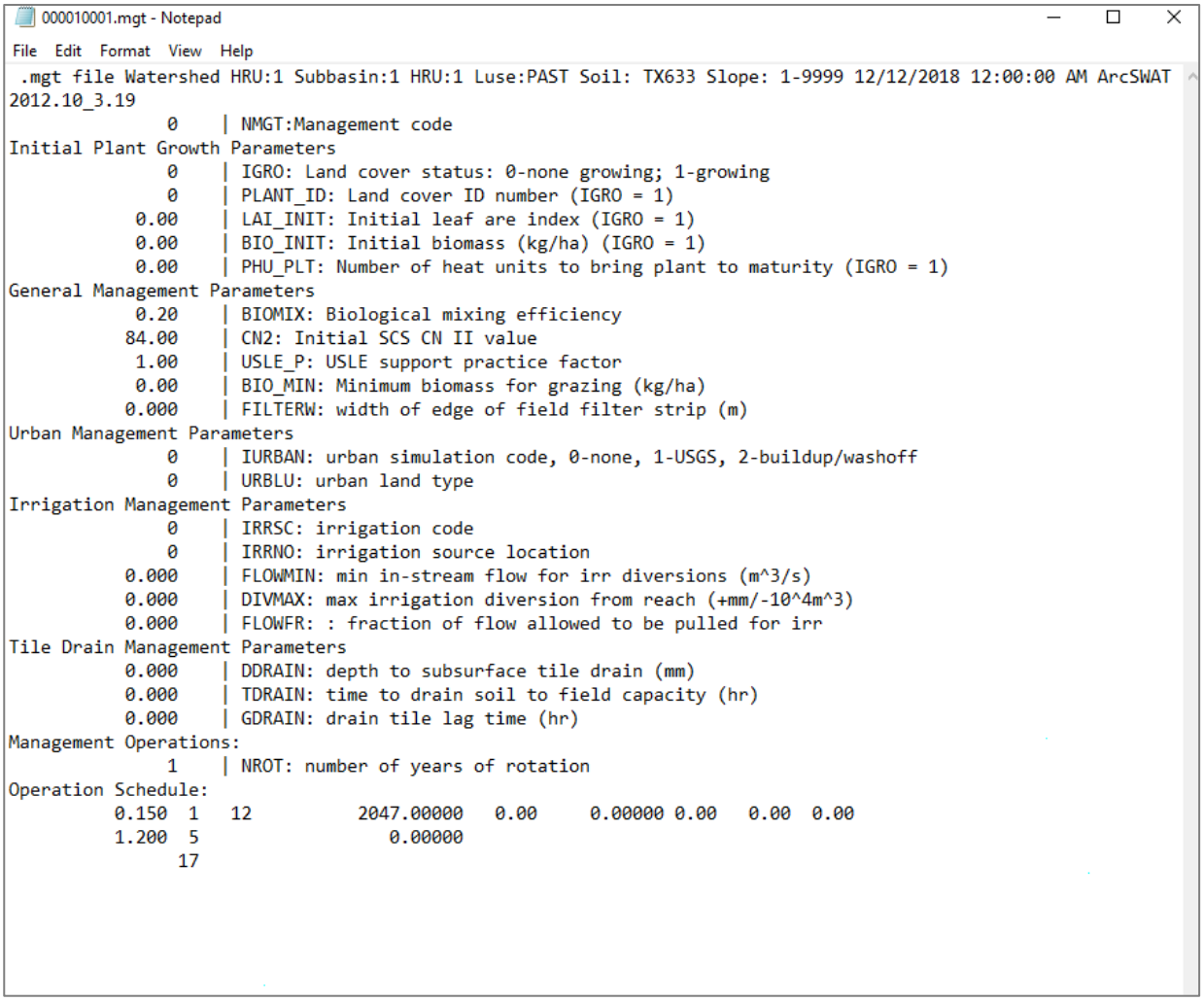

Figure 6.5: Initial Management File

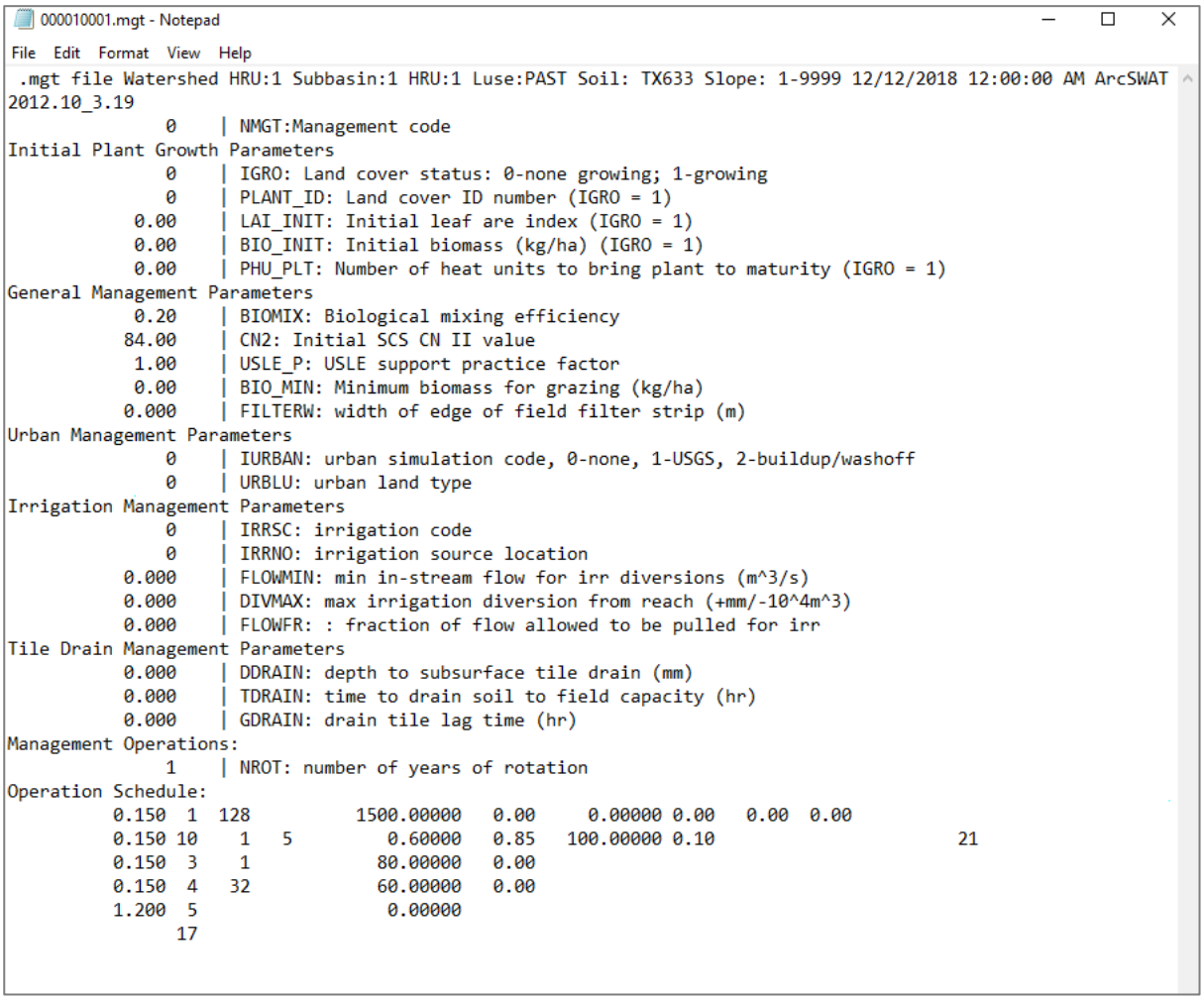

Figure 6.6: New Management Operation Schedule

Once these files are changed, the interface initiates a SWAT rerun using these new files and start the development of result tables that will be later used by the MOEA.

In order to evaluate a different management practice, it is necessary to change the parameters and click OK again. This will create a second result table for the MOEA. The user can evaluate as many management practices as desired.

6.4 RESULT TABLES

Every time a management practice is evaluated, a result table for that management practice is created. The size of the table is an 8xHRU matrix, where HRU is the number of HRUs in the simulation. An example of one result table for a simulation with 8 HRUs is demonstrated in figure

6.7. The columns identify the number of every HRU. The first row identifies the number of management practice. In this example, the table corresponds to the first management practice evaluated. The second row saves the results of biomass for each HRU. Rows 3, 4, and 5 save the results from the optimization parameters selected in the SWAT interface. Rows 6, 7 and 8 save the CO_2, CH_4, and N_2O results from the GREET ethanol pathway selected in the GREET GUI. In the MOEA, the objective is to maximize row 2 and minimize rows 3, 4, 5, 6, 7, and 8. More details about this are provided in the following subsection. The process in which these values are obtained is explained next.

HRU	1	2	3	4	5	6	7	8
Management Practice	1	1	1	1	1	1	1	1
Maximize	Biomass Yield	Biomass Yield	Biomass Yield	Biomass Yield	Biomass Yield	Biomass Yield	Biomass Yield	Biomass Yield
Minimize	SWAT GUI 1	SWAT GUI 1	SWAT GUI 1	SWAT GUI 1	SWAT GUI 1	SWAT GUI 1	SWAT GUI 1	SWAT GUI 1
Minimize	SWAT GUI 2	SWAT GUI 2	SWAT GUI 2	SWAT GUI 2	SWAT GUI 2	SWAT GUI 2	SWAT GUI 2	SWAT GUI 2
Minimize	SWAT GUI 3	SWAT GUI 3	SWAT GUI 3	SWAT GUI 3	SWAT GUI 3	SWAT GUI 3	SWAT GUI 3	SWAT GUI 3
Minimize	CO_2	CO_2	CO_2	CO_2	CO_2	CO_2	CO_2	CO_2
Minimize	CH_4	CH_4	CH_4	CH_4	CH_4	CH_4	CH_4	CH_4
Minimize	N_2O	N_2O	N_2O	N_2O	N_2O	N_2O	N_2O	N_2O

Figure 6.7: Example of Result Table

After the SWAT management files are modified to the new management practice setting, the interface calls for a SWAT rerun, using these new files. When the simulation execution is finalized, the output.std file is used to extract the biomass values for each HRU. Figure 6.8 shows an example of the output.std file. These values are saved in row 2 of the result table, which corresponds to biomass yield.

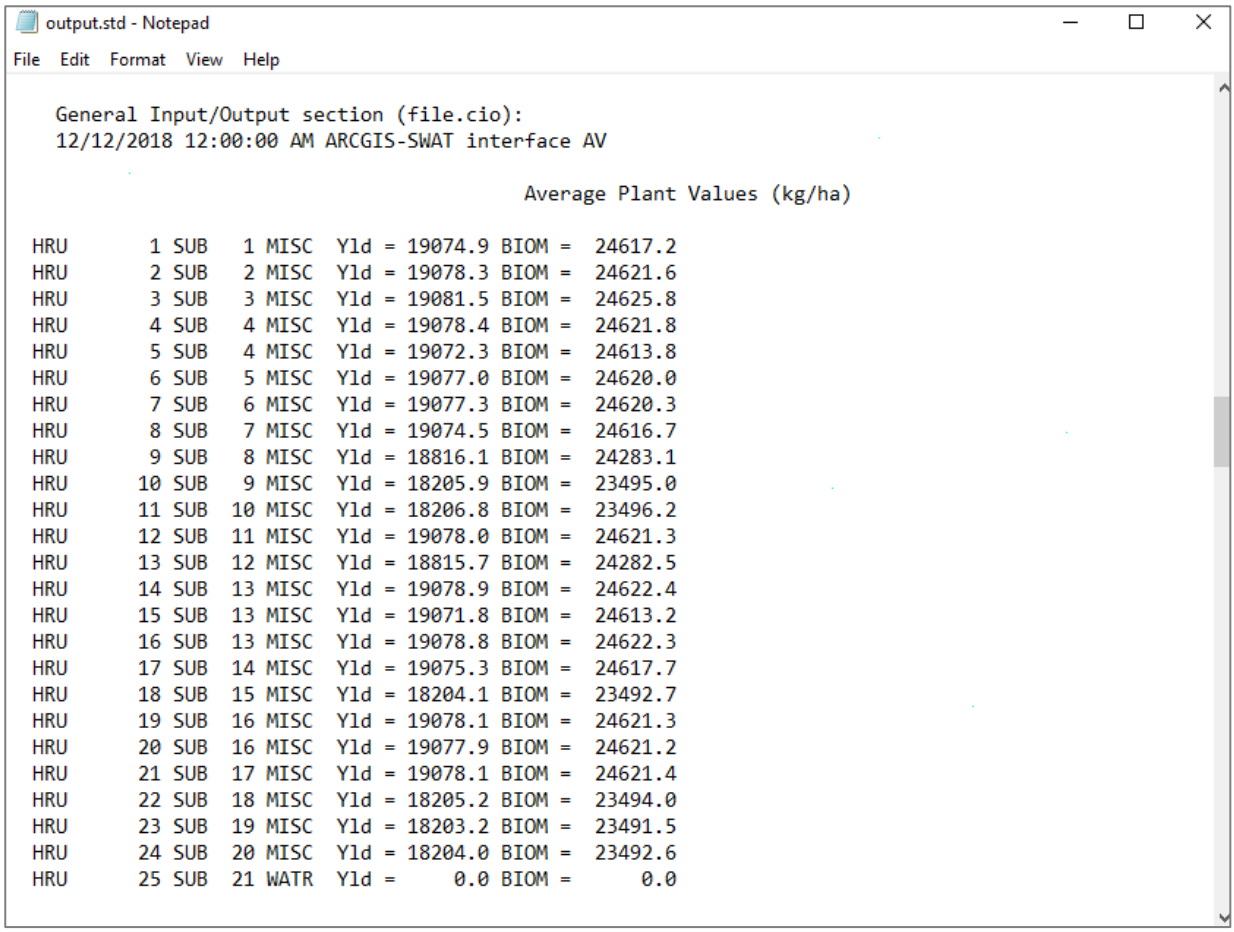

Figure 6.8: Example of the output.std file

Similarly, the parameters selected in the SWAT interface are extracted from the output.hru file. This file contains the output information for every HRU, for every year simulated. At the end of the file, the average values for each HRU of the entire simulation are provided. The average values that correspond to the parameters selected are saved in rows 3, 4, and 5 in the result tables. An example of the output.hru file is shown in figure 6.9.

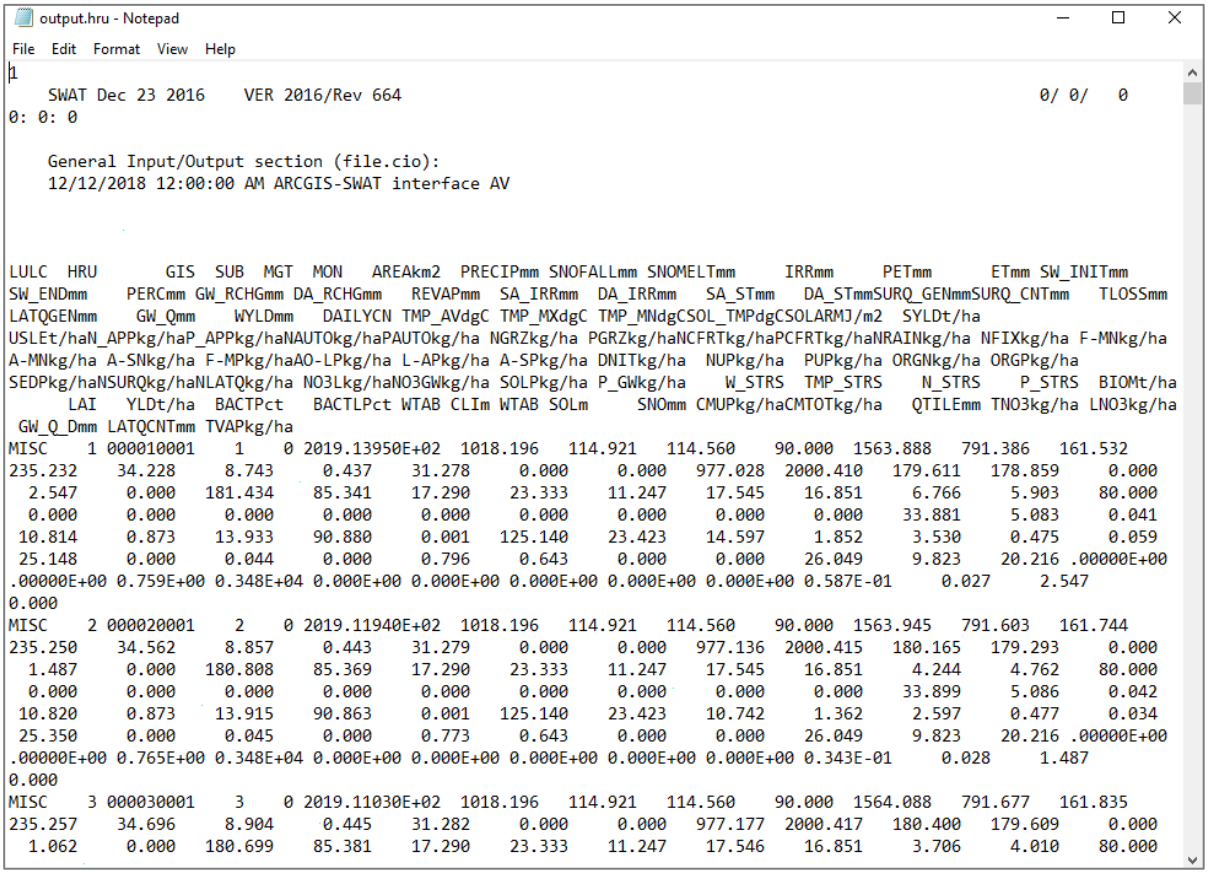

output.hru - Notepad

File Edit Format View Help

```
1
    SWAT Dec 23 2016    VER 2016/Rev 664                                                    0/ 0/   0
0: 0: 0

    General Input/Output section (file.cio):
    12/12/2018 12:00:00 AM ARCGIS-SWAT interface AV



LULC  HRU       GIS  SUB  MGT  MON   AREAkm2  PRECIPmm SNOFALLmm SNOMELTmm     IRRmm     PETmm      ETmm SW_INITmm
SW_ENDmm    PERCmm GW_RCHGmm DA_RCHGmm   REVAPmm  SA_IRRmm  DA_IRRmm   SA_STmm   DA_STmmSURQ_GENmmSURQ_CNTmm   TLOSSmm
LATQGENmm    GW_Qmm    WYLDmm   DAILYCN TMP_AVdgC TMP_MXdgC TMP_MNdgCSOL_TMPdgCSOLARMJ/m2  SYLDt/ha
USLEt/haN_APPkg/haP_APPkg/haNAUTOkg/haPAUTOkg/ha NGRZkg/ha PGRZkg/haNCFRTkg/haPCFRTkg/haNRAINkg/ha NFIXkg/ha F-MNkg/ha
A-MNkg/ha A-SNkg/ha F-MPkg/haAO-LPkg/ha L-APkg/ha A-SPkg/ha DNITkg/ha  NUPkg/ha  PUPkg/ha ORGNkg/ha ORGPkg/ha
SEDPkg/haNSURQkg/haNLATQkg/ha NO3Lkg/haNO3GWkg/ha SOLPkg/ha P_GWkg/ha    W_STRS  TMP_STRS    N_STRS    P_STRS  BIOMt/ha
      LAI   YLDt/ha  BACTPct   BACTLPct WTAB CLIm WTAB SOLm     SNOmm CMUPkg/haCMTOTkg/ha   QTILEmm TNO3kg/ha LNO3kg/ha
 GW_Q_Dmm LATQCNTmm TVAPkg/ha
MISC    1 000010001    1    0 2019.13950E+02  1018.196   114.921   114.560    90.000  1563.888   791.386   161.532
235.232    34.228     8.743     0.437    31.278     0.000     0.000   977.028  2000.410   179.611   178.859     0.000
  2.547     0.000   181.434    85.341    17.290    23.333    11.247    17.545    16.851     6.766     5.903    80.000
  0.000     0.000     0.000     0.000     0.000     0.000     0.000     0.000     0.000    33.881     5.083     0.041
 10.814     0.873    13.933    90.880     0.001   125.140    23.423    14.597     1.852     3.530     0.475     0.059
 25.148     0.000     0.044     0.000     0.796     0.643     0.000     0.000    26.049     9.823    20.216 .00000E+00
.00000E+00 0.759E+00 0.348E+04 0.000E+00 0.000E+00 0.000E+00 0.000E+00 0.000E+00 0.587E-01     0.027     2.547
0.000
MISC    2 000020001    2    0 2019.11940E+02  1018.196   114.921   114.560    90.000  1563.945   791.603   161.744
235.250    34.562     8.857     0.443    31.279     0.000     0.000   977.136  2000.415   180.165   179.293     0.000
  1.487     0.000   180.808    85.369    17.290    23.333    11.247    17.545    16.851     4.244     4.762    80.000
  0.000     0.000     0.000     0.000     0.000     0.000     0.000     0.000     0.000    33.899     5.086     0.042
 10.820     0.873    13.915    90.863     0.001   125.140    23.423    10.742     1.362     2.597     0.477     0.034
 25.350     0.000     0.045     0.000     0.773     0.643     0.000     0.000    26.049     9.823    20.216 .00000E+00
.00000E+00 0.765E+00 0.348E+04 0.000E+00 0.000E+00 0.000E+00 0.000E+00 0.000E+00 0.343E-01     0.028     1.487
0.000
MISC    3 000030001    3    0 2019.11030E+02  1018.196   114.921   114.560    90.000  1564.088   791.677   161.835
235.257    34.696     8.904     0.445    31.282     0.000     0.000   977.177  2000.417   180.400   179.609     0.000
  1.062     0.000   180.699    85.381    17.290    23.333    11.247    17.546    16.851     3.706     4.010    80.000
```

Figure 6.9: Example of output.hru file

Since GREET calculates emissions of greenhouse gases based on the energy consumption from the field, the biomass values (kg/ha) obtained in SWAT are multiplied to the farming energy use suggested in the GREET excel input spreadsheet and then converted to imperial tons. The farming energy use per dry ton harvested for each crop are shown in table 6.5.

Table 6.5: Farming Energy Use

Crop	**Farming energy use: Btu**
Corn (per bushel)	6,924
Willow (per d.ton harvested)	185,416
Poplar (per d.ton harvested)	268,597
Switchgrass (per d.ton harvested)	59,361
Miscanthus (per d.ton harvested)	45,433
Corn Stover (per d.ton collected)	192,500
Forage sorghum (per wet tonne)	60,014
Sugarcane (per tonne)	95,000

In GREET, greenhouse gas emissions derived from the use of fertilizers and pesticides are calculated based on the energy required to their manufacture. In order to obtain these GHG emissions, GREET requires the amounts of fertilizer and pesticide use in grams. Therefore, it is necessary to calculate the total amount of fertilizer and pesticide use in each HRU and convert this amount to grams, since the amount specified in the management practice interface are in kg/ha. This is calculated with the product of each HRU area and amount entered in the management practice interface. Each HRU area is obtained in the input.std file, as seen in figure 6.10.

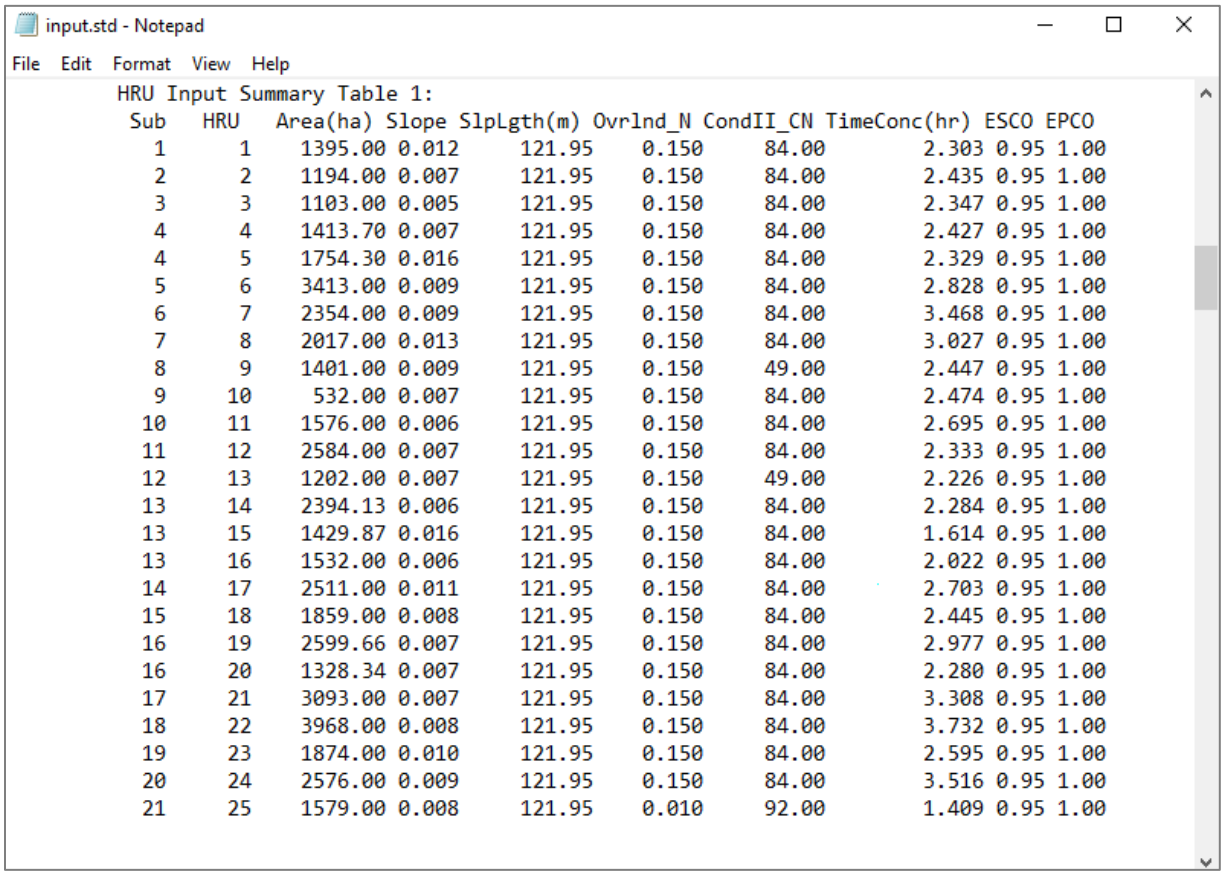

Figure 6.10: Example of input.std file

The calculated farming energy use and the grams of fertilizer and pesticide use for each HRU individually are sent to the GREET_2018 spreadsheet and the output CO_2, CH_4 and N_2O emissions that correspond to the ethanol pathway selected in the GREET interface are saved in rows 6, 7 and 8, respectively.

This process is repeated when new management practices are evaluated. New results are saved in separate tables so that they can be later used by the MOEA. This methodology is explained in the next subsection.

6.5 MOEA

The optimization methodology implemented to the interactive control model was developed by Taboada and Coit (2008), which modifies certain aspects from numerous metaheuristic methods to accomplish quality approximations to global optimal solutions. In this MOEA, three different fitness functions are adjusted to ensure that multiple objectives are all taken into account when searching for the optimal solution. Figure 6.11 shows the MOEA flowchart.

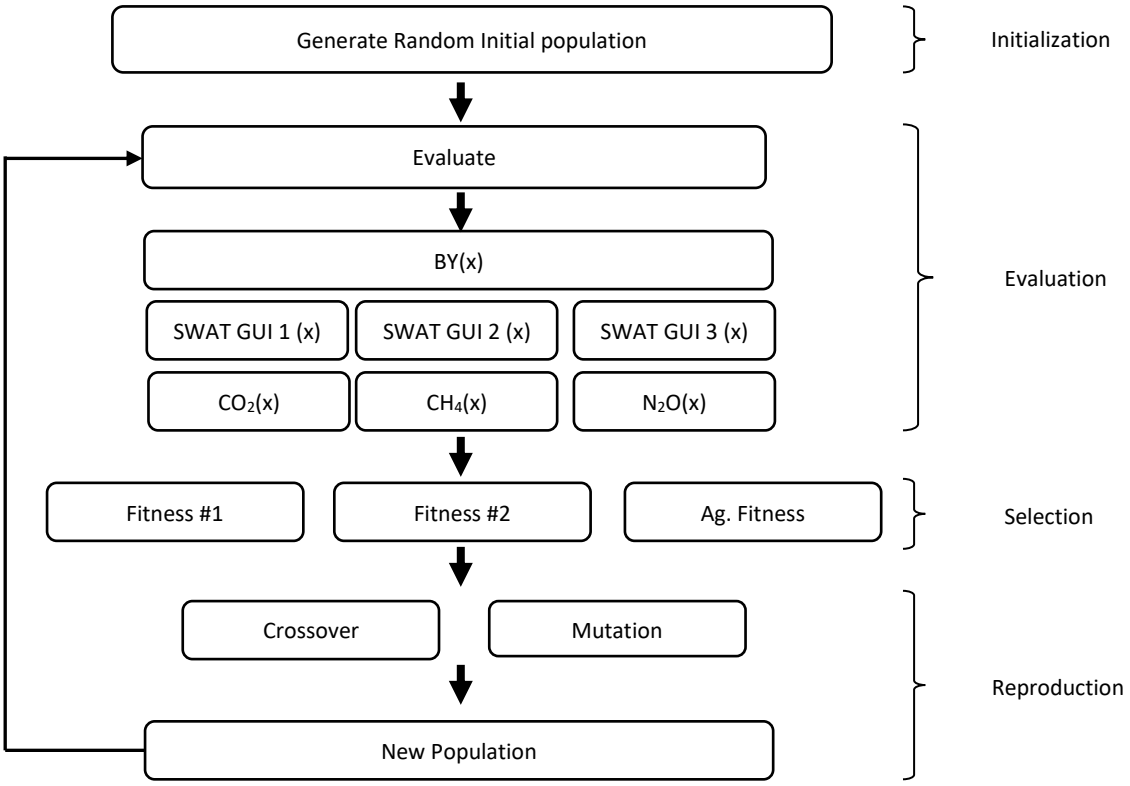

Figure 6.11: MOEA Flowchart

In general, the algorithm is initiated with a random initial population in which every individual is evaluated to quantify its environmental performance. After that, all individuals are

evaluated using the metric functions proposed by Taboada and colleagues. The best-fitted individuals are considered to create a new population. The process continues until a stopping criterion is reached, and the optimal solution is given by Pareto optimality. A detailed description in which this MOEA was employed to the interactive control model, is provided in the following subsections.

This MOEA was fully coded in Matlab. Its parameters must be defined at the first stage of the algorithm and remain constant throughout its evolutionary process. These are defined in the MOEA interface shown in figure 6.12. Each of these parameters is explained in the following subsections.

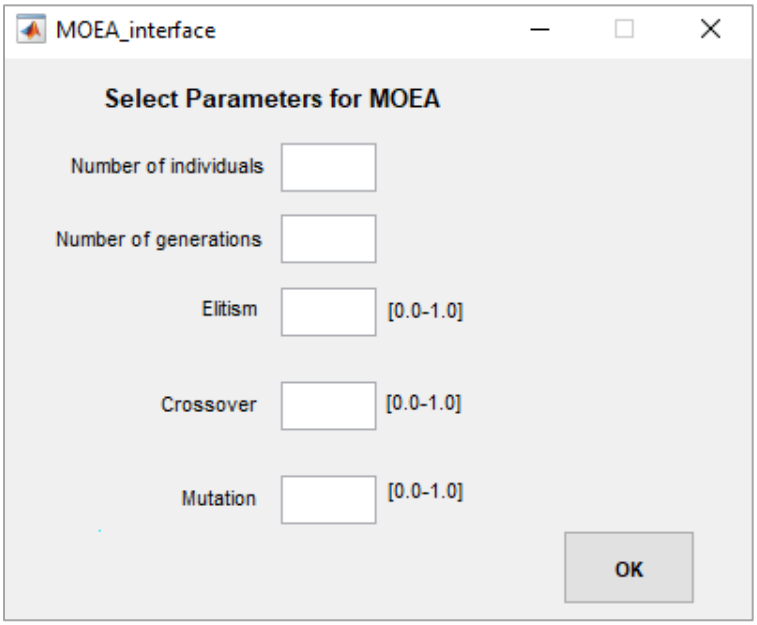

Figure 6.12: MOEA Interface

6.5.1 Initialization

The algorithm begins by producing an initial set of possible solutions called individuals. An individual is distinguished from others by the configuration of their genes, which is known as chromosome encoding. The number of genes of an individual is equal to the number of HRUs defined in the SWAT interface. These individuals are possible landscape scenarios and are

produced by mixing the columns, corresponding to the simulation outputs of each HRU, from the result tables saved when management practices were evaluated. Thus, one can identify the corresponding information for each HRU and recognize the set of factors that belong to a possible landscape scenario. Vital to maintaining a diverse population that guarantees the thoroughly and effectiveness of the search space, such initial set is created randomly. Figure 6.13 illustrates the process by which an individual is created. In this example, the possible individual is created by mixing the result tables from 4 different management practices. HRUs 1, 7, 13, and 14 from this individual correspond to the output information obtained from the same HRUs in management practice 1. HRUs 2, 5, and 11 correspond to the output information obtained from the same HRUs in management practice 2. HRUs 3, 4, and 10 correspond to the output information obtained from the same HRUs in management practice 3. HRUs 6, 8, 9, and 12 correspond to the output information obtained from the same HRUs in management practice 4.

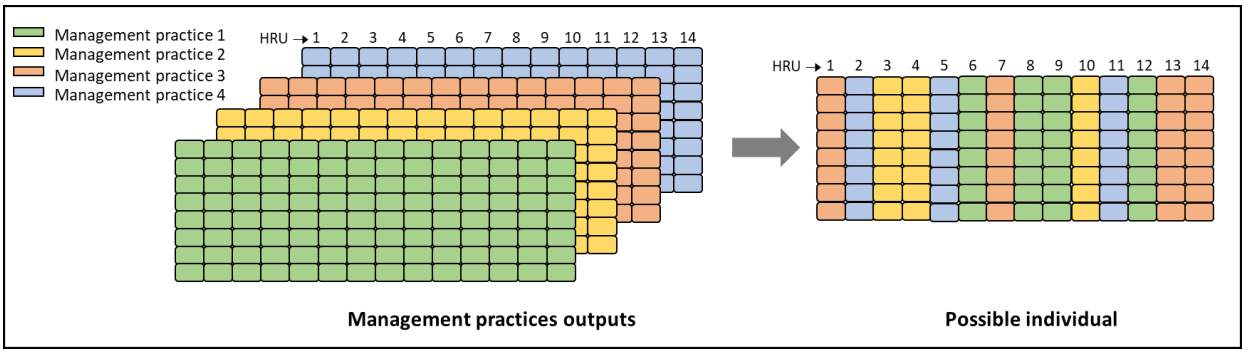

Figure 6.13: Chromosome encoding

The initial population is a set of random individuals, in which its size is a variable, predefined in the MOEA interface. The size of this population remains constant in the entire iterative process of the algorithm. The initial population guides the MOEA towards the Pareto-optimal front by providing a base for succeeding populations. Figure 6.14 illustrates an initial population of 20 random individuals

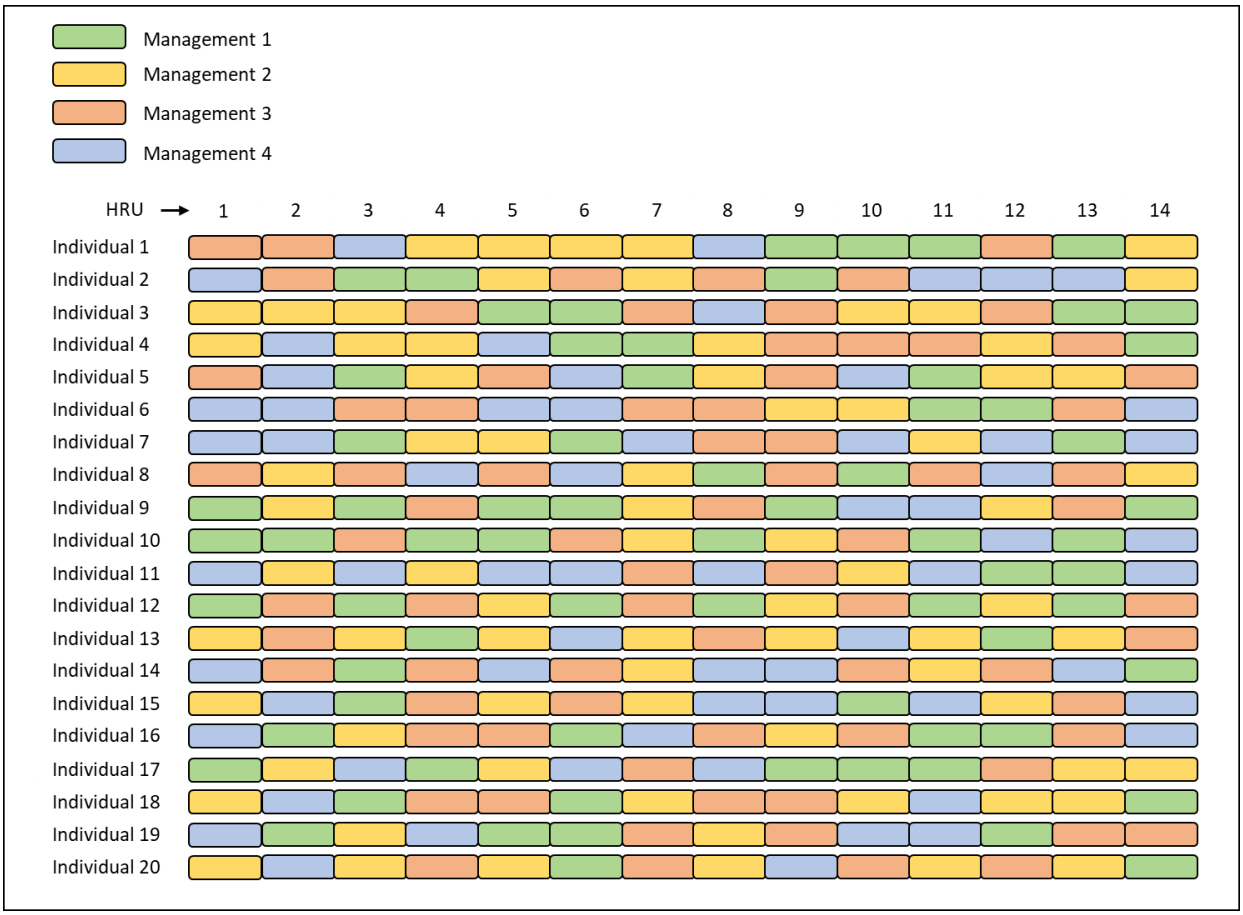

Figure 6.14: Example of Initial Population

6.5.2 Evaluation

In the evaluation stage, every individual in the current generation is evaluated according to seven objective functions. The algorithm includes the concept of Pareto dominance. In this sense, only the nondominated individuals survive, whereas the dominated individuals are removed. The Pareto criterion begins with dominance count, which represents the number of individuals dominated by a single solution.

6.5.3 Fitness assignment

The MOEA used in this research has two main goals; (1) Diversity of population; and (2) Proximity to the Pareto front. These two are evaluated according to the following fitness metrics:

- Fitness Metric 1: Distance-based, $f_1(i)$

This fitness metric aims to maintain the diversity of the Pareto optimal solutions giving higher fitness to those individuals that are farther away from other individuals in the Pareto front. The following steps are needed to measure individuals.

1. Normalization: to avoid unit discrepancies, every objective's result is normalized according to equation 6.3.

$$\frac{f_i(x) - f_i^{min}}{f_i^{max} - f_i^{min}} \quad \text{(Eq. 6.1)}$$

where $f_i(x)$ = value in the nondominated set, f_i^{min}= minimum value in the nondominated set and f_i^{max}= maximum value in the nondominated set.

2. Distances. Euclidean distance between solutions is measured, and all the summation of all distances is computed. The individuals are categorized using the ranks that begin with the minimum distance obtained and end at the maximum.

- Fitness Metric 2: Dominance count-based, $f_2(i)$

This fitness metric aims to approximate the true Pareto front by selecting those individuals who are more dominating than others. The metric is based on the dominance count concept.

- Aggregated fitness Metric

The objective of this fitness metric is to obtain the most two common desirable characteristics in MOEAs; Proximity and diversity. In this metric, equal weights for individuals in fitness metric 1 and 2 are aggregated.

6.5.4 Selection

In each iteration, a portion of the most fitted individuals is selected to survive into the next generation; a process called elitism. The remaining spots are filled by reproduction in which the individuals with highest fittest value are given greater probability to reproduce. This MOEA

considers tournament selection where two individuals are selected randomly, and the most fitted is chosen to be parent 1. The process repeats to find parent 2. Both parents produce new individuals through a process called crossover.

6.5.5 Crossover

Different types of crossovers can achieve the reproduction of parents. Its effectiveness depends on employing a suitable crossover method which, to a large extent, has to do with the type of chromosome encoding of the problem. Among the different types of crossover, a random single-point crossover was the technique selected for the reproduction of parents. Figure 6.15 shows how the crossover process is executed. First, a random point divides the chromosome into two segments. The first segment of parent 1 is joint with the second segment of parent 2. Similarly, the second segment of parent 1 is joint with the first segment of parent 2. In this extent, two new individuals are created to populate the next generation. Note that the increasing order of HRUs is kept. This operation is repeated until the empty places, that were not occupied by elitism, are filled.

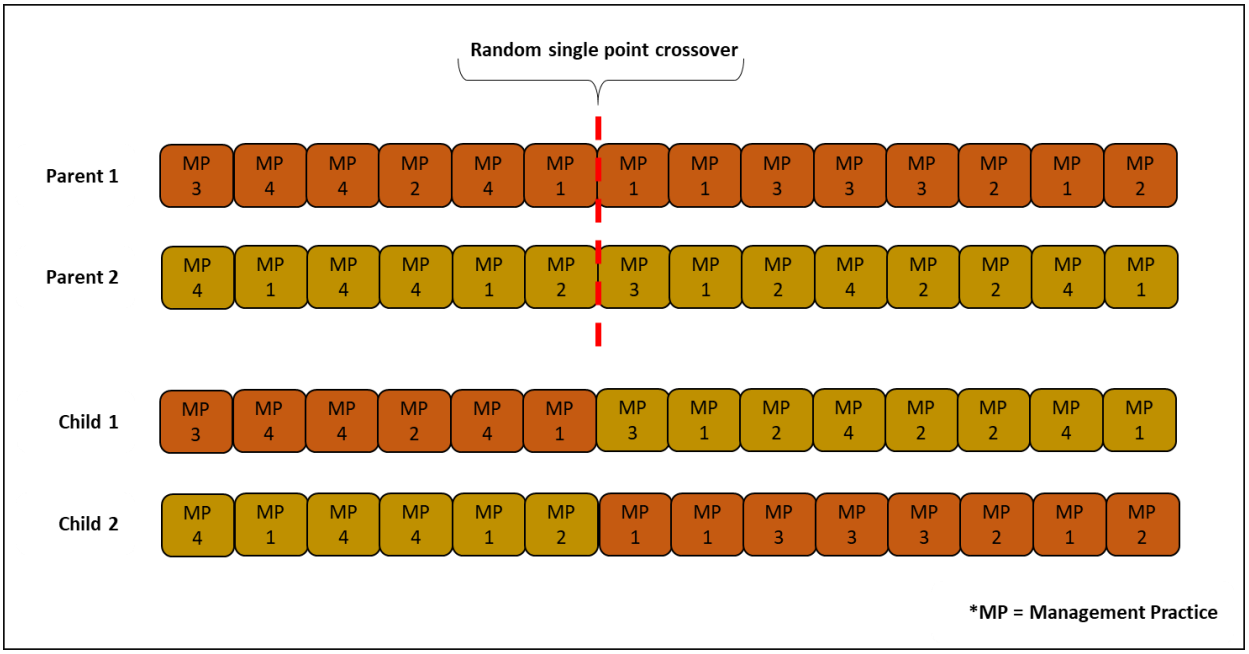

Figure 6.15: Example of crossover process

6.5.6 Mutation

To avoid falling into local optimum, new individuals will undergo a small percent chance of mutation, increasing the variation of solutions. If a set of new individuals will mutate, four random genes will be swapped, as shown in figure 6.16.

Figure 6.16: Example of Random Mutation Process

6.5.7 Termination

There are different ways in which the iterative process can end. Among the processes used include criteria such as reaching a predetermined number of generations, reaching a satisfying solution or detecting a steady-state system in which the quality of solutions is no longer evolving. The criterion chosen to stop the iterations of this MOEA is to predetermine a specific number of generations at the beginning of the algorithm. The user selects this number in the MOEA interface.

6.6 Chapter Conclusions

In this chapter, the methodology applied to optimize allocation design in Land-Use and Land-Cover change was explained. This methodology considered the coupling of the SWAT and GREET models to quantify the environmental performance on soil, water, and atmosphere

associated with the production of biofuel feedstock and its conversion to biofuel. This methodology included a Multi-Objective Evolutionary Algorithm to provide a near-optimal solution for allocation design to reduce the effects of natural resource exploitation when considering the production of clean, renewable fuels. The objective was to maximize the biomass yields and reduce variant objectives that affect ecosystem services. The next chapter illustrates how this model is employed to optimize allocation design in Land-Use and Land-Cover Changes in different case studies.

Chapter 7: Case Studies

This chapter is dedicated to present different case studies applying the developed optimization model presented in chapter 6. This case studies demonstrate the flexibility of the model by using two SWAT simulations and selecting different optimization objectives. Furthermore, this chapter demonstrates that the Land-Use and Land-Cover change parameters can be modified to meet the needs that may arise in different scenarios.

7.1 Case Studies

The following subsections used the Lake Fork Watershed SWAT simulation, which is located in the Texas Gulf region. This simulation was divided into 21 sub-basins. The land cover in the 48,683 hectares basin is comprised of Pasture (PAST), Forest-Deciduous (FRSD), Range Grasses (RNGE) and water (WATR) and TX633 dominates the soil type in this area. Two slopes levels (0-1 and 1-9999) were considered. The weather was simulated with the SWAT user weather station Database (station count 4) while the rainfall, temperature, relative humidity, solar radiation, and wind speed data were set to default simulation. In this model, 25 HRUs were used to be distributed according to similar land use, soil type, and slope along the 21 sub-basins. The description of each HRU is shown in table 7.1 and figures 7.1, 7.2, and 7.3 show the shapefiles for land use, soil, and slope, respectively.

Table 7.1: Description of Lake Fork Watershed

Sub-basin	HRU	Land Use	Soil Type	Slope	Area (ha)
1	1	PAST	TX633	1-9999	1395.00
2	2	PAST	TX633	0-1	1194.00
3	3	PAST	TX633	0-1	1103.00
4	4	PAST	TX633	0-1	1413.70
4	5	PAST	TX633	1-9999	1754.30
5	6	PAST	TX633	0-1	3413.00
6	7	PAST	TX633	0-1	2354.00
7	8	PAST	TX633	0-1	2017.00
8	9	PAST	TX619	0-1	1401.00
9	10	PAST	TX620	0-1	532.00
10	11	PAST	TX620	0-1	1576.00
11	12	PAST	TX633	0-1	2584.00
12	13	PAST	TX619	0-1	1202.00
13	14	PAST	TX633	0-1	2394.13
13	15	PAST	TX633	1-9999	1429.87
13	16	RNGE	TX633	0-1	1532.00
14	17	PAST	TX633	0-1	2511.00
15	18	PAST	TX620	0-1	1859.00
16	19	PAST	TX633	0-1	2599.66
16	20	RNGE	TX633	0-1	1328.34
17	21	PAST	TX633	0-1	3093.00
18	22	PAST	TX620	0-1	3968.00
19	23	PAST	TX620	0-1	1874.00
20	24	PAST	TX620	0-1	2576.00
21	25	WATR	TX357	0-1	1579.00

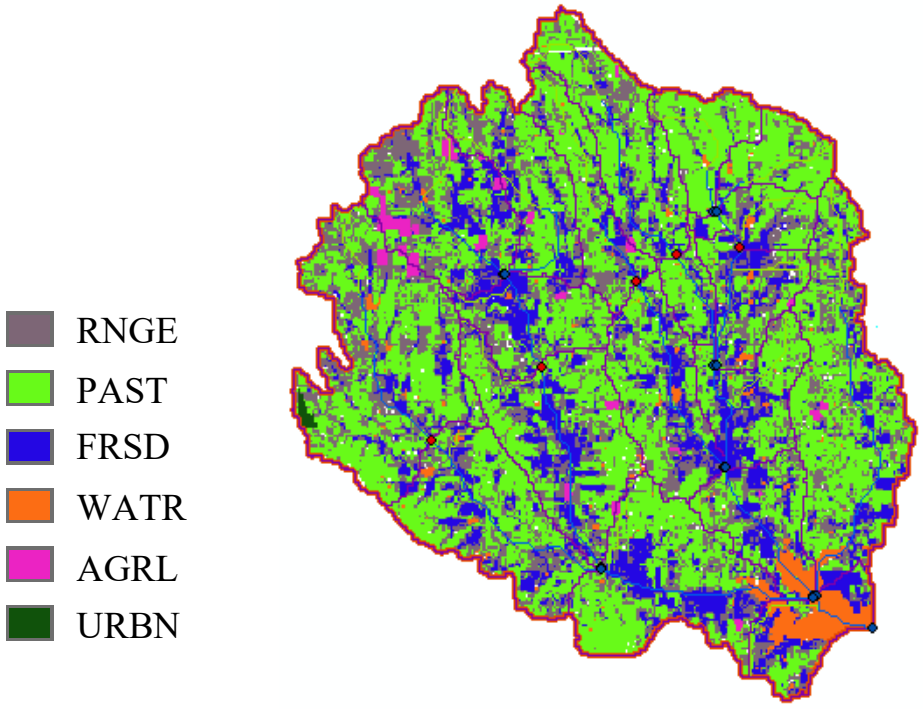

Figure 7.1: Land Use Shape

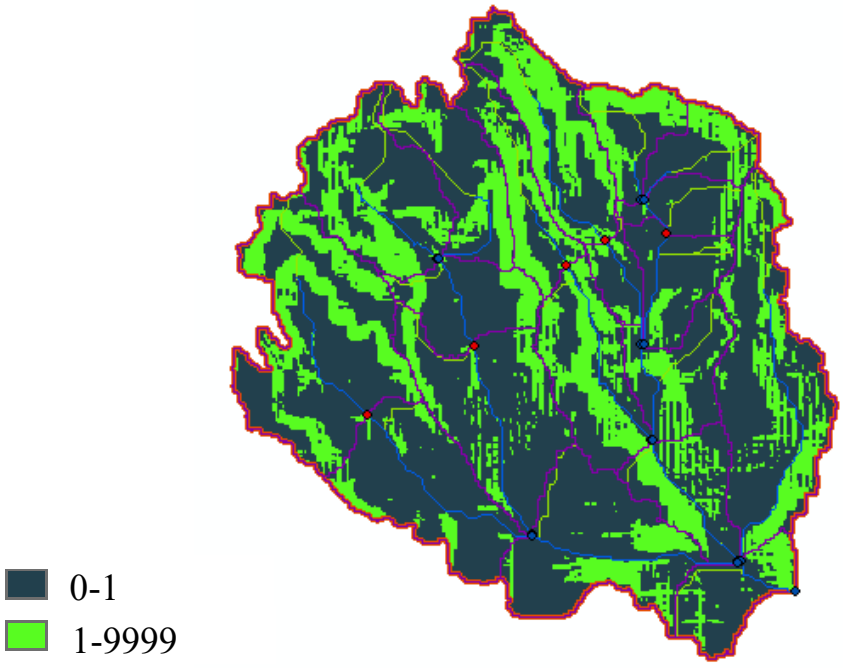

Figure 7.2: Slope Shape

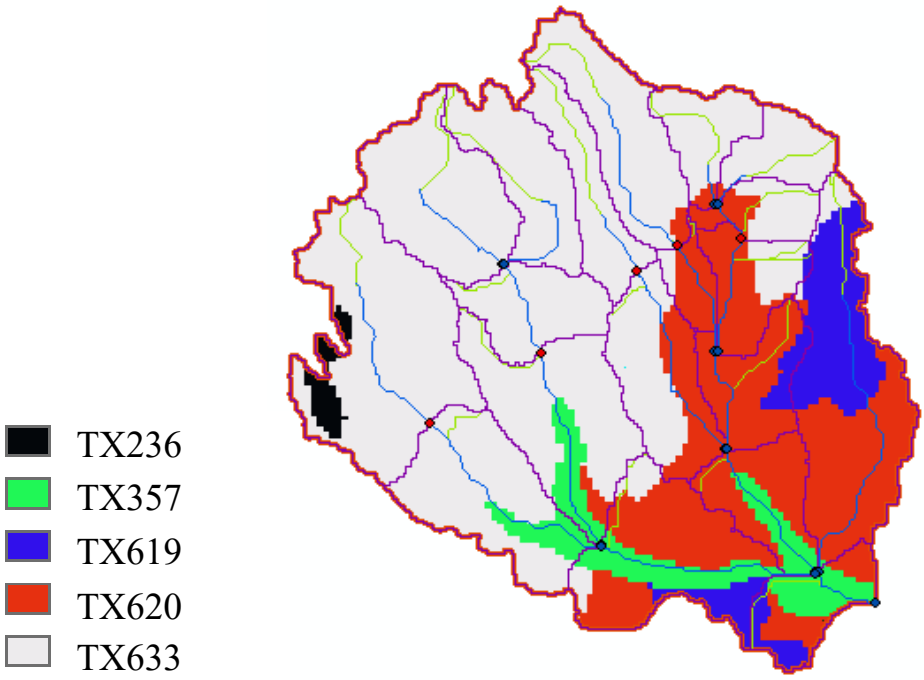

Figure 7.3: Soil Shape

7.2 CASE STUDY 1

The scheduled management operation used in Case Study 1, are listed in table7.2. The Management code (from 1 to 12) indicates the schedule management operation evaluated in the entire watershed. This number will help to identify the type of management practice used when the MOEA is executed, and it is found on the first row of every possible individual. The SWAT operation number and name are used in the same sequence as shown in this table. The first operation (Plant/begin growing season) initializes the growth of the specified land cover type in all HRUs. In this study, two perennial crops were considered for land cover; Alamo Switchgrass and Miscanthus. The second operation initializes auto irrigation within every HRU. This operation applies water whenever the plant experiences a user-specified level of water stress. The water stress threshold that triggers irrigation in this study is 0.60. Plants are irrigated with water diverted from an unlimited outside source with an irrigation efficiency of 0.85. Also, a surface runoff ratio

of 0.10 was used in this study. The third operation (fertilizer application) adds nutrients to the soil in every HRU. In this study, nitrogen was the fertilizer applied with three different levels of application (40, 60, and 80 kg/ha). In order to compare the impacts of fertilizer application on the soil, each nitrogen level was scheduled in different evaluations for every land cover. The fourth operation applies a pesticide to the plant and soil in every HRU. This study used Glufosinate Ammonia as a pesticide with two levels of application (30 and 60 kg/ha). These two levels of pesticide were scheduled with every level of fertilizer application to evaluate their performance. The last operation skips one-year operation to January 1st and harvest in the 2nd year.

Table 7.2: Crop Management Practices Case Study 1

SWAT Operation No.	1	10	3	4	5	17
	SWAT Operation Name					
Management Code	Plant/begin growing season	Auto Irrigation	Fertilizer Application	Pesticide Application	Harvest and Kill	Skip a Year Operation
1	Alamo Switchgrass	PWD*	40 kg/ha	30 kg/ha	SBY**	1 Year
2	Alamo Switchgrass	PWD*	40 kg/ha	60 kg/ha	SBY**	1 Year
3	Alamo Switchgrass	PWD*	60 kg/ha	30 kg/ha	SBY**	1 Year
4	Alamo Switchgrass	PWD*	60 kg/ha	60 kg/ha	SBY**	1 Year
5	Alamo Switchgrass	PWD*	80 kg/ha	30 kg/ha	SBY**	1 Year
6	Alamo Switchgrass	PWD*	80 kg/ha	60 kg/ha	SBY**	1 Year
7	Miscanthus	PWD*	40 kg/ha	30 kg/ha	SBY**	1 Year
8	Miscanthus	PWD*	40 kg/ha	60 kg/ha	SBY**	1 Year
9	Miscanthus	PWD*	60 kg/ha	30 kg/ha	SBY**	1 Year
10	Miscanthus	PWD*	60 kg/ha	60 kg/ha	SBY**	1 Year
11	Miscanthus	PWD*	80 kg/ha	30 kg/ha	SBY**	1 Year
12	Miscanthus	PWD*	80 kg/ha	60 kg/ha	SBY**	1 Year

* Plant Water Demand **Skip to Beginning of Year

This study aims to evaluate the biomass yield, sediment yield, organic nitrogen yield, and the organic phosphorous yield effects of these management practices.

The GREET Well to Pump pathway considered for each crop in this study was from farming until Low-Level EtOH Blend with Gasoline (E10) is delivered to the pump. The ethanol production was done via fermentation. Figure 7.4 shows the GREET's life cycle system boundary used in this example.

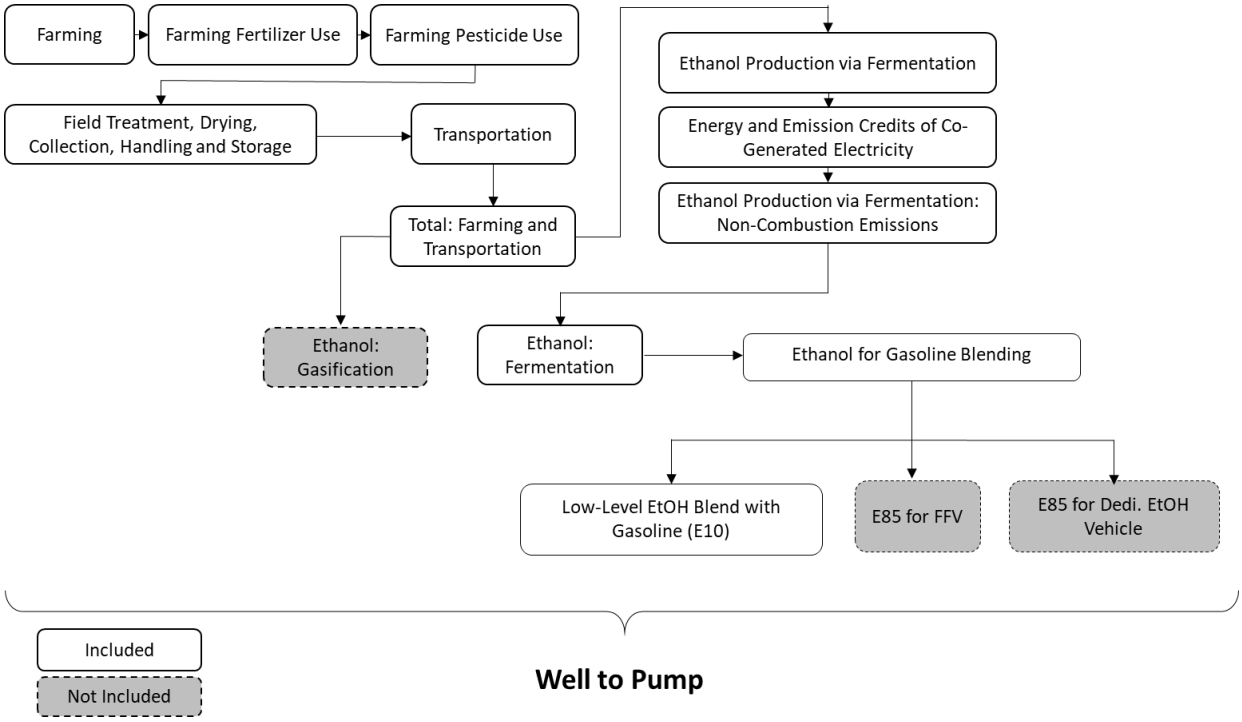

Figure 7.4: GREET's Life Cycle System Boundary Case Study 1

The MOEA was executed using 500 individuals and 500 iterations. In each iteration, the top 25% of the most fitted individuals were selected for reproduction with a 75% chance of reproduction and a 1% chance of mutation. The management operations and the MOEA were run on an HP computer, with an Intel® Core™ i5 6200U CPU processor operating at 2.30 GHz 2.40 GHz and 8 GB of RAM.

The optimal solution given with these settings is displayed in table 7.3. Under these settings, 1,918,198.80 kg/ha of biomass is produced on the watershed. The environmental impact

corresponding to this biomass yield in terms of sediment yield is 53.51 metric tons, 18.75 kg/ha of organic nitrogen yield, and 32.18 of organic phosphorus yield. The greenhouse gas emissions evaluated, CO_2, CH_4 and N_2O yield a total of 515,581,925.79, 1,004,993.21 and 831,156.28 grams/mmBtu, respectively. While management operations 1, 2, 3, 4, 6, 7, 8, 9 and 11 are considered in the optimal solution, the management practices 5 and 12 were not considered optimal; therefore they were discarded.

Table 7.3: Optimal Solution Case Study 1

Sub-basin	Area (ha)	HRU	MP	Biomass Yield (kg/ha)	Sediment Yield (metric tons)	Org. Nitrogen Yield (kg N/ha)	Org. Phosphorous Yield (kg P/ha)	CO2 (grams/mmBtu)	CH4 (grams/mmBtu)	N2O (grams/mmBtu)
1	1395	1	3	19,559.10	1.82	0.57	1.03	12,725,554.56	25,608.59	25,563.56
2	1194	2	3	19,547.40	1.19	0.40	0.72	10,893,814.72	21,935.06	21,880.40
3	1103	3	11	24,625.80	2.99	1.11	1.98	11,056,030.08	22,976.30	26,907.71
4	1413	4	9	23,210.20	3.94	1.25	2.24	12,894,607.14	25,950.15	25,906.28
	1754	5	6	21,888.00	1.76	0.63	1.13	28,829,155.16	55,634.63	42,997.82
5	3413	6	11	24,620.00	4.11	1.36	2.44	34,186,572.01	70,858.53	83,257.31
6	2354	7	2	17,142.50	1.56	0.46	0.83	34,441,929.08	63,070.13	29,120.39
7	2017	8	9	23,204.20	6.24	1.53	2.73	18,392,558.01	36,976.23	36,961.26
8	1401	9	9	22,683.50	0.95	0.07	0.10	12,778,844.02	25,718.00	25,673.57
9	532	10	7	17,939.80	3.10	1.45	2.18	4,380,447.82	8,531.16	6,520.83
10	1576	11	3	17,973.20	1.08	0.57	0.87	14,374,927.30	28,916.46	28,880.24
11	2584	12	8	19,491.10	3.80	1.29	2.31	37,804,493.05	69,221.18	31,965.55
12	1202	13	4	17,787.00	0.25	0.02	0.03	18,674,854.81	35,207.47	22,165.75
13	2394	14	2	17,147.40	1.14	0.48	0.87	35,028,866.43	64,143.40	29,616.80
	1429	15	3	19,544.00	2.24	0.81	1.47	13,043,328.41	26,245.88	26,202.53
	1532	16	11	24,622.30	3.32	1.27	2.27	15,351,702.03	31,868.72	37,372.64
14	2511	17	1	17,136.10	1.74	0.60	1.09	20,635,517.85	39,847.86	30,772.63
15	1859	18	3	17,969.50	1.44	0.70	1.07	16,953,942.78	34,088.65	34,065.98
16	2599	19	1	17,145.70	1.33	0.44	0.81	21,363,686.41	41,250.85	31,859.12
	1328	20	6	21,916.50	0.96	0.36	0.66	21,832,305.90	42,153.57	32,557.88
17	3093	21	1	17,146.00	1.43	0.42	0.77	25,415,506.47	49,057.63	37,904.80
18	3968	22	11	23,494.00	3.95	1.51	2.32	39,743,853.70	82,362.63	96,795.85
19	1874	23	3	17,965.10	1.58	0.76	1.18	17,090,639.44	34,362.79	34,340.85
20	2576	24	2	15,791.30	1.61	0.70	1.09	37,688,788.61	69,007.35	31,866.53
21	1579	25	---	0.00	0.00	0.00	0.00	0.00	0.00	0.00

Total	**1,918,199**	**53.51**	**18.75**	**32.18**	**515,581,925.79**	**1,004,993.21**	**831,156.28**

The Lake Fork Watershed map and the land change distribution according to the optimal solution is illustrated in figure 7.5. This map displays the entire optimal solution, including the water outlet.

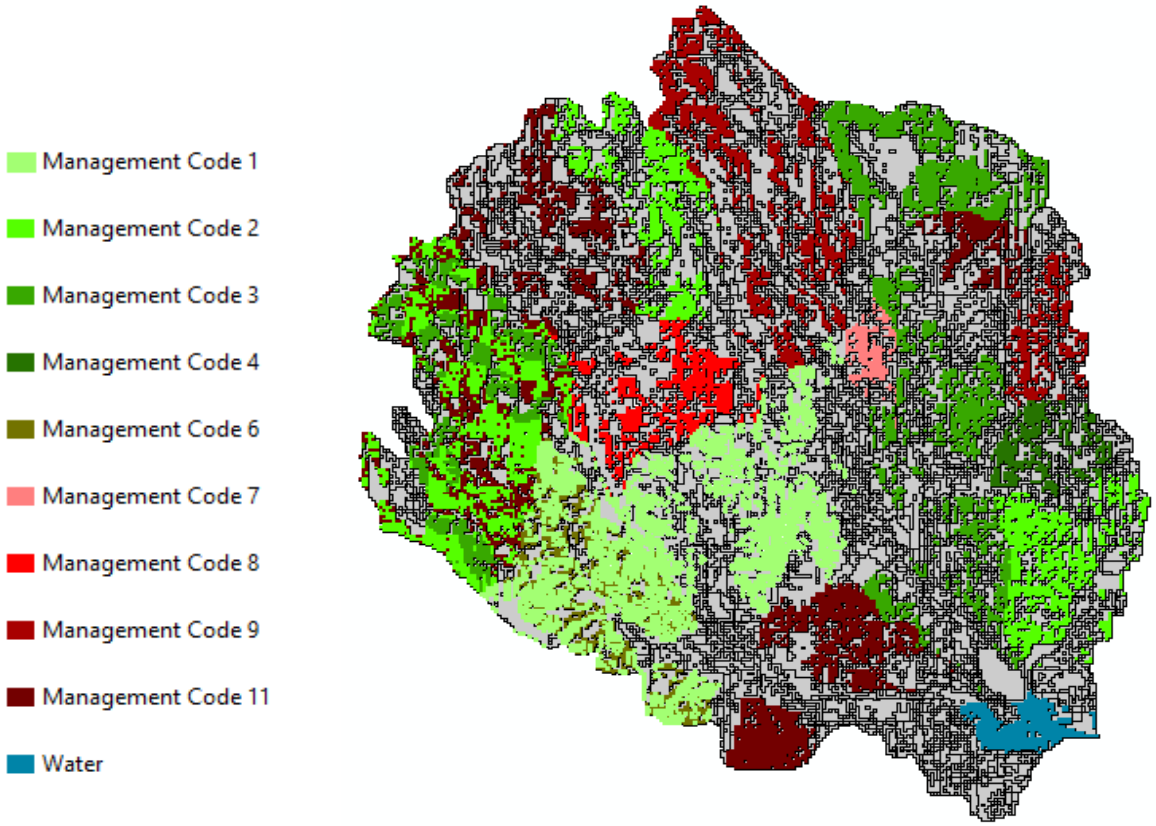

Figure 7.5: Optimal solution Case Study 1

The sum of all non-dominated solutions found in the execution of this MOEA was 114,729. In order to avoid dominance within all dominated solutions, one last dominance check was performed at the end of the algorithm. In this last dominance check, 230 non dominated solutions were found. The Pareto graphs for the last non-dominance check are shown in figure 7.6. Blue dots represent non-dominated solutions, while the red dot represents the solution that is closest to the ideal point [1 0 0 0 0 0 0].

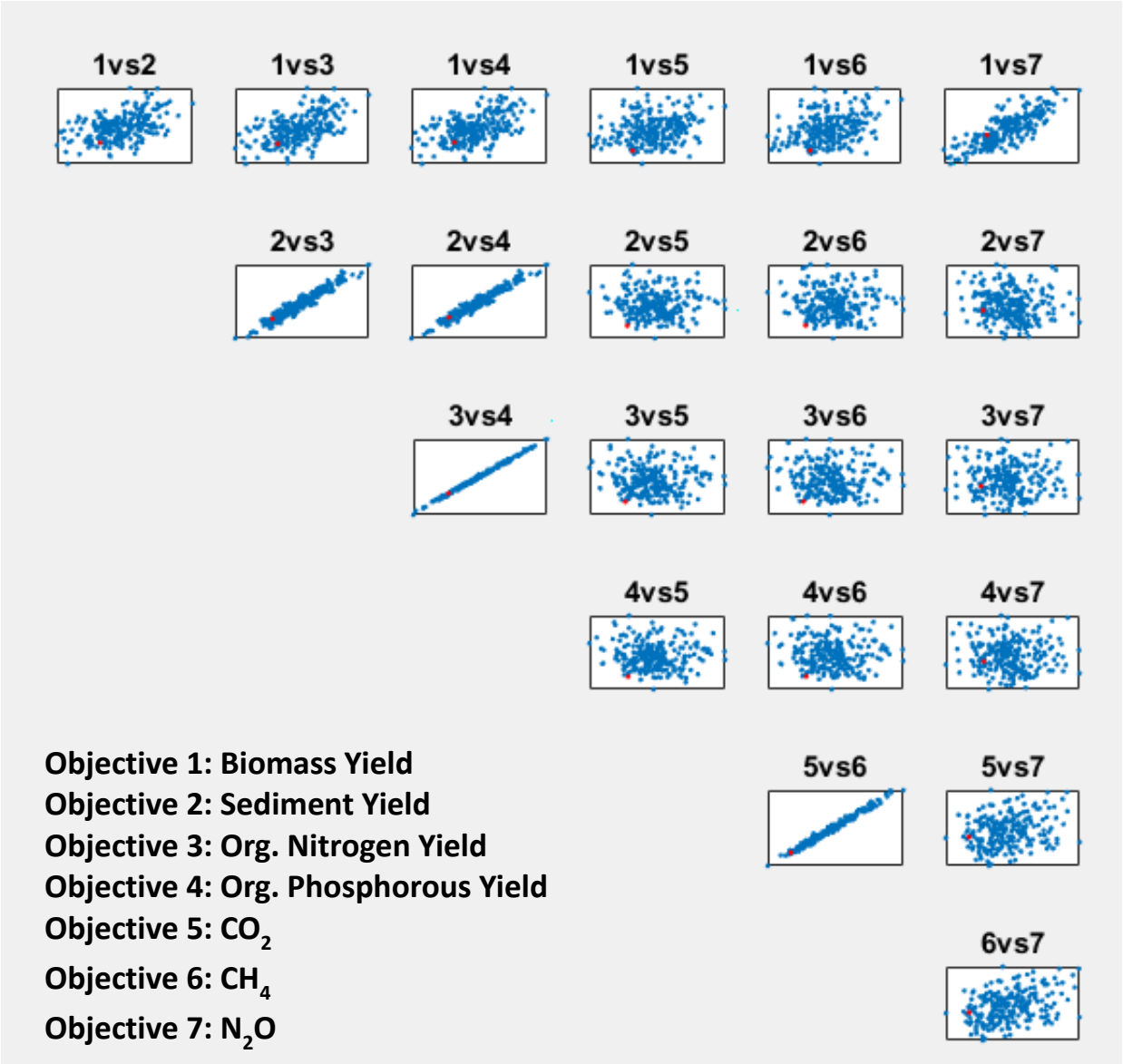

Figure 7.6: Pareto Graphs Case Study 1

The computational time to execute each management operation is 15 minutes. The MOEA computational time in this example was 1.25 hrs. Therefore, the total computational time to obtain the optimal solution shown in Case Study 1 was 3.25 hrs.

7.3 CASE STUDY 2

The scheduled management operation used in Case Study 2, are listed in table 7.4. Similar to Case Study 1, the Management code (from 1 to 10) indicates the schedule management operation evaluated in the entire watershed and the SWAT operation number and name are used in the same sequence as shown in this table. The first operation (Plant/begin growing season) initializes the growth of the specified land cover type in all HRUs. However, in order to show additional crop growth, this study supplements three new land cover. The total land covers considered in this study are Willow, Poplar, Alamo Switchgrass, Miscanthus, and Sorghum. Instead of using auto irrigation, the second operation irrigates every HRU by diverting water from a deep aquifer, assuming the irrigation source location was in the sub-basin 21. The depth of irrigation applied to every HRU is 50 mm. No concentration of salt was considered, an irrigation efficiency of 0.80, and a 0.15 surface runoff ratio was considered. As an alternative to nitrogen, the third operation (fertilizer application) applied Urea to every HRU. Two levels of Urea application were considered (30 and 60 kg/ha). Similarly, instead of using Glufosinate Ammonia as a pesticide, the fourth operation applies Mecroprop Amine to plants and soils in every HRU. The levels of application considered were 20 and 40 kg/ha. These two levels of pesticide were scheduled respectively to the level of fertilizer application. The last operation skips one-year operation to January 1st and harvest in the 2nd year.

Table 7.4: Crop Management Practices Case Study 2

SWAT Operation No.	1	10	3	4	5	17
	SWAT Operation Name					
MOEA Code	Plant/begin growing season	Irrigation	Fertilizer Application	Pesticide Application	Harvest and Kill	Skip a Year Operation
1	Willow	DWFDA*	30 kg/ha	20 kg/ha	SBY**	1 Year
2	Willow	DWFDA*	60 kg/ha	40 kg/ha	SBY**	1 Year
3	Poplar	DWFDA*	30 kg/ha	20 kg/ha	SBY**	1 Year
4	Poplar	DWFDA*	60 kg/ha	40 kg/ha	SBY**	1 Year
5	Alamo Switchgrass	DWFDA*	30 kg/ha	20 kg/ha	SBY**	1 Year
6	Alamo Switchgrass	DWFDA*	60 kg/ha	40 kg/ha	SBY**	1 Year
7	Miscanthus	DWFDA*	30 kg/ha	20 kg/ha	SBY**	1 Year
8	Miscanthus	DWFDA*	60 kg/ha	40 kg/ha	SBY**	1 Year
9	Sorghum	DWFDA*	30 kg/ha	20 kg/ha	SBY**	1 Year
10	Sorghum	DWFDA*	60 kg/ha	40 kg/ha	SBY**	1 Year

* Divert Water from Deep Aquifer
**Skip to Beginning of Year

This study aims to evaluate the biomass yield, sediment yield, organic nitrogen yield, and the organic phosphorous yield effects of these management practices.

The GREET Well to Pump pathway considered for each crop in this study was from farming until E85 for FFV is delivered to the pump. The ethanol production was done via fermentation — figure7.7 shows the GREET's life cycle system boundary used in this example.

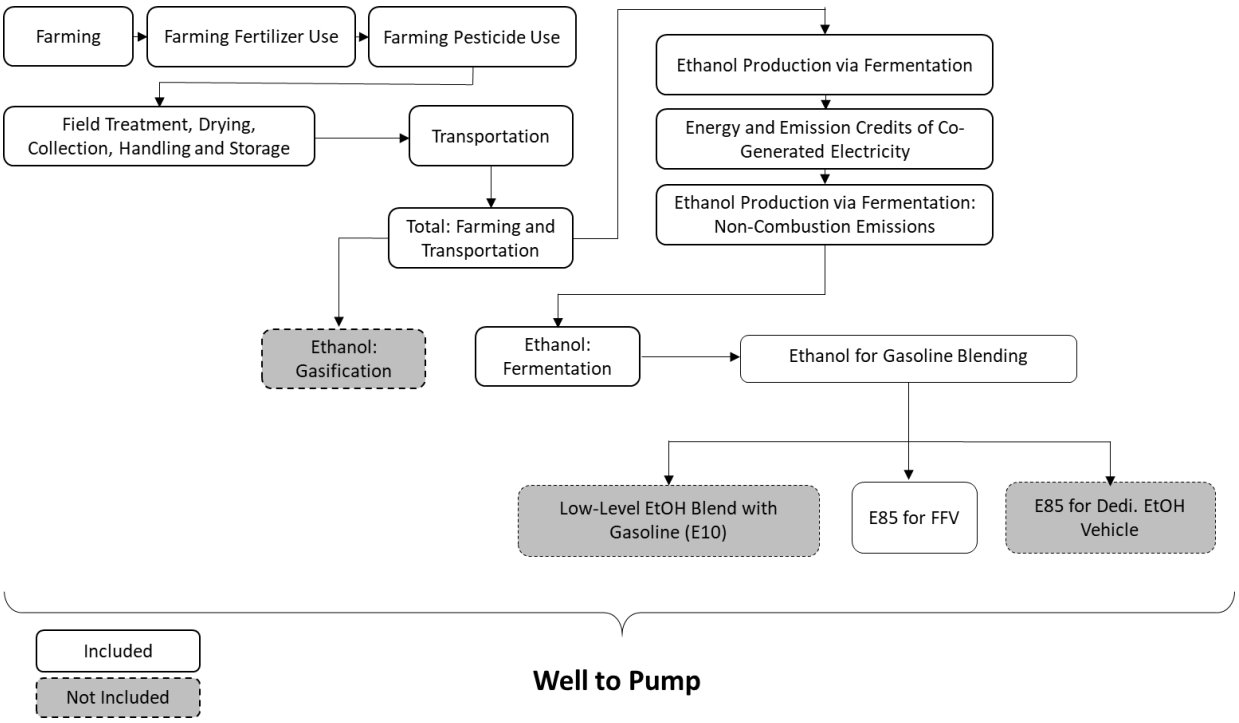

Figure 7.7: GREET's Life Cycle System Boundary Case Study 2

The MOEA was executed using 1000 individuals and 1000 iterations. In each iteration, the top 25% of the most fitted individuals were selected for reproduction with a 75% chance of reproduction and a 1% chance of mutation. The management operations and the MOEA were run on an HP computer, with an Intel® Core™ i5 6200U CPU processor operating at 2.30 GHz 2.40 GHz and 8 GB of RAM.

The optimal solution given with these settings is displayed in table 7.5. Under these settings, 424,529.10 kg/ha of biomass is produced on the watershed. The environmental impact corresponding to this biomass yield in terms of sediment yield is 45.40 metric tons, 10.30 kg/ha of organic nitrogen yield, and 18.77 of organic phosphorus yield. The greenhouse gas emissions evaluated, CO_2, CH_4 and N_2O yield a total of 4,149,085,335.84, 8,085,128.87 and 6,771,901.37 grams/mmBtu, respectively. While management operations 1, 2, 3, 4, 5, 8 and 9 are considered in the optimal solution, the management practices 6, 7 and 10 were not considered optimal; therefore they were discarded.

Table 7.5: Optima Solution Case Study 2

Sub-basin	Area (ha)	HRU	MP	Biomass Yield (kg/ha)	Sediment Yield (metric tons)	Org. Nitrogen Yield (kg N/ha)	Org. Phosphorous Yield (kg P/ha)	CO2 (grams/mmBtu)	CH4 (grams/mmBtu)	N2O (grams/mmBtu)
1	1395	1	5	10,617.80	3.46	0.95	1.78	90,149,667.17	175,752.77	147,224.82
2	1194	2	9	4,258.10	15.39	1.94	3.42	339,929,711.1	662,192.07	553,949.48
3	1103	3	5	10,628.50	2.20	0.63	1.18	71,269,750.06	138,974.74	116,410.37
4	1413	4	4	23,013.20	0.34	0.09	0.18	160,836,122.4	313,401.71	262,496.51
	1754	5	4	23,008.10	0.64	0.16	0.32	199,583,250.3	388,881.03	325,736.81
5	3413	6	2	23,217.00	0.40	0.10	0.21	388,258,620.6	756,435.14	633,712.36
6	2354	7	3	20,388.70	0.42	0.09	0.18	133,901,214.9	260,937.84	218,547.50
7	2017	8	1	20,530.20	0.57	0.12	0.25	114,713,904.4	223,574.44	187,261.01
8	1401	9	5	9,235.80	0.74	0.06	0.10	90,536,571.75	176,507.11	147,857.98
9	532	10	3	19,090.80	0.36	0.16	0.27	30,260,806.25	59,049.19	49,399.12
10	1576	11	3	19,089.90	0.33	0.16	0.27	89,644,269.43	174,728.03	146,320.54
11	2584	12	5	10,624.80	1.86	0.77	1.44	167,027,175.8	325,509.96	272,698.75
12	1202	13	2	22,221.50	0.02	0.00	0.00	136,730,115.4	266,459.62	223,188.84
13	2394	14	5	10,626.50	2.16	0.72	1.36	154,750,699.8	301,595.42	252,661.97
	1429	15	8	15,116.70	7.31	1.90	3.40	184,842,168.0	360,240.35	301,798.00
	1532	16	3	20,387.50	0.32	0.10	0.20	87,145,264.33	169,857.37	142,235.81
14	2511	17	8	15,122.00	6.23	1.39	2.49	324,648,016.8	632,581.79	529,979.04
15	1859	18	1	19,286.00	0.38	0.19	0.33	105,724,269.0	206,064.37	172,592.77
16	2599	19	4	23,013.00	0.34	0.09	0.17	295,752,625.8	576,218.72	482,697.52
	1328	20	1	20,529.00	0.35	0.10	0.20	75,542,429.27	147,268.50	123,328.15
17	3093	21	3	20,388.10	0.36	0.09	0.17	175,936,061.1	342,821.62	287,153.75
18	3968	22	1	19,286.30	0.40	0.16	0.27	225,685,696.1	439,748.93	368,385.17
19	1874	23	2	22,423.90	0.44	0.20	0.34	213,178,199.4	415,380.02	347,961.25
20	2576	24	2	22,425.70	0.39	0.16	0.27	293,038,725.9	570,948.12	478,303.85
21	1579	25	3	0.00	0.00	0.00	0.00	0.00	0.00	0.00
Total				**424,529.10**	**45.40**	**10.30**	**18.77**	**4,149,085,335.84**	**8,085,128.87**	**6,771,901.37**

The Lake Fork Watershed map and the land change distribution according to the optimal solution is illustrated in figure 7.8. This map displays the entire optimal solution, including the water outlet.

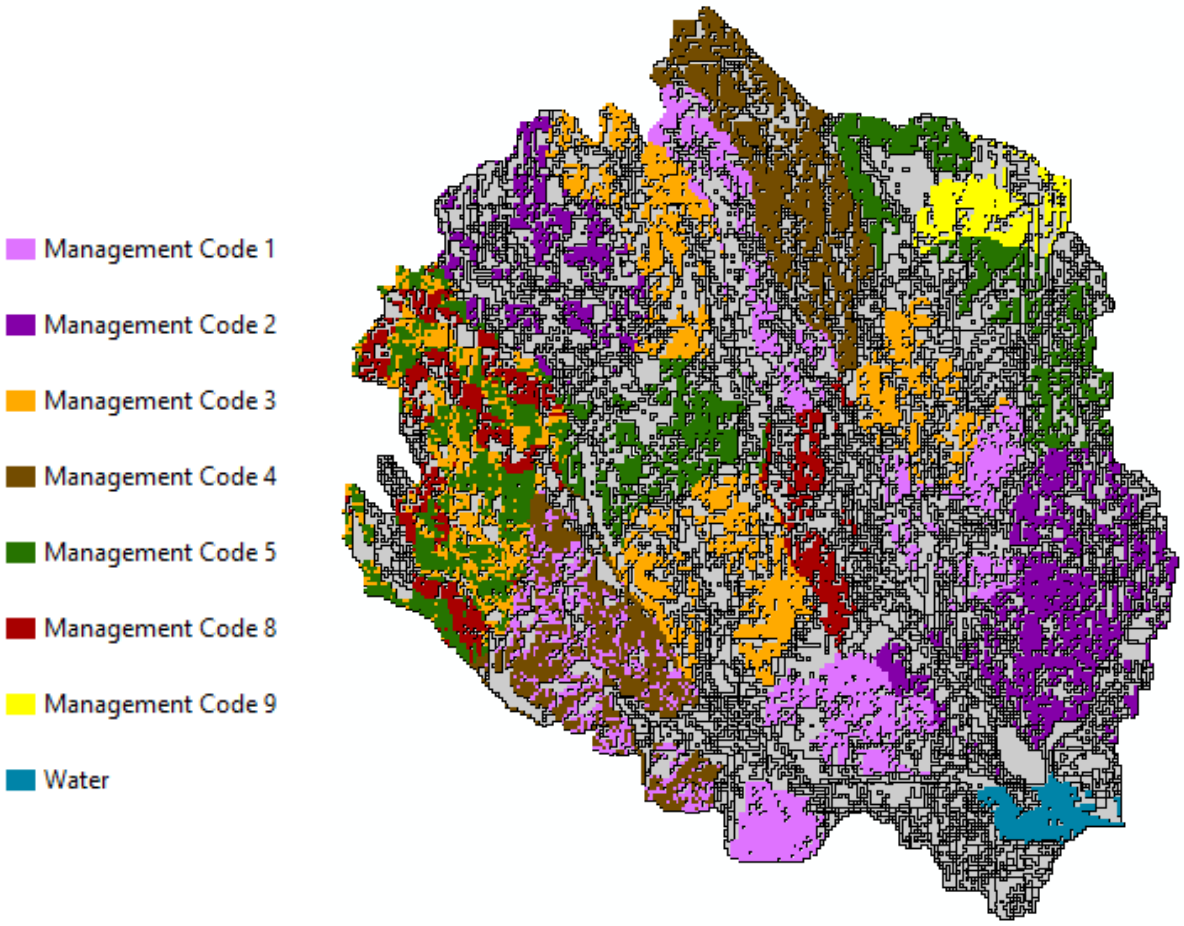

Figure 7.8: Optimal Solution Case Study 2

The sum of all non-dominated solutions found in the execution of this MOEA was 9,009. In order to avoid dominance within all dominated solutions, one last dominance check was performed at the end of the algorithm. In this last dominance check, ten non dominated solutions were found. The Pareto graphs for the last non-dominance check are shown in figure 7.9. Blue dots represent non-dominated solutions, while the red dot represents the solution that is closest to the ideal point [1 0 0 0 0 0 0].

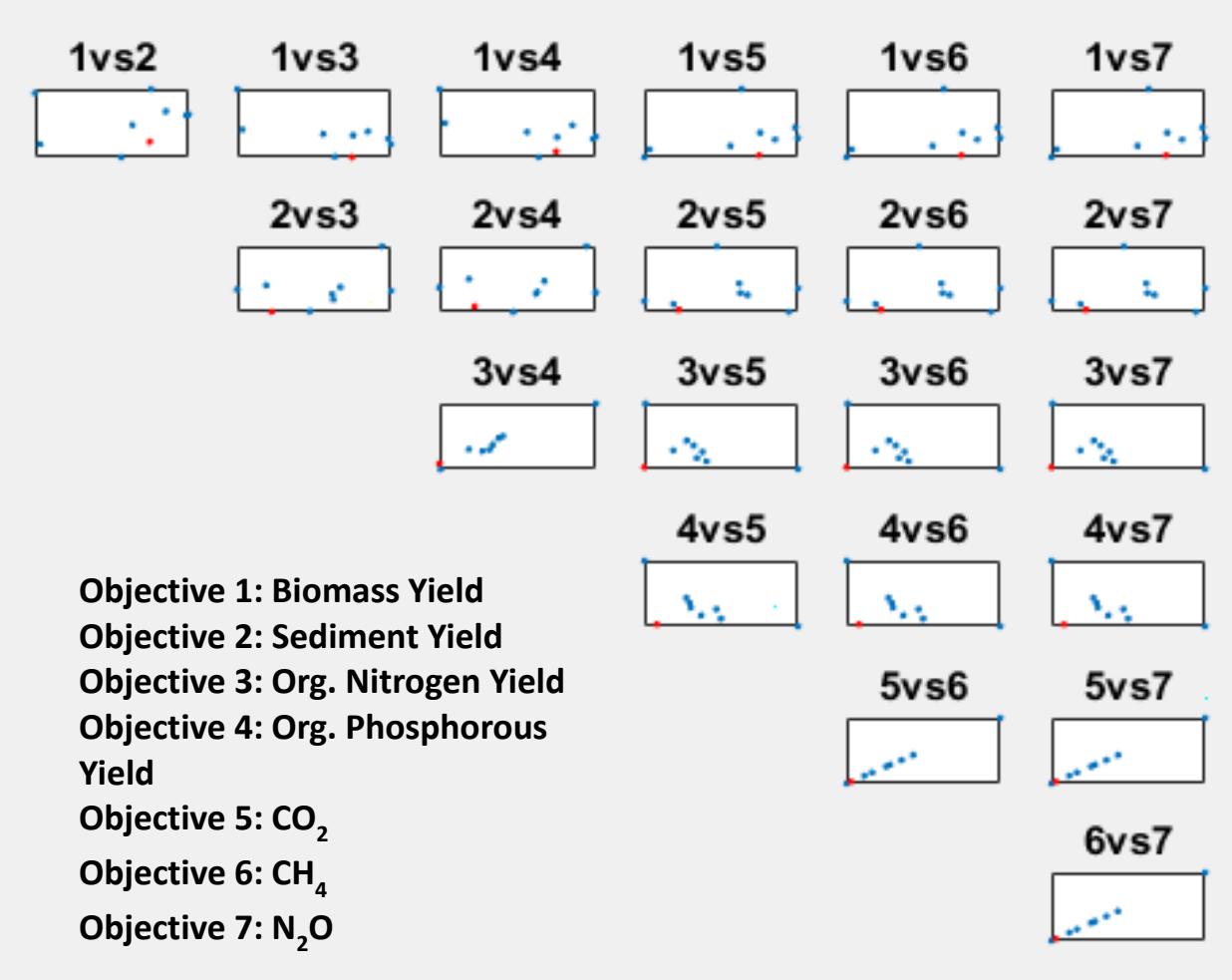

Figure 7.9: Pareto Graphs Case Study 2

The computational time to execute each management operation is 15 minutes. The MOEA computational time in this example was 23 minutes. Therefore, the total computational time to obtain the optimal solution shown in Case Study 2 was 2.88 hrs.

7.4 Case Study 3

The scheduled management operation used in Case Study 3, are listed in table 7.6. Similar to Case Study 1 and Case Study 2, the Management code (from 1 to 12) indicates the schedule management operation evaluated in the entire watershed and the SWAT operation number and name are used in the same sequence as shown in this table. Instead of using second-generation biofuel feedstock, this example introduces the use of first-generation feedstock for biofuel

production. The first operation (Plant/begin growing season) initializes the growth of Corn and Sugarcane as land covers in all HRUs. Instead of using irrigation, the second operation uses two different types of machinery for tillage operations (Chisel Plow Gt 21 ft and Moldboard Plow Reg DE 10b). Similar to Case Study 1, the fertilizer and pesticide applications are Nitrogen and Glufosinate using two levels of application, 0 and 20 kgs. These two levels were scheduled, as shown in the table below. The last operation skips one-year operation to January 1st and harvest in the 2nd year.

Table 7.6: Management Practices Case Study 3

SWAT Operation No.	1	10	3	4	5	17
	SWAT Operation Name					
Management Code	Plant/begin growing season	Tillage	Fertilizer Application	Pesticide Application	Harvest and Kill	Skip a Year Operation
1	Corn	Chisel*	0 kg/ha	0 kg/ha	SBY***	1 Year
2	Corn	Chisel*	20 kg/ha	0 kg/ha	SBY***	1 Year
3	Corn	Chisel*	20 kg/ha	20 kg/ha	SBY***	1 Year
4	Corn	Chisel*	0 kg/ha	0 kg/ha	SBY***	1 Year
5	Corn	Chisel*	20 kg/ha	0 kg/ha	SBY***	1 Year
6	Corn	Chisel*	20 kg/ha	20 kg/ha	SBY***	1 Year
7	Sugarcane	MP**	0 kg/ha	0 kg/ha	SBY***	1 Year
8	Sugarcane	MP**	20 kg/ha	0 kg/ha	SBY***	1 Year
9	Sugarcane	MP**	20 kg/ha	20 kg/ha	SBY***	1 Year
10	Sugarcane	MP**	0 kg/ha	0 kg/ha	SBY***	1 Year
11	Sugarcane	MP**	20 kg/ha	0 kg/ha	SBY***	1 Year
12	Sugarcane	MP**	20 kg/ha	20 kg/ha	SBY***	1 Year

* Chisel Plow Gt 21 ft
** Moldboard Plow Reg DE 10b
**Skip to Beginning of Year

This study aims to evaluate the biomass yield, sediment yield, water yield, and NO_3 surface runoff effects of these management practices.

The GREET Well to Pump pathway considered for each crop in this study was from farming until E85 for Dedi EtOH vehicle is delivered to the pump. The ethanol production was

done via fermentation. Figure 7.10 shows the GREET's life cycle system boundary used in this example.

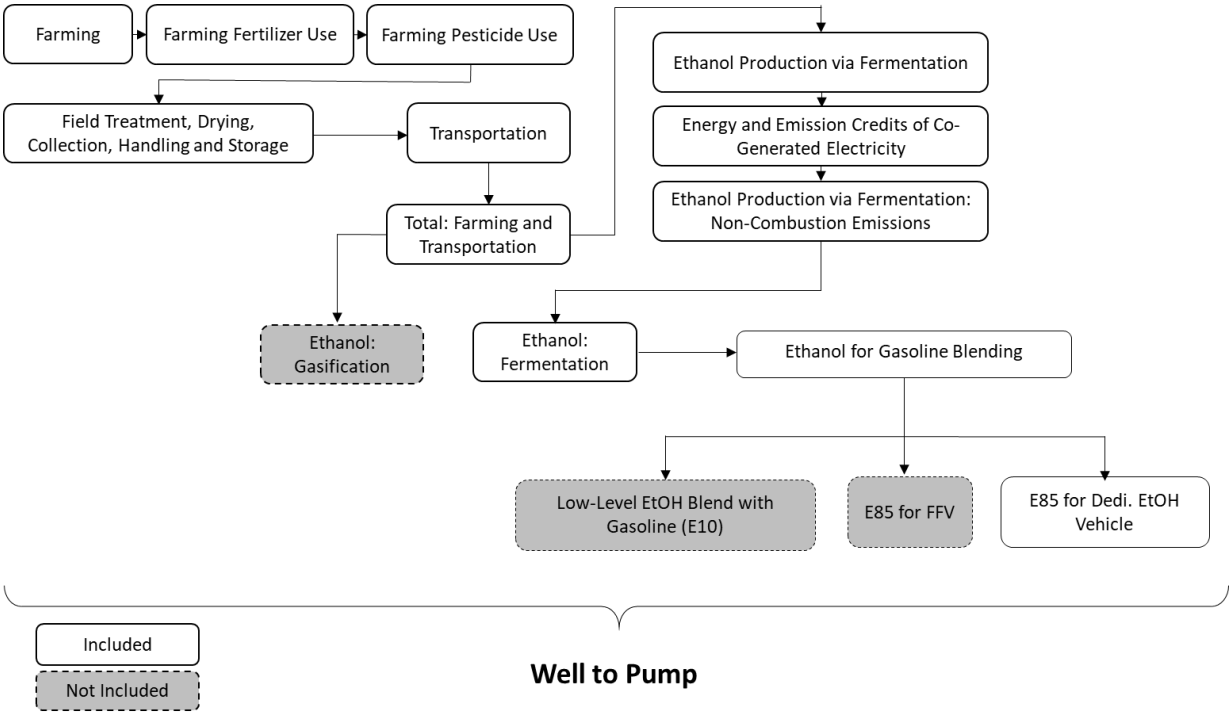

Figure 7.10: GREET's Life Cycle System Boundary Case Study 3

The MOEA was executed using 500 individuals and 1000 iterations. In each iteration, the top 25% of the most fitted individuals were selected for reproduction with a 75% chance of reproduction and a 1% chance of mutation. The management operations and the MOEA were run on an HP computer, with an Intel® Core™ i5 6200U CPU processor operating at 2.30 GHz 2.40 GHz and 8 GB of RAM.

The optimal solution given with these settings is displayed in table 7.7. Under these settings, 207,193.20kg/ha of biomass is produced on the watershed. The environmental impact corresponding to this biomass yield in terms of sediment yield is 116.74metric tons, the water leaving the HRU and entering the main channel is 1,964.94 mm/H_2O and 0.31 of NO_3 Surface Runoff. The greenhouse gas emissions evaluated, CO_2, CH_4 and N_2O yield a total of 4,705,751,467.37, 9,482,000.90 and 8,874,515.44 grams/mmBtu, respectively. While

management operations 1, 2, 4, 5, 6, 7, 8, 9, 10, 11 and 12 are considered in the optimal solution, only the management practices 3 was not considered optimal; therefore it was discarded.

Table 7.7: Optimal Solution Case Study 3

Sub-basin	Area (ha)	HRU	MP	Biomass Yield (kg/ha)	Sediment Yield (metric tons)	Water Yield (mm/H_2O)	NO_3 Surface Runoff (kg N/ha)	CO2 (grams/mmBtu)	CH4 (grams/mmBtu)	N2O (grams/mmBtu)
1	1395	1	7	9,620.20	1.23	82.32	0.02	-16,552.99	175.88	14.10
2	1194	2	5	5,905.00	9.09	82.49	0.01	248,896,793.36	678,172.69	1,678,456.56
3	1103	3	2	5,903.80	7.52	82.50	0.01	229,926,555.34	626,495.62	1,550,534.73
4	1413.7	4	9	13,715.90	0.69	82.45	0.02	210,961,006.77	414,386.73	270,081.32
	1754.3	5	8	13,705.90	1.33	82.42	0.04	50,047,074.69	158,190.44	330,583.34
5	3413	6	10	9,623.40	1.50	82.33	0.01	-16,543.43	175.91	14.10
6	2354	7	7	9,618.50	0.91	82.33	0.01	-16,558.07	175.87	14.10
7	2017	8	10	9,631.00	2.21	82.32	0.02	-16,520.72	175.97	14.10
8	1401	9	7	6,947.00	0.19	57.35	0.03	-24,541.56	152.70	13.84
9	532	10	12	13,340.40	0.88	86.47	0.01	79,384,498.88	156,069.55	101,645.32
10	1576	11	11	13,341.30	0.95	86.47	0.01	44,958,960.19	142,130.91	296,985.62
11	2584	12	7	9,613.40	0.84	82.34	0.01	-16,573.31	175.82	14.10
12	1202	13	10	6,944.80	0.32	57.36	0.02	-24,548.13	152.68	13.83
13	2394.13	14	6	5,903.70	8.47	82.49	0.01	2,874,994,043.1	5,405,648.05	3,408,288.26
	1429.87	15	10	9,630.50	2.29	82.30	0.02	-16,522.21	175.97	14.10
	1532	16	4	2,796.40	15.36	85.83	0.00	-14,464.32	112.65	9.58
14	2511	17	12	13,715.00	1.30	82.43	0.03	374,710,205.37	735,865.53	479,704.53
15	1859	18	4	1,985.20	18.67	89.62	0.00	-15,790.87	109.66	9.54
16	2599.66	19	1	2,797.40	16.36	85.83	0.00	-14,462.68	112.65	9.58
	1328.34	20	10	9,621.70	0.90	82.33	0.01	-16,548.51	175.89	14.10
17	3093	21	10	9,622.80	1.00	82.33	0.01	-16,545.22	175.90	14.10
18	3968	22	12	13,339.40	1.22	86.46	0.01	592,136,027.50	1,162,723.31	758,043.15
19	1874	23	4	1,983.30	21.91	89.60	0.00	-15,793.98	109.65	9.54
20	2576	24	10	7,887.20	1.60	86.56	0.01	-21,731.87	160.85	13.93
21	1579	25	7	0.00	0.00	0.00	0.00	0.00	0.00	0.00
Total				**207,193.2**	**116.74**	**1,965**	**0.31**	**4,705,751,467.3**	**9,482,000.90**	**8,874,515.44**

The Lake Fork Watershed map and the land change distribution according to the optimal solution is illustrated in figure 7.11. This map displays the entire optimal solution, including the water outlet.

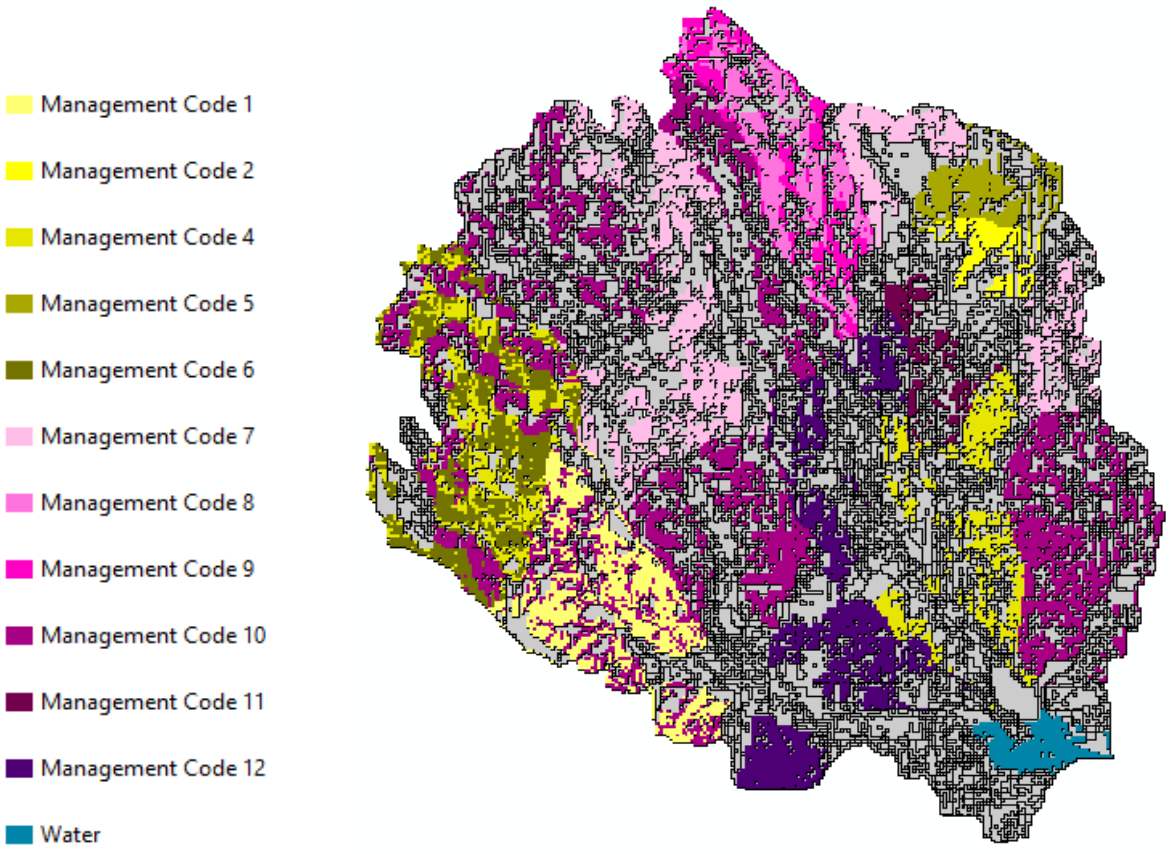

Figure 7.11: Optimal Solution Case Study 3

The sum of all non-dominated solutions found in the execution of this MOEA was 169,169. In order to avoid dominance within all dominated solutions, one last dominance check was performed at the end of the algorithm. In this last dominance check, 170 non dominated solutions were found. The Pareto graphs for the last non-dominance check are shown in figure 7.12. Blue dots represent non-dominated solutions, while the red dot represents the solution that is closest to the ideal point [1 0 0 0 0 0 0].

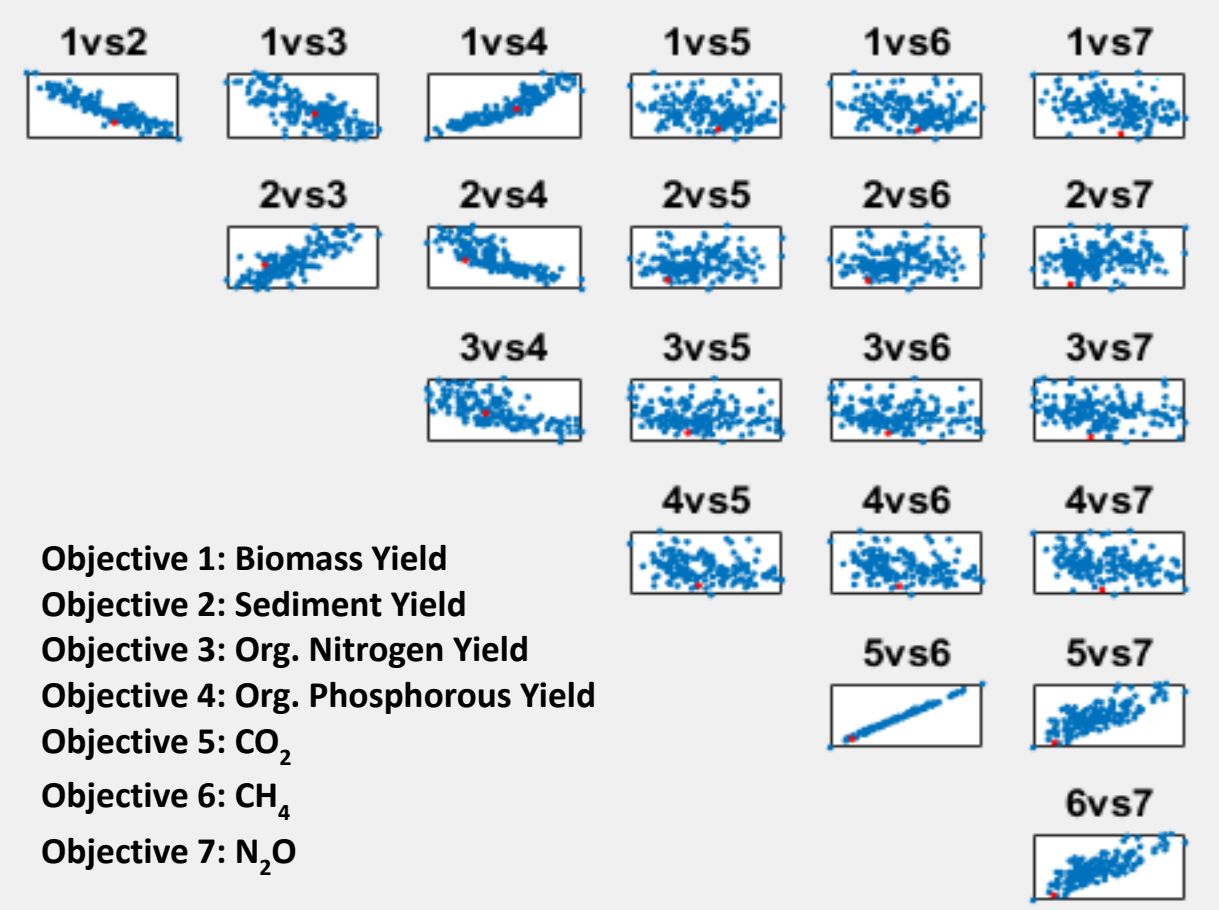

Figure 7.12: Pareto Graphs Case Study 3

The computational time to execute each management operation is 15 minutes. The MOEA computational time in this example was 2.60 hrs. Therefore, the total computational time to obtain the optimal solution shown in Case Study 3 was 5.60 hrs.

The following subsections used the SWAT simulation corresponding to the Lake Tawakoni watershed in Quinlan, TX. This simulation was divided into 26 sub-basins. The land cover in the 40,9535 hectares basin is comprised of Agricultural Land-Row Crops (AGRR), Pasture (PAST), Forest-Deciduous (FRSD), Range Grasses (RNGE) and water (WATR) and TX236 dominates the soil type in this area. Two slopes levels (0-1 and 1-9999) were considered. The weather was simulated with the SWAT user weather station Database (station count 4) while the rainfall, temperature, relative humidity, solar radiation, and wind speed data were set to default simulation.

In this model, 30 HRUs were used to be distributed according to similar land use, soil type, and slope along the 26 sub-basins. The description of each HRU is shown in table 7.8 and figures 7.13, 7.14 and 7.15 show the shapefiles for land use, soil, and slope, respectively

Table 7.8: Description of Lake Tawakoni Watershed

Sub-basin	HRU	Land Use	Soil Type	Slope	Area (ha)
1	1	AGRR	TX236	0-1	1026.62
	2	AGRR	TX236	1-9999	1005.02
	3	PAST	TX236	0-1	1209.35
2	4	AGRR	TX236	0-1	1393.16
	5	AGRR	TX236	1-9999	1211.59
	6	PAST	TX236	0-1	972.24
3	7	AGRR	TX236	0-1	3803.00
4	8	AGRR	TX236	0-1	2099.00
5	9	PAST	TX610	0-1	1747.00
6	10	PAST	TX610	0-1	1168.00
7	11	PAST	TX736	0-1	3241.00
8	12	PAST	TX212	0-1	1242.00
9	13	PAST	TX633	1-9999	1009.00
10	14	FRSD	TX212	0-1	493.00
11	15	PAST	TX212	0-1	1205.00
12	16	FRSD	TX193	0-1	469.00
13	17	PAST	TX610	0-1	2697.00
14	18	PAST	TX212	0-1	943.00
15	19	PAST	TX212	0-1	706.00
16	20	PAST	TX212	0-1	523.00
17	21	PAST	TX212	0-1	165.00
18	22	PAST	TX633	0-1	1455.00
19	23	PAST	TX212	0-1	1449.00
20	24	PAST	TX212	0-1	1129.00
21	25	PAST	TX193	0-1	509.00

22	26	FRSD	TX212	0-1	2402.00
23	27	WATR	TXW	0-1	35.00
24	28	WATR	TXW	0-1	2246.00
25	29	PAST	TX212	1-9999	2254.00
26	30	PAST	TX212	0-1	1128.00

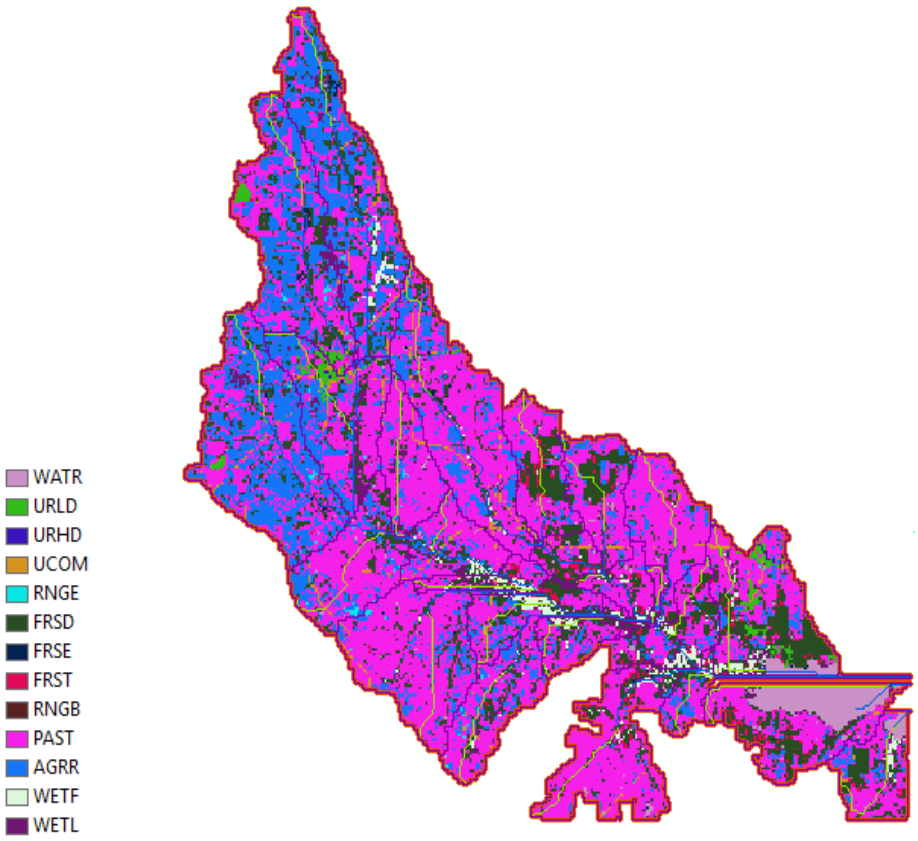

Figure 7.13: Land Use Shape

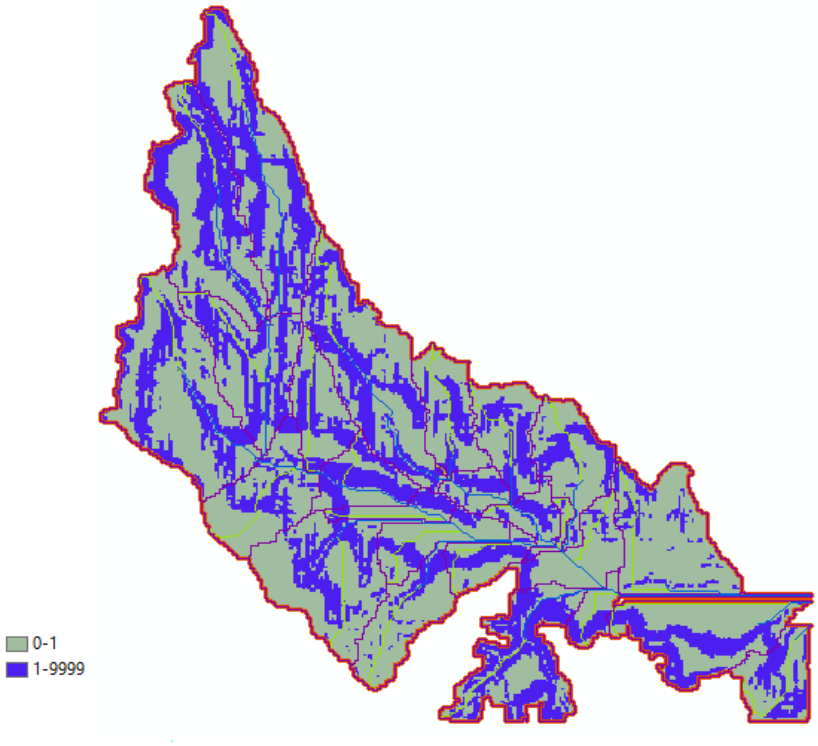

Figure 7.14: Slope Shape

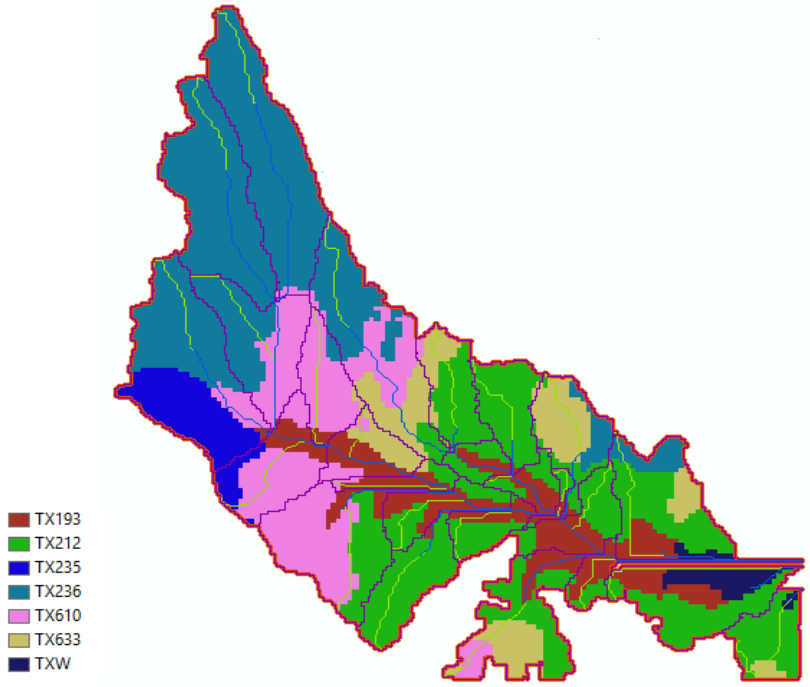

Figure 7.15: Soil Shape

The purpose of case studies 4 and 5 is to determine if pesticides influence biomass yields, water yield, NO_3 Surface Runoff, CO_2, CH_4, and N_2O. This is carried out by evaluating the same basin using different levels of fertilizers in case study 4 and adding a single level of fertilizer in case study 5.

7.5 CASE STUDY 4

The scheduled management operation used in Case Study 4, are listed in table 7.9. Similar to the previous case studies, the Management code (from 1 to 4) indicates the schedule management operation evaluated in the entire watershed and the SWAT operation number and name are used in the same sequence as shown in this table. The first operation (Plant/begin growing season) initializes the growth of switchgrass in all HRUs. The second operation (fertilizer application) applied Nitrogen to every HRU. Four levels of Nitrogen application were considered (0, 20, 40, and 60 kg/ha). No pesticide application is considered in this case study. The last operation skips one-year operation to January 1st and harvest in the 2nd year.

Table 7.9: Management Practices for Case Study4

SWAT Operation No.	1	3	4	5	17
	SWAT Operation Name				
Management Code	Plant/begin growing season	Fertilizer Application	Pesticide Application	Harvest and Kill	Skip a Year Operation
1	Switchgrass	0 kg/ha	0 kg/ha	SBY***	1 Year
2	Switchgrass	20 kg/ha	0 kg/ha	SBY***	1 Year
3	Switchgrass	40 kg/ha	0 kg/ha	SBY***	1 Year
4	Switchgrass	60 kg/ha	0 kg/ha	SBY***	1 Year

**Skip to Beginning of Year

This study aims to evaluate the biomass yield, sediment yield, water yield, and NO_3 surface runoff effects of these management practices.

The GREET Well to Wheel pathway considered for each crop in this study was from farming until Low-Level EtOH Blend with Gasoline (E10) is in its usage stage. The ethanol production was done via gasification. Figure 7.16 shows the GREET's life cycle system boundary used in this example.

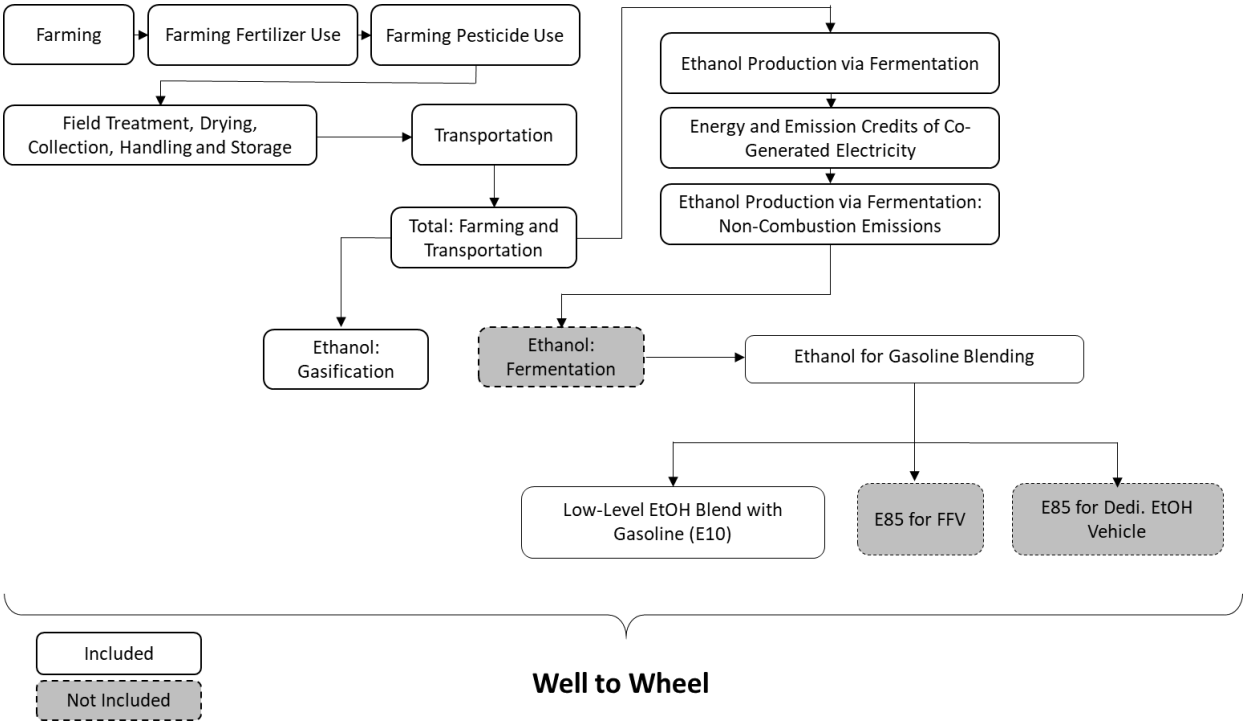

Figure 7.16: GREET's Life Cycle System Boundary Case Study 4

The MOEA was executed using 500 individuals and 1000 iterations. In each iteration, the top 25% of the most fitted individuals were selected for reproduction with a 75% chance of reproduction and a 1% chance of mutation. The management operations and the MOEA were run on an HP computer, with an Intel® Core™ i5 6200U CPU processor operating at 2.30 GHz 2.40 GHz and 8 GB of RAM.

The optimal solution given with these settings is displayed in table 7.10. Under these settings, 287,310.2 kg/ha of biomass is produced on the watershed. The environmental impact corresponding to this biomass yield in terms of sediment yield is 39.68 metric tons, the water leaving the HRU and entering the main channel is 2,268.43 mm/H_2O and 0.079 of NO_3 Surface Runoff. The greenhouse gas emissions evaluated, CO_2, CH_4, and N_2O yield a total of 170,276.4, 462.27, and 1133.75 grams/mmBtu, respectively.

Table 7.10: Optimal Solution for Case Study 4

Sub-basin	Area (ha)	HRU	MP	Biomass Yield (kg/ha)	Sediment Yield (metric tons)	Water Yield (mm/ H_2O)	NO_3 Surface Runoff (kg N/ha)	CO2 (grams/mmBtu)	CH4 (grams/mmBtu)	N2O (grams/mmBtu)
1	1026	1	4	11728.6	1.131	85.823	0	11155.87	30.33283	74.70777
2	1005	2	2	8654	3.018	85.906	0	3691.816	10.00105	24.38095
3	1209	3	4	11180.4	0.895	80.336	0	13127.59	35.70422	88.00459
4	1393	4	4	11729	0.974	85.823	0	15111.24	41.10773	101.38
	1211	5	2	8655	2.286	85.906	0	4434.821	12.02508	29.39124
5	972	6	4	11180.5	0.895	80.336	0	10568.9	28.73408	70.75067
6	3803	7	2	8657.6	1.488	85.903	0	13756.23	37.41764	92.24814
7	2099	8	1	6396.2	2.116	86.372	0	76.09193	0.152243	0.00306
8	1747	9	2	10693.1	1.25	77.666	0.003	6361.245	17.27213	42.37809
9	1168	10	1	6906.5	2.668	80.885	0.002	76.22533	0.15242	0.003063
10	3241	11	1	6727.4	2.357	81.36	0	76.17851	0.152358	0.003062
11	1242	12	3	11584.7	0.899	82.169	0.004	9012.497	24.49411	60.25467
12	1009	13	3	11268	1.482	80.895	0.016	7336.193	19.92779	48.95143
13	493	14	3	11781	1.232	81.152	0.005	3624.182	9.815662	23.91938
	1205	15	3	11581.6	1.114	82.165	0.005	8746.315	23.769	58.45973
	469	16	4	13666.7	0.295	59.401	0	5139.029	13.94158	34.13111
14	2697	17	1	6907.7	2.189	80.884	0.002	76.22565	0.15242	0.003063
15	943	18	3	11584.3	1.087	82.168	0.004	6861.467	18.63446	45.74966
16	706	19	3	11579.3	1.307	82.162	0.006	5156.468	13.98986	34.25238
	523	20	3	11581.3	1.114	82.164	0.005	3839.952	10.40352	25.37473
17	165	21	4	13007.8	0.778	82.039	0.006	1858.355	5.004905	12.00975
18	1455	22	2	9599.1	1.639	81.076	0.007	5310.623	14.41052	35.29537
19	1449	23	1	5865.6	2.41	85.129	0.002	75.95322	0.15206	0.003057
20	1129	24	2	9838.7	0.885	82.366	0.002	4138.051	11.21621	27.38796
21	509	25	4	13564.2	0.408	62.467	0	5570.647	15.1174	37.04181
	2402	26	2	9976	0.986	81.362	0.002	8717.119	23.69006	58.26568

35	27	---	0	0	0	0	0	0	0
2246	28	---	0	0	0	0	0	0	0
2254	29	2	9832.6	1.673	82.357	0.004	8184.72	22.23979	54.67581
1128	30	3	11583.3	1.106	82.166	0.004	8192.371	22.25999	54.72433
Total			**287310**	**39.682**	**2268.438**	**0.079**	**170276.4**	**462.2711**	**1133.751**

The Lake Tawakoni Watershed map and the land change distribution according to the optimal solution is illustrated in figure 7.17. This map displays the entire optimal solution, including the water outlets.

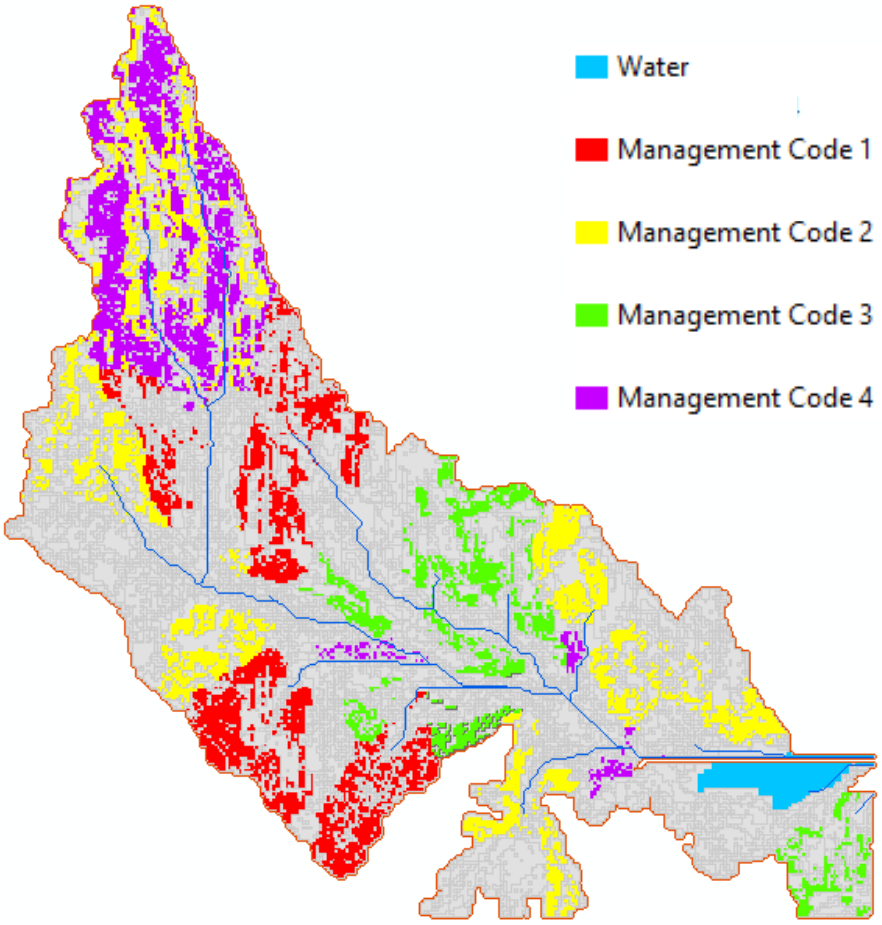

Figure 7.17: Optimal Solution Case Study 4

The sum of all non-dominated solutions found in the execution of this MOEA was 123,123. In order to avoid dominance within all dominated solutions, one last dominance check was performed at the end of the algorithm. In this last dominance check, 124 non dominated solutions were found. The Pareto graphs for the last non-dominance check are shown in figure 7.18. Blue dots represent non-dominated solutions, while the red dot represents the solution that is closest to the ideal point [1 0 0 0 0 0 0].

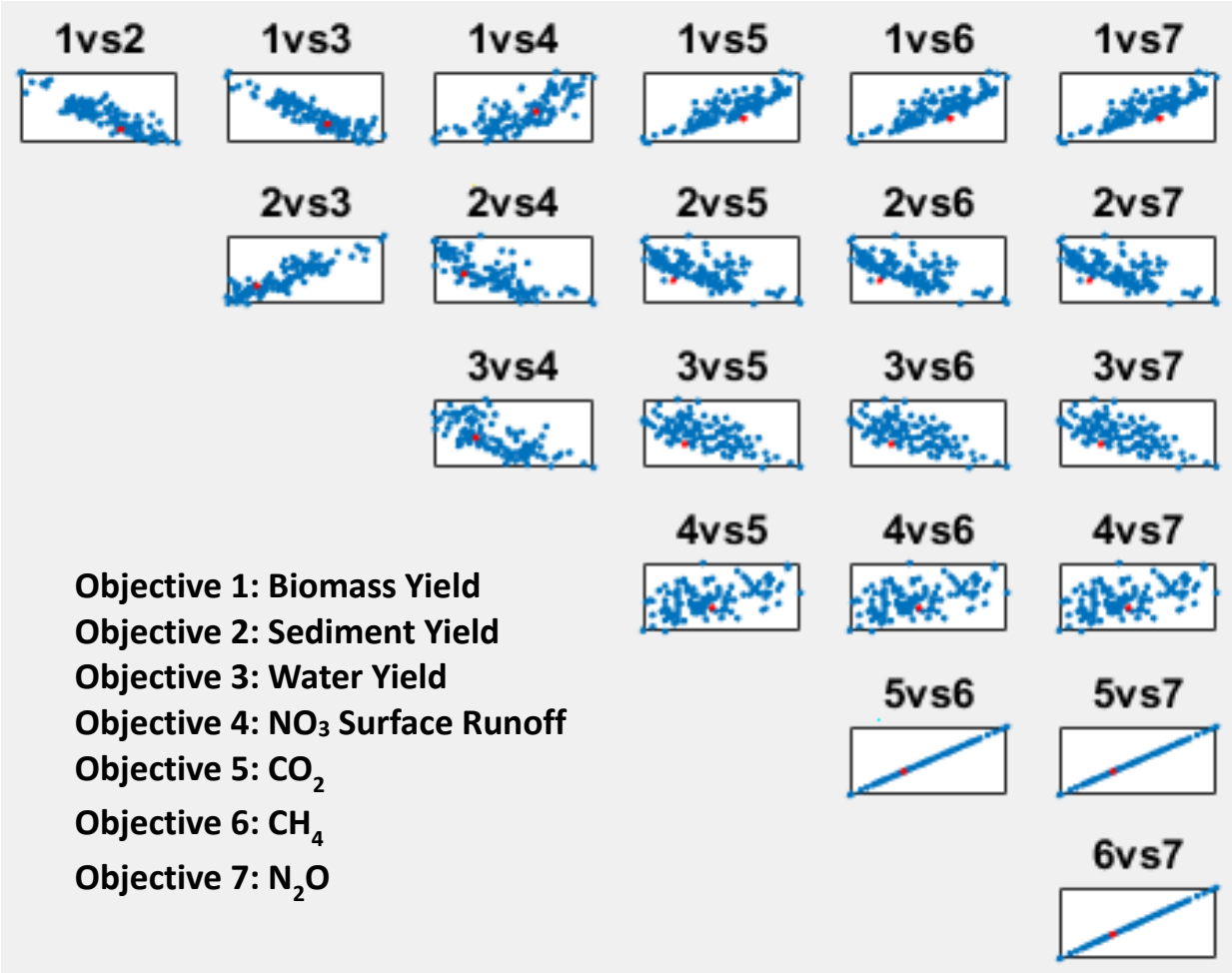

Figure 7.18: Pareto Graphs Case Study 4

The computational time to execute each management operation is 15 minutes. The MOEA computational time in this example was 1.47 hrs. Therefore, the total computational time to obtain the optimal solution shown in Case Study 4 was 2.47 hrs.

7.6 CASE STUDY 5

As previously mentioned, this case study uses the same management operation schedule used in Case Study 4, plus a single application of pesticide in all HRUs. The management practices are listed in table 7.11. The management code (from 1 to 4) indicates the schedule management operation evaluated in the entire watershed and the SWAT operation number and name are used in the same sequence as shown in this table. The first operation (Plant/begin growing season) initializes the growth of switchgrass in all HRUs. The second operation (fertilizer application) applied Nitrogen to every HRU. Four levels of Nitrogen application were considered (0, 20, 40, and 60 kg/ha). The third operation considers a single level of pesticide application (Glufosinate - 30 kg/ha). The last operation skips one-year operation to January 1st and harvest in the 2nd year.

Table 7.11: Management Operations for Case Study 5

SWAT Operation No.	1	3	4	5	17
	SWAT Operation Name				
Management Code	Plant/begin growing season	Fertilizer Application	Pesticide Application	Harvest and Kill	Skip a Year Operation
1	Switchgrass	0 kg/ha	30 kg/ha	SBY***	1 Year
2	Switchgrass	20 kg/ha	30 kg/ha	SBY***	1 Year
3	Switchgrass	40 kg/ha	30 kg/ha	SBY***	1 Year
4	Switchgrass	60 kg/ha	30 kg/ha	SBY***	1 Year

**Skip to Beginning of Year

As in case study 4, this study aims to evaluate the biomass yield, sediment yield, water yield, and NO_3 surface runoff effects of these management practices.

The GREET Well to Wheel pathway considered for each crop in this study is the equivalent to that of case study 4. For reference, see figure 7.16 for the GREET's life cycle system boundary.

The MOEA was executed using 500 individuals and 1000 iterations. In each iteration, the top 25% of the most fitted individuals were selected for reproduction with a 75% chance of reproduction and a 1% chance of mutation. The management operations and the MOEA were run

on an HP computer, with an Intel® Core™ i5 6200U CPU processor operating at 2.30 GHz 2.40 GHz and 8 GB of RAM.

As shown in table 7.12, the same optimal solution obtained in case study 4 was found in this case study. Therefore, no influence on biomass yields, water yield, NO_3 Surface Runoff, CO_2, CH_4, and N_2O was found by adding pesticide to the management practices.

Table 7.12: Optimal Solution for Case Study 5

Sub-basin	Area (ha)	HRU	MP	Biomass Yield (kg/ha)	Sediment Yield (metric tons)	Water Yield (mm/H_2O)	NO_3 Surface Runoff (kg N/ha)	CO2 (grams/mmBtu)	CH4 (grams/mmBtu)	N2O (grams/mmBtu)
1	1026	1	4	11728.6	1.131	85.823	0	11155.87	30.33283	74.70777
2	1005	2	2	8654	3.018	85.906	0	3691.816	10.00105	24.38095
3	1209	3	4	11180.4	0.895	80.336	0	13127.59	35.70422	88.00459
4	1393	4	4	11729	0.974	85.823	0	15111.24	41.10773	101.38
	1211	5	2	8655	2.286	85.906	0	4434.821	12.02508	29.39124
5	972	6	4	11180.5	0.895	80.336	0	10568.9	28.73408	70.75067
6	3803	7	2	8657.6	1.488	85.903	0	13756.23	37.41764	92.24814
7	2099	8	1	6396.2	2.116	86.372	0	76.09193	0.152243	0.00306
8	1747	9	2	10693.1	1.25	77.666	0.003	6361.245	17.27213	42.37809
9	1168	10	1	6906.5	2.668	80.885	0.002	76.22533	0.15242	0.003063
10	3241	11	1	6727.4	2.357	81.36	0	76.17851	0.152358	0.003062
11	1242	12	3	11584.7	0.899	82.169	0.004	9012.497	24.49411	60.25467
12	1009	13	3	11268	1.482	80.895	0.016	7336.193	19.92779	48.95143
13	493	14	3	11781	1.232	81.152	0.005	3624.182	9.815662	23.91938
	1205	15	3	11581.6	1.114	82.165	0.005	8746.315	23.769	58.45973
	469	16	4	13666.7	0.295	59.401	0	5139.029	13.94158	34.13111
14	2697	17	1	6907.7	2.189	80.884	0.002	76.22565	0.15242	0.003063
15	943	18	3	11584.3	1.087	82.168	0.004	6861.467	18.63446	45.74966
16	706	19	3	11579.3	1.307	82.162	0.006	5156.468	13.98986	34.25238
	523	20	3	11581.3	1.114	82.164	0.005	3839.952	10.40352	25.37473
17	165	21	4	13007.8	0.778	82.039	0.006	1858.355	5.004905	12.00975
18	1455	22	2	9599.1	1.639	81.076	0.007	5310.623	14.41052	35.29537
19	1449	23	1	5865.6	2.41	85.129	0.002	75.95322	0.15206	0.003057
20	1129	24	2	9838.7	0.885	82.366	0.002	4138.051	11.21621	27.38796
21	509	25	4	13564.2	0.408	62.467	0	5570.647	15.1174	37.04181
	2402	26	2	9976	0.986	81.362	0.002	8717.119	23.69006	58.26568
	35	27	---	0	0	0	0	0	0	0
	2246	28	---	0	0	0	0	0	0	0

2254	29	2	9832.6	1.673	82.357	0.004	8184.72	22.23979	54.67581
1128	30	3	11583.3	1.106	82.166	0.004	8192.371	22.25999	54.72433
Total			**287310**	**39.682**	**2268.4**	**0.079**	**170276.4**	**462.2711**	**1133.751**

The optimal solution map and the Pareto graphs are equivalent to figures 7.17 and 7.18, respectively.

7.7 CHAPTER CONCLUSIONS

In this chapter, it was demonstrated that the proposed optimization model described in chapter 6 could be employed for optimal allocation design in Land-Use and Land-Cover change to produce biofuel feedstock. The different case studies presented verified that the optimization model can accommodate different simulation scenarios and that the optimization objectives can be modified to satisfy the different needs or constrains in different landscape scenarios.

The conclusions of this project are provided in the next chapter. Also, the future work and how this optimization model can be expanded to increase the research in different areas are explained.

Chapter 8: Conclusions and Future Work

8.1 Conclusions

Expanding the production of bioethanol has reduced the U.S. reliance on foreign oil and can potentially reduce the anthropogenic GHG concentration levels in the atmosphere that are attributed to the combustion of fossil fuels. However, the natural resource exploitation for biofuel feedstock production may intensify the environmental impacts in ecosystem services. Tradeoffs between these services must be carefully considered when deciding for land use/land change covers and management practices to optimize their performance. Therefore, an exhaustive understanding of agroecosystems is needed for optimal performance of future biofuel feedstock land cover that can improve environmental health while reducing the effects on soil, water, and atmosphere.

The rising demand for clean, renewable fuels has forced the need to develop more suitable tools to analyze these land-use changes, along with variant agricultural management practices. Coupling hydrological and life cycle assessment models with heuristic multiple objective evolutionary algorithms is a viable approach to identifying optimal factors that would ultimately lessen the effects of natural resource exploitation.

This study proposed a coupled modeling framework to optimize land use and land change allocation for biofuel feedstock production. This interactive framework coupled the Soil and Water Assessment Tool to quantify the effects of land change and land management practices at the watershed scaled and the Greenhouse gases, Regulated Emissions, and Energy use in Transportation Model (GREET) to quantify the potential GHG emissions effects from a life cycle assessment perspective. A multi-objective genetic algorithm was integrated for optimal allocation design in Land-Use and Land-Cover changes. This algorithm takes into account the environmental

effects on soil and water from replacing regional crops for biofuel feedstock (SWAT) and the GHG emissions produced in every stage of the life cycle (cradle to gate) from converting these feedstocks into biofuel (GREET) while increasing the performance of the system by maximizing biomass yields.

This innovative optimization approach can be applied to assist the decision-making process when exploiting resources in ecosystem services to reduce the anthropogenic effects from conventional fossil fuels. It was demonstrated that the proposed model is flexible and can be used to accommodate the different needs that might arise. However, to verify the accuracy of the results, the initial SWAT simulation needs further calibration and validation. Ideally, these should be processed and spatially based considering uncertainties in parameters inputs and outputs. Many techniques for calibration and validation of SWAT simulations can be found in literature (Arnold et al., 2012). It is strongly recommended that the application of the proposed optimization model for decision making, be carried out with proper model calibration.

8.2 Future Work

For future research, the methodology developed in the proposed model will be used to study different Land-Use and Land-Cover changes in the calibrated simulation watershed models of Oklahoma, with the support of the Agricultural Research Service – USDA in El Reno, OK. Furthermore, it is likely to integrate new watershed simulations with the intent of assessing the effects of biofuel feedstock cultivation and the conversion of these feedstocks to biofuel in different regions. Findings from these studies are expected to be disseminated in peer-reviewed journals.

Additionally, to obtain the maximum benefit from all the work and effort made on this project, it is planned to develop an executable version of the proposed optimization model and make it

available through a digital platform for researchers and stakeholders to use in different research areas.

Currently, the proposed model considers eight different crops that can be used to analyze Land-Cover changes for biofuel feedstock production (alamo switchgrass, corn, corn silage, poplar, sorghum hay, sugarcane, willow, and miscanthus). However, in order to evaluate additional Land-Cover changes, besides to those crops established in this model, it is necessary to integrate additional life cycle assessment models and databases, such as the GaBi Software. This will extend the capability of the model in the assessment of biofuel feedstock production when the aim is converting feedstocks to bioethanol.

Similarly, the model can be extended to optimize and quantify the environmental effects of Land-Use and Land-Cover change for optimal allocation design in biofuel feedstock production, considering the conversion of the feedstock to biodiesel. In that instance, the GREET life cycle assessment model can be used to analyze the Land-Cover changes to Soybean, Palm Oil, Canola, Jatropha, Camelina, Tallow, and Carinata. From these crops, the SWAT database only includes Soybean. Therefore, the growth parameters for the remaining biofuel feedstock should be added to the SWAT database.

Future extensions to the model also include addressing the current and future climate change challenges as a decision-making variable of resilient food-energy-water-ecosystem services systems (FEWES) in optimal allocation design for biofuel feedstock production. In this context, the aim is to assess the climate variability and change impacts on soil and water resources to produce clean, renewable fuels.

Lastly, it is intended to integrate the water footprint to indicate the direct and indirect freshwater used to produce biofuel. The objective is to generate the blue water footprint that refers

to the consumption of blue water resources from the available surfaces and groundwater, associated to water evaporation, the transportation of water to a tributary channel and main channel or reach. Also, the development of the green water footprint, which refers to the consumption of green water resources associated with the rainwater stored in the soil as soil moisture. Finally, the development of the gray water footprint, which refers to pollution associated with the required volume of freshwater to assimilate pollution load as stated by existing water quality standards.

References

Arabi, M., R. S. Govindaraju, and M. M. Hantush (2006), Cost-effective allocation of watershed management practices using a genetic algorithm, *Water Resour. Res*., 42, W10429, doi:10.1029/2006WR004931.

Arnold, J.G. Kiniry, J.R. Srinivasan, R. Williams, J.R. Haney, E.B. Neitsch, S.L. (2012) SWAT Input/Output fiel documentation, Version 2012, *Texas Water Resources Institute*

Azapagic, A. Clift, R. (1999a) Life cycle assessment and multiobjective optimisation. *Journal of Cleaner Production,* Volume 7, Pages 135-143.

Azapagic, A. Clift, R. (1999b) The application of life cycle assessment to process optimization, *Computers and Chemical Engineering,* Volume 23, Pages 1509-1526.

Batidzirai B., E. Smeets, and A. Faaij (2012). Harmonising bioenergy resource potentials—Methodological lessons from review of state of the art bioenergy potential assessments. Renewable and Sustainable Energy Reviews 16, 6598–6630.

Batidzirai B., E. Smeets, and A. Faaij (2012). Harmonising bioenergy resource potentials—Methodological lessons from review of state of the art bioenergy potential assessments. Renewable and Sustainable Energy Reviews 16, 6598–6630.

Bazaraa, M., Jarvis, J., Sherali, H., (2010) Linear programming and network flows. John Wiley & Sons, Inc., Hoboken, New Jersey.

Beringer T., W. Lucht, and S. Schaphoff (2011). Bioenergy production potential of global biomass plantations under environmental and agricultural constraints. GCB Bioenergy 3, 299–312. doi: 10.1111/j.1757-1707.2010.01088.x, ISSN: 1757-1707.

Berndes G., S. Ahlgren, P. Börjesson, and A. L. Cowie (2013). Bioenergy and land use change—state of the art. Wiley Interdisciplinary Reviews: Energy and Environment 2, 282–303. doi: 10.1002/wene.41, ISSN: 2041-840X

Blanco G., R. Gerlagh, S. Suh, J. Barrett, H.C. de Coninck, C.F. Diaz Morejon, R. Mathur, N. Nakicenovic, A. Ofosu Ahenkora, J. Pan, H. Pathak, J. Rice, R. Richels, S.J. Smith, D.I. Stern, F.L. Toth, and P. Zhou, 2014: Drivers, Trends and Mitigation. In: Climate Change 2014: Mitigation of Climate Change. Contribution of Working Group III to the Fifth Assessment Report of the Intergovernmental Panel on Climate Change [Edenhofer, O., R. Pichs-Madruga, Y. Sokona, E. Farahani, S. Kadner, K. Seyboth, A. Adler, I. Baum, S. Brunner, P. Eickemeier, B. Kriemann, J. Savolainen, S. Schlömer, C. von Stechow, T. Zwickel and J.C. Minx (eds.)]. Cambridge University Press, Cambridge, United Kingdom and New York, NY, USA.

Bojarski, A.D. Laínez, J.M. Espuña, A. Puigjaner, L. (2009) Incorporating environmental impacts and regulations in a holistic supply chains modeling: an LCA approach, *Computers and Chemical Engineering*, Volume 33 (10), Pages 1747-1759.

Brandão M., L. Milà i Canals, and R. Clift (2011). Soil organic carbon changes in the cultivation of energy crops: Implications for GHG balances and soil quality for use in LCA. Biomass and Bioenergy 35, 2323–2336. doi: 10.1016/j.biombioe.2009.10.019, ISSN: 0961-9534.

Bucak, T. Trolle, D. Andersen, H., E. Thodsen, H. Erdogan, S. Levi, E., E. Filiz, N. Jeppesen, E. Beklioglu, M. (2017) Future water availability in the largest freshwater Mediterranean lake is at great risk as evidenced from simulations with the SWAT model, *Science of The Total Environment*, 581–582, 413–425

California Air Resources Board. Proposed regulation for implemeing low carbon fuel standards. In: Staff report: initial statement of reasons, vol. 1. Sacramento, CA: California Envirionmental Protection Agency, Air Resources Board; March 5, 2009. 374p

Carvalho, M. Serra, L.M. Lozano, M.A. (2011) Optimal synthesis of trigeneration systems subject to environmental constraints, *Energy*, Volume 36, Pages 3779-3790

Cherubini F., G. Guest, and A. Strømman (2012). Application of probability distributions to the modeling of biogenic CO2 fluxes in life cycle assessment. GCB Bioenergy 4, 784–798. doi: 10.1111/j.1757-1707.2011.01156.x, ISSN: 1757-1707.

Chichakly, K. J. Bowden, W. B. Eppstein, M. J. (2013) Minimization of cost, sediment load, and sensitivity to climate change in a watershed management application, *Environmental Modelling & Software*, Volume 50, Pages 158-168.

Chum H., A. Faaij, J. Moreira, G. Berndes, P. Dhamija, H. Dong, B. Gabrielle, A. G. Eng, W. Lucht, M. Mapako, O. M. Cerutti, T. McIntyre, T. Minowa, and K. Pingoud (2011). Bioenergy. In: IPCC Special Report on Renewable Energy Sources and Climate Change Mitigation [O. Edenhofer, R. Pichs-Madruga, Y. Sokona, K. Seyboth, P. Matschoss, S. Kadner, T. Zwickel, P. Eickemeier, G. Hansen, S. Schlömer, C. von Stechow (eds)],. Cambridge University Press, Cambridge, United Kingdom and New York, NY, USA, pp. 209–332.

Coelho S., O. Agbenyega, A. Agostini, K. H. Erb, H. Haberl, M. Hoogwijk, R. Lal, O. Lucon, O. Masera, and J. R. Moreira (2012). Chapter 20—Land and Water: Linkages to Bioenergy. In: Global Energy Assessment—Toward a Sustainable Future. Cambridge University Press, Cambridge, UK and New York, NY, USA and the International Institute for Applied Systems Analysis, Laxenburg, Austria, Cambridge, UK, pp. 1459–1526. ISBN: 9780521182935

Coello, C. A. Lamont, G. B. Van Veldhuizen, D. A. (2007) Evolutionary Algorithms for Solving Multi-Objective Problems. Springer

Confesor, R, B. Whittaker, G, W. (2007) Automatic calibration of hydrologic models with multi-objective evolutionary algorithm and pareto optimization, *American water resources association*, Volume 43, Page 4.

Cools, J. Broekx, S. Vandenberghe, V. Sels, H. Meynaerts, E. Vercaemst, P. Seuntjens, P. Hulle, S. V. Wustenberghs, H. Bauwens, W. Huygens, M. (2011) Coupling a hydrological waterquality model and aneconomic optimization model to set up a cost-effective emission reduction scenario for nitrogen, *Environmental Modelling & Software,* Volume 26, Pages 44-51.

Daigneault A., B. Sohngen, and R. Sedjo (2012). Economic Approach to Assess the Forest Carbon Implications of Biomass Energy. Environmental Science & Technology 46, 5664–5671. doi: 10.1021/es2030142, ISSN: 0013-936X.

Das, S., Maitya, S., Qub, B., Sugantha, P. N., (2011) Real-parameter evolutionary multimodal optimization - A survey of the state-of-the-art. *Swarm and Evolutionary Computation 1, 71–88*

Davis S. C., R. M. Boddey, B. J. R. Alves, A. L. Cowie, B. H. George, S. M. Ogle, P. Smith, M. van Noordwijk, and M. T. van Wijk (2013). Management swing potential for bioenergy crops. GCB Bioenergy 5, 623–638. doi: 10.1111/gcbb.12042, ISSN: 1757-1707.

De Wit M., M. Junginger, and A. Faaij (2013). Learning in dedicated wood production systems: Past trends, future outlook and implications for bioenergy. Renewable and Sustainable Energy Reviews 19, 417–432. doi: 10.1016/j. rser.2012.10.038, ISSN: 1364-0321.

Deb, K., 2001, Multiobjective Optimization Using Evolutionary Algorithms, Wiley, New York

Dornburg V., D. van Vuuren, G. van de Ven, H. Langeveld, M. Meeusen, M. Banse, M. van Oorschot, J. Ros, G. Jan van den Born, H. Aiking, M. Londo, H. Mozaffarian, P. Verweij, E.

Lysen, and A. Faaij (2010). Bioenergy revisited: Key factors in global potentials of bioenergy. Energy and Environmental Science 3, 258–267. doi: 10.1039/b922422j, ISSN: 1754-5692.

Eliceche, A. Corvalán, S. Martínez, P. (2007) Environmental life cycle impact as a tool for process optimization of a utility plant. *Computers and Chemical Engineering*, Volume 31, Pages 648-656.

Ercan, M. B., Goodall, J. L. (2016). Design and implementation of a general software library for using NSGA-II with SWAT for multi-objective model calibration, *Environmental Modeling & Software*, Volume 84, Pages 112-120.

Faaij A. (2006). Modern Biomass Conversion Technologies. Mitigation and Adaptation Strategies for Global Change 11, 335–367. doi: 10.1007/s11027-005-900 4-7, ISSN: 1381-2386, 1573–1596.

Fischer G., S. Prieler, H. Van Velthuizen, G. Berndes, A. Faaij, M. Londo, and M. De Wit (2010). Biofuel production potentials in Europe: Sustainable use of cultivated land and pastures, Part II: Land use scenarios. Biomass and Bioenergy 34, 173–187

Frank, E.D. Han, J. Palou-Rivera, I. Elgowainy, A. Wang, M. Q. (2011) Life-Cycle Analyisis of Algal Lipid Fuels with the GREET Model, *Energy Systems Division, Argonne National Laboratory*.

Garg K. K., L. Karlberg, S. P. Wani, and G. Berndes (2011). Jatropha production on wastelands in India: opportunities and trade-offs for soil and water management at the watershed scale. Biofuels, Bioproducts and Biorefining 5, 410–430. doi: 10.1002/bbb.312, ISSN: 1932-1031.

Gassman, P. W. Reyes, M. R. Green, C. H. Arnold, J. G. (2007) The Soil and Water Assessment Tool: Historical Development, Applications, and Future Research Directions, *American Society of Agricultural and Biological Engineers*, Volume 50(4), Pages 1211-1250.

GEA (2012). Global Energy Assessment—Toward a Sustainable Future. Cambridge University Press, Cambridge, UK and New York, NY, USA and the International Institute for Applied Systems Analysis, Laxenburg, Austria, 1802 pp.

Gebreslassie, B.H. Guillén-Gosálbez, G. Jiménez, L. Boera, D. (2010) A systematic tool for the minimization of the life cycle impact of solar assisted absorption cooling systems, *Energy*, Volume 35, Issue 9, Pages 3849-3862

Gelfand I., R. Sahajpal, X. Zhang, R. C. Izaurralde, K. L. Gross, and G. P. Robertson (2013). Sustainable bioenergy production from marginal lands in the US Midwest. Nature 493, 514–517. doi: 10.1038/nature11811, ISSN: 0028-0836, 1476–4687.

Gerbens-Leenes W., A. Y. Hoekstra, and T. H. Van der Meer (2009). The water footprint of bioenergy. Proceedings of the National Academy of Sciences 106, 10219–10223. Available at: http:/ /www.pnas.org/content/106/25/10219. short.

Ghosh, A. Dehuri, S. (2004) Evolutionary Algorithms for Multi-Criterion Optimization: A Survey. *International Journal of Computing & Information Sciences* Vol. 2, No. 1

Gibbs H. K., M. Johnston, J. A. Foley, T. Holloway, C. Monfreda, N. Ramankutty, and D. Zaks (2008). Carbon payback times for crop-based biofuel expansion in the tropics: the effects of changing yield and technology. Environmental Research Letters 3, 034001 (10pp). doi: 10.1088/1748-9326/3/3/034001, ISSN: 1748-9326

Green, W. H. Ampt, G. A. (1911) Studies on Soil Physics. *The Journal of Agricultural Science,* 4:1

GREET Life Cycle Model (2014) *Center for Transportation Research Energy Systems Division Argonne National Laboratory*

Groom M., E. Gray, and P. Townsend (2008). Biofuels and Biodiversity: Principles for Creating Better Policies for Biofuel Production. Conservation Biology 22, 602–609. doi: 10.1111/j.1523-1739.2007.00879.x, ISSN: 1523-1739.

Guillén-Gosálbez, G. Caballero, J. Jiménez, L. (2008) Application of life cycle assessment to the structural optimization of process flowsheets, *Industrial & Engineering Chemistry Research,* Volume 47, Pages 777-789.

Haberl H., T. Beringer, S. C. Bhattacharya, K.-H. Erb, and M. Hoogwijk (2010). The global technical potential of bio-energy in 2050 considering sustainability constraints. Current Opinion in Environmental Sustainability 2, 394–403. doi: 10.1016/j.cosust.2010.10.007, ISSN: 1877-3435.

Harper R. J., S. J. Sochacki, K. R. J. Smettem, and N. Robinson (2010). Bioenergy Feedstock Potential from Short-Rotation Woody Crops in a Dryland Environment†. Energy & Fuels 24, 225–231. doi: 10.1021/ef9005687, ISSN: 0887-0624.

Heijungs, R., Guinee, J. B., Huppes, G., Lankreijer, R. M., Udo de Haes, H. A., Wegener Sleeswijk, A., Ansems, A. M. M., Eggels, A. M. M., van Duin, R., & de Goede, H. P. (1992). En6ironmental Life Cycle Assessment of Products : Background and Guide. MultiCopy, Leiden.

Hejazi, M, I. Cai, X. Borah, D, K. (2008) Calibrating a watershed simulation model involving human interference: an application of multi-objective genetic algorithms, *Journal of Hydroinformatics*, 10.1

Hugo, A. Pistikopoulos, E. (2005) Environmentally conscious long-range planning and design of supply chain networks, *Journal of Cleaner Production,* Volume 13 (15), Pages 1471-1491.

Immerzeel D. J., P. Verweij, F. Hilst, and A. P. Faaij (2013). Biodiversity impacts of bioenergy crop production: a state-of-the-art review. GCB Bioenergy.

IPCC (2011). IPCC Special Report on Renewable Energy Sources and Climate Change Mitigation. Prepared by Working Group III of the Intergovernmental Panel on Climate Change [O. Edenhofer, R. Pichs-Madruga, Y. Sokona, K. Seyboth, P. Matschoss, S. Kadner, T. Zwickel, P. Eickemeier, G. Hansen, S. Schlömer, C. von Stechow (eds.)]. Cambridge University Press, Cambridge, United Kingdom and New York, NY, USA, 1075 pp.

Johnston M., J. A. Foley, T. Holloway, C. Kucharik, and C. Monfreda (2009). Resetting global expectations from agricultural biofuels. Environmental Research Letters 4, 014004 (9pp). doi: 10.1088/1748-9326/4/1/014004, ISSN: 1748-9326

Ki, S., J. Sugimura, T. Kim, A., S. (2015) Open MP-accelerated SWAT simulation using Intel C and FORTRAN complilers: Development and benchmark, *Computer & Geosciences*, Volume 75, Pages 66-72.

Kløverpris J. H., and S. Mueller (2013). Baseline time accounting: Considering global land use dynamics when estimating the climate impact of indirect land use change caused by biofuels. The International Journal of Life Cycle Assessment 18, 319–330

Lal R. (2011). Sequestering carbon in soils of agro-ecosystems. Food Policy 36, S33–S39. doi: 10.1016/j.foodpol.2010.12.001, ISSN: 03069192.

Lamers P., and M. Junginger (2013). The "debt" is in the detail: A synthesis of recent temporal forest carbon analyses on woody biomass for energy. Biofuels, Bioproducts and Biorefining 7, 373–385. doi: 10.1002/bbb.1407, ISSN: 1932- 1031.

Latta G. S., J. S. Baker, R. H. Beach, S. K. Rose, and B. A. McCarl (2013). A multisector intertemporal optimization approach to assess the GHG implications of U.S. forest and agricultural biomass electricity expansion. Journal of Forest Economics 19, 361–383. doi: 10.1016/j.jfe.2013.05.003, ISSN: 1104-6899.

Li, M., Li, G., Azarm, S., (2008) A Kriging Metamodel Assisted Multi-Objective Genetic Algorithm for Design Optimization. *Journal of Mechanical Design Vol. 130 (3) 031401–031410*

Liu, P. Pistikopoulos, E.N. Li, Z. (2010) An energy systems engineering approach to the optimal design of energy systems in commercial buildings, *Energy Policy,* Volume 38, Issue 8, Pages 4224-4231

Luz Santos, H. and Legey, L. (2010) Environmental costs on along-term expansion model of hydrothermal generation systems, *In: 2nd International Conference on Engineering Optimization Lisbon, Portugal*.

McKone, T. (2009, May 27) The Coming of Biofuels: Study Shows Reducing Gasoline Emissions Will Benefit Human Health. Berkeley Lab News Center. Retrieved from https://newscenter.lbl.gov/2009/05/27/biofuels-and-human-health/

Neitsch, S.L., Arnold, J.G., Kiniry, J.R., Williams, J.R., (2011). Soil and Water Assessment Tool Theoretical Documentation, Version 2009. Grassland, Soil and Water Research Laboratory, ARS. Texas Water Resources Institute Technical Report No. 406

Nijsen M., E. Smeets, E. Stehfest, and D. P. Vuuren (2012). An evaluation of the global potential of bioenergy production on degraded lands. GCB Bioenergy 4, 130–147. doi: 10.1111/j.1757-1707.2011.01121.x, ISSN: 1757-1707

Noori, N., Kalin, L. (2016) Coupling SWAT and ANN models for enhanced daily streamflow prediction, *Journal of Hydrology*, Volume 533, Pages 141-151.

Pacca S., and J. R. Moreira (2011). A Biorefinery for Mobility? Environmental Science & Technology 45, 9498–9505. doi: 10.1021/es2004667, ISSN: 0013-936X

Pai, N. Saraswat, D. Srinivasan, R. (2012) Field_SWAT: A tool for mapping SWAT output to field boundaries, *Computers & Geosciences*, Volume 40, Pages 175–184

Pieragostini, C. Mussati, M, C. Aguirre, P. (2012) On process optimization considering LCA methodology, *Journal of Environmental Management,* Volume 96,Pages 43-54.

Pietrapertosa, F. Cosmi, C. Macchiato, M. Salvia, M. Cuomo, V. (2009) Life Cycle Assessment, ExternE and Comprehensive Analysis for an integrated evaluation of the environmental impact of anthropogenic activities. *Renewable and Sustainable Energy Reviews*, Volume 13, Pages 1039-1048.

Pinto-Varela, T. Barbosa-Póvoa, A.P. Novais, A. (2010) Supply chain network optimization with environmental impacts. *In: 2nd International Conference on Engineering Optimization, Portugal.*

Popp A., J. P. Dietrich, H. Lotze-Campen, D. Klein, N. Bauer, M. Krause, T. Beringer, D. Gerten, and O. Edenhofer (2011). The economic potential of bioenergy for climate change mitigation with special attention given to implications for the land system. Environmental Research Letters 6, 34–44. doi: 10.1088/17 48-9326/6/3/034017, ISSN: 1748-9326.

Popp A., S. Rose, K. Calvin, D. Vuuren, J. Dietrich, M. Wise, E. Stehfest, F. Humpenöder, P. Kyle, J. Vliet, N. Bauer, H. Lotze-Campen, D. Klein, and E. Kriegler (2013). Land-use transition for bioenergy and climate stabilization: model comparison of drivers, impacts and interactions with other land use based mitigation options. Climatic Change, 1–15. doi: 10.1007/s10584-013-0926-x, ISSN: 0165-0009.

Psomas, A., Panagopoulos, T., Konsta, D., Mimikou, M. (2016) Designing water efficiency measures in a catchment in Greece using WEAP and SWAT models, *Procedia Engineering*, Volume 162, Pages 269-276.

Qi, H. Altinakar, M. S. (2011) A conceptual framework of agricultural land use planning with BMP for integrated watershed management, *Journal of Environmental Management*, Volume 92, Pages 149-155.

Rallison, R. E. and N. Miller; (1981) Past, Present, and Future SCS Runoff Procedure in Rainfall-Runoff Relationship, Proceedings of the International Symposium on Rainfall-Runoff Modelling, edited by V. P. Singh.

Renewable Fuels Association. Going global, 2015 ethanol industry outlook. Washington, D. C; Jan. 2015

Repo A., M. Tuomi, and J. Liski (2011). Indirect carbon dioxide emissions from producing bioenergy from forest harvest residues. GCB Bioenergy 3, 107–115. doi: 10.1111/j.1757-1707.2010.01065.x, ISSN: 1757-1707.

Rogner H. H., R. F. Aguilera, C. L. Archer, R. Bertani, S. C. Bhattacharya, I. Bryden, R. R. Charpentier, M. B. Dusseault, L. Gagnon, Y. Goswami, H. Haberl, M. M. Hoogwijk, A. Johnson, P. Odell, H. Wagner, and V. Yakushev (2012). Chapter 7—Energy resources and potentials. In: Global Energy Assessment: Toward a Sustainable Future. L. Gomez-Echeverri, T.B. Johansson, N. Nakicenovic, A. Patwardhan, (eds.), IIASA and Cambridge University Press, Laxenburg, Austria, Cambridge, UK, pp. 425–512.

Rose S., R. Beach, K. Calvin, B. McCarl, J. Petrusa, B. Sohngen, R. Youngman, A. Diamant, F. de la Chesnaye, J. Edmonds, R. Rosenzweig, and M. Wise (2013). Estimating Global Greenhouse Gas Emissions Offset Supplies: Accounting for Investment Risks and Other Market Realties. EPRI, Palo Alto, CA, 23 pp

Schrage, L., (2009) Optimization modeling with LINGO. Lindo systems inc.

Scown C. D., W. W. Nazaroff, U. Mishra, B. Strogen, A. B. Lobscheid, E. Masanet, N. J. Santero, A. Horvath, and T. E. McKone (2012). Lifecycle greenhouse gas implications of US national scenarios for cellulosic ethanol production. Environmental Research Letters 7, 014011. doi: 10.1088/1748-9326/7/1/014011, ISSN: 1748-9326.

SCS, 1972 - (Soil Conservation Service). National Engineering Handbook, Section 4, U.S. Department of Agriculture, Washington, D.C.

Sedjo R., and X. Tian (2012). Does Wood Bioenergy Increase Carbon Stocks in Forests? Journal of Forestry 110, 304–311.

Smith P., M. Bustamante, H. Ahammad, H. Clark, H. Dong, E.A. Elsiddig, H. Haberl, R. Harper, J. House, M. Jafari, O. Masera, C. Mbow, N.H. Ravindranath, C.W. Rice, C. Robledo Abad, A. Romanovskaya, F. Sperling, and F. Tubiello, 2014: Agriculture, Forestry and Other Land Use (AFOLU). In: Climate Change 2014: Mitigation of Climate Change. Contribution of Working Group III to the Fifth Assessment Report of the Intergovernmental Panel on Climate Change [Edenhofer, O., R. Pichs-Madruga, Y. Sokona, E. Farahani, S. Kadner, K. Seyboth, A. Adler, I. Baum, S. Brunner, P. Eickemeier, B. Kriemann, J. Savolainen, S. Schlömer, C. von Stechow, T. Zwickel and J.C. Minx (eds.)]. Cambridge University Press, Cambridge, United Kingdom and New York, NY, USA.

Smith W. K., C. C. Cleveland, S. C. Reed, N. L. Miller, and S. W. Running (2012b). Bioenergy Potential of the United States Constrained by Satellite Observations of Existing Productivity. Environmental Science & Technology 46, 3536–3544. doi: 10.1021/es203935d, ISSN: 0013-936X

Smith W. K., M. Zhao, and S. W. Running (2012). Global Bioenergy Capacity as Constrained by Observed Biospheric Productivity Rates. BioScience 62, 911–922. doi: 10.1525/bio.2012.62.10.11, ISSN: 0006-3568, 1525–3244.

Sochacki S. J., R. J. Harper, and K. R. J. Smettem (2012). Bio-mitigation of carbon following afforestation of abandoned salinized farmland. GCB Bioenergy 4, 193–201. doi: 10.1111/j.1757-1707.2011.01139.x, ISSN: 17571693.

Sochacki S. J., R. J. Harper, K. R. J. Smettem, B. Dell, and H. Wu (2013). Evaluating a sustainability index for nutrients in a short rotation energy cropping system. GCB Bioenergy 5, 315–326. doi: 10.1111/j.1757-1707.2012.01202.x, ISSN: 1757-1707.

Sterner M., and U. Fritsche (2011). Greenhouse gas balances and mitigation costs of 70 modern Germany-focused and 4 traditional biomass pathways including land-use change effects. Biomass and Bioenergy 35, 4797–4814. doi: 10.1016/j.biombioe.2011.08.024, ISSN: 0961-9534.

Taboada, H., and Coit, D. (2008). MOEA-DAP: a new multiple objective evolutionary algorithm for solving design allocation problems. Department of Industrial and Systems Engineering, Rutgers University. Piscataway, NJ.

Tan, R. (2005) Application of symmetric fuzzy linear programming in life cycle assessment, *Environmental Modelling & Software*, Volume 20, Pages 1343-1346.

Tan, R.R. Culaba, A.B. Purvis, M.R.I. (2004) POLCAGE 1.0 possibilistic life-cycle assessment model for evaluating alternative transportation fuels, *Environmental Modelling & Software*, Volume 19 (10), Pages 907-918.

Tilman D., J. Hill, and C. Lehman (2006). Carbon-Negative Biofuels from LowInput High-Diversity Grassland Biomass. Science 314, 1598–1600. doi: 10.1126/science.1133306, ISSN: 0036-8075, 1095–9203.

U.S. Congress. (2007). Energy Independence and Security Act of 2007. HR 6. 110th Congress. 1st session. December 2007.

Van Dam J., A. P. C. Faaij, J. Hilbert, H. Petruzzi, and W. C. Turkenburg (2009). Large-scale bioenergy production from soybeans and switchgrass in Argentina: Part A: Potential and economic feasibility for national and international markets. Renewable and Sustainable Energy Reviews 13, 1710–1733.

Van der Hilst F., J. P. Lesschen, J. M. C. van Dam, M. Riksen, P. A. Verweij, J. P. M. Sanders, and A. P. C. Faaij (2012). Spatial variation of environmental impacts of regional biomass chains. Renewable and Sustainable Energy Reviews 16, 2053–2069. doi: 10.1016/j.rser.2012.01.027, ISSN: 1364-0321.

Van Vuuren D. P., J. van Vliet, and E. Stehfest (2009). Future bio-energy potential under various natural constraints. Energy Policy 37, 4220–4230. doi: 16/j. enpol.2009.05.029, ISSN: 0301-4215

Wagena, M. B., Bock, E. M., Sommerlot, A. R., Fuka, D. R., Easton, Z. M. (2017). Development of a nitrous oxide routine for the SWAT model to assess greenhouse gas emissions from agroecosystems, *Environmental Modelling & Software*, Volume 89, pages 131-143.

Wicke B., E. Smeets, A. Tabeau, J. Hilbert, and A. Faaij (2009). Macroeconomic impacts of bioenergy production on surplus agricultural land—A case study of Argentina. Renewable and Sustainable Energy Reviews 13, 2463–2473. doi: 16/j.rser.2009.05.010, ISSN: 1364-0321.

Wicke B., E. Smeets, H. Watson, and A. Faaij (2011). The current bioenergy production potential of semi-arid and arid regions in sub-Saharan Africa. Biomass and Bioenergy 35, 2773–2786. doi: 10.1016/j.biombioe.2011.03.010, ISSN: 0961-9534

Ximenes F. de A., B. H. George, A. Cowie, J. Williams, and G. Kelly (2012). Greenhouse Gas Balance of Native Forests in New South Wales, Australia. Forests 3, 653–683. doi: 10.3390/f3030653.

Zanchi G., N. Pena, and N. Bird (2012). Is woody bioenergy carbon neutral? A comparative assessment of emissions from consumption of woody bioenergy and fossil fuel. GCB Bioenergy 4, 761–772. doi: 10.1111/j.1757-1707.2011.01 149.x, ISSN: 1757-1707.

Zhang, D. Chen, X. Yao, H. Lin, B. (2015) Improved calibration scheme of SWAT by separating wet and dry seasons, *Ecological Modeling*, Volume 301, Pages 54-61.

Zhang, P., Liu, Y., Pan, Y., Yu, Z. (2013b) Land use pattern optimization base on CLUE-S and SWAT models for agricultural non-point source pollution control, *Mathematical and Computer Modelling*, Volume 58, issues (3-4), Pages 588-595.

Zhang, X. Beeson, P. Link, R. Manowitz, D. Izaurralde, R, C. Sadeghi, A. Thomson, A, M. Sahajpal, R. Srinivasan, R. Arnold, J, G. (2013a) Efficient multi-objective calibration of a computationally intensive hydrologic model with parallel computing software in Python, *Environmental Modelling & Software*, Volume 46,Pages 208-218.

Zhou, C. Yin, G. Hu, X. (2009) Multi-objective optimization of material selection for sustainable products: artificial neural networks and genetic algorithm approach, *Materials & Design,* Volume 30 (4), Page 1209-1215.

Vita

Ana C. Cram was born in Ciudad Juarez, Chihuahua, Mexico. The fourth child of Armando Davila Cardenas and Martha Dolores Mena Olveda. She studied her fundamental education and high school in Mexico to later migrate to the U.S. to pursue higher education. She is the first in obtaining a Ph. D. in her family.

She graduated with a B. S. in Industrial Engineering in 2011 and with an M.S. in Manufacturing Engineering in 2013 from the University of Texas at El Paso. During her graduate school years, she was a research assistant in the Industrial Manufacturing and Systems Engineering department. Also, Ana had the opportunity to intern in Washington D.C. at USDA's National Institute of Food and Agriculture in the Institute of Bioenergy, Climate and Environment.